

https://dspace.org/

Fabrication of a label-free DNA/graphene based electrochemical DNA hybridisation sensor for product authentication and tracing

Hlongwane, Gloria Ntombenhle

2017

https://hdl.handle.net/10539/24969

Hlongwane, Gloria Ntombenhle (2017) Fabrication of a label-free DNA/graphene based electrochemical DNA hybridisation sensor for product authenticating and tracking, University of the Witwatersrand, Johannesburg, https://hdl.handle.net/10539/24969

Downloaded from a DSpace repository. https://dspace.org/



FABRICATION OF A LABEL-FREE DNA/GRAPHENE BASED ELECTROCHEMICAL DNA HYBRIDISATION SENSOR FOR PRODUCT AUTHENTICATION AND TRACING

Gloria Ntombenhle Hlongwane

A thesis submitted to the Faculty of Engineering and Built Environment,

University of the Witwatersrand. Johannesburg, in fulfilment of the requirements for the Degree of Doctor of Philosophy

August, 2017

Declaration

I declare that this thesis is my unaided work. It is being submitted for the Degree of Doctor of Philosophy to the University of the Witwatersrand, Johannesburg. It has not been submitted before for any degree or examination to any other University.

_____

(Signature of Candidate)

_____day of _____year _____

day *month* *year*

Abstract

Poor understanding of the interactions at graphene/DNA interfaces has brought tremendous limitations to the development of label-free DNA-graphene based electrochemical/electrical biosensors. The aim of this study was to develop a label-free DNA/graphene-based electrochemical DNA hybridisation sensor, evaluate and benchmark its output electronic signal as a function of the effect of DNA on graphene's electronic properties. In addition, the study sought to understand the effect of graphene on the nature of DNA. Herein, results of the investigation of the effects of DNA self-immobilisation and subsequent DNA hybridisation on the electronic structure of CVD-grown graphene using a combination of Raman spectroscopy and conductance measurements are presented. A novel UV-Vis spectroscopy dependent measurement technique for the label-free study of the interaction between DNA-graphene interfaces during DNA hybridisation on graphene is reported. Also presented in this work, is a new method of representing electronic events and DNA conformational changes during DNA detection on graphene from current-voltage measurements. Non-covalent assembly was used to immobilise single-stranded (ssDNA) probes on CVD-grown graphene. On CVD-grown graphene, Raman peak frequency shifts, intensities and widths of the G and 2D bands after adsorption of the ssDNA probe and its hybridisation with complementary and mismatched ssDNA strands were analysed. The effect of graphene on the structural and conformational changes of DNA upon hybridisation of the ssDNA on the graphene surface both before and after hybridisation with complementary and triple-base mismatch DNA targets were investigated by monitoring UV-Vis absorption peaks at the 200 nm to 300 nm range. The findings were further confirmed through XRD analysis. Using Riemann approximation method, the rate at which the energy is transformed (power) was computed from the area under current-voltage curves.

Significant sequence-specific features in Raman peaks of graphene upon self-immobilisation of ssDNA and subsequent hybridisation with complementary and mismatched target strands were observed. The shifts in G and 2D peak positions indicate a donor-acceptor interaction between ssDNA and graphene and charge transfer effects on graphene upon hybridisation. While n-type doping (red shift of the G peak) was observed during hybridisation with complementary strands, p-type doping (blue shift of the G peak) was observed for mismatched strands. These features can serve as fingerprints for the identification of the electronic structure of graphene that uniquely evolves during DNA immobilisation and DNA hybridisation. These findings demonstrate that Raman spectroscopy can be sufficiently used to fingerprint differences between graphene and samples of graphene coated with biological adsorbates and clusters such as DNA.

Hyperchromic and hypochromic effects were related to structural and conformational changes of DNA on graphene. An increase and a decrease in absorption for hybridisation with a complementary and triple-base mismatch target was observed, respectively (Wilk' Lambda = 0.172, F (3,636) = 1020, p =0.000 < 0.05). Differences in structure between perfectly complementary DNA duplexes and those that contain mismatches were also seen by complexities between 2θ = 11° to around 2θ =25° that appeared only in the XRD pattern of ssDNA-coated graphene when hybridised with a triple-base mismatch. Bathochromic and hypsochromic shift in absorption wavelengths confirmed DNA adsorption and desorption on graphene. Adsorption of ssDNA probe on graphene shifted the maximum absorption wavelength to longer wavelengths (bathochromic shift) and shifted to shorter wavelengths (hypsochromic shift) during desorption of DNA upon hybridisation of ssDNA coated-graphene with a complementary and triple-base mismatch. DNA Adsorption and desorption on graphene was further confirmed by the shift of kα1 and kα2 to lower angles in the XRD patterns. The effects of graphene on the chromophoric

structure of DNA was evident through the re-appearance of the signature DNA absorbance wavelength peak at 260 nm in the absence of graphene in solution. Findings of the study provide an alternative application of hyperchromic and hypochromic effects when concerning the illumination of interactions between DNA and graphene. Furthermore, it is proposed that by monitoring the absorbance wavelength and absorption intensity changes of DNA on the graphene surface (before and after hybridisation), interactions in DNA-graphene interfaces could be clarified and the influence of graphene on the conformational changes that occur to the DNA can be better understood. Therefore, the findings of this study shed more light on the understanding of DNA-graphene interfaces and can be instrumental to the design and fabrication of improved devices with consistent output signals.

The power obtained through the method presented in this work represents the electronic charge transfer events and conformational changes in DNA structure holistically. Two distinct electronic circuit configurations, parallel and series, were studied. Using this simple integrative approach of geometric interpretation of current-voltage measurements, a consistent general trend in DNA hybridisation on graphene was obtained, a trend that has not been established using Dirac point's back gate (V_g) values in this work and previous work reported in literature. It was observed that in both parallel and series configuration; hybridisation of the ssDNA coated graphene with a complementary DNA target results in a decrease in Power. When the ssDNA coated graphene was hybridised with triple-base mismatched strands, an increase in power was observed for both parallel and series configurations. This offers a consistent output electronic signal that deciphers selective and specific DNA hybridisation characteristics on graphene.

Acknowledgements

First and foremost I would like to thank my supervisors and advisors (Dr. Daniel Wamwangi, Dr. David Dodoo-Arhin, Prof. Michael Daramola and Prof. Sunny Iyuke) for their guidance and assistance in the planning, executing and writing up of this work. This thesis would not have been possible without their unwavering support and guidance. I thank the African Materials Science and Engineering Network, AMSEN (A Carnegie-IAS RISE Network) and the University of the Witwatersrand for their financial support. I also acknowledge and sincerely appreciate everyone (colleagues, friends, family, and acquaintances) who have played a role either directly or indirectly in making this thesis possible. Lastly, I give thanks to God for giving me the strength and courage to carry on during hard times.

Table of Contents

Declaration i

Abstract ii

Acknowledgements v

Table of Contents vi

List of Figures ix

List of tables xiii

Nomenclature xiv

Chapter 1 Introduction 1

1. 1 Background and motivation 1

1.2 Research questions 5

1.3 Aims and objectives of the study 5

1.4 Thesis layout 6

Chapter 2 Literature review and state of the art 8

2.1 Background 8

2.1.1 Consumer Expectation 8

2.1.2 Product Authenticity 9

2.2 Analysis of Product Samples 10

2.2.1 Technology based techniques 10

2.2.2 Cellular and molecular biology techniques 12

2.2.3 Biosensing technologies 15

2.3 Current limitations and Challenges of DNA biosensing technologies 43

2.4 Future outlook 46

Chapter 3 Experimental 49

3.1 Target region 49

3.2 Sequence Selection 49

3.3 DNA strands preparation 51

3.4 Graphene samples 51

3.4 DNA self-immobilisation and hybridisation on graphene 52

Chapter 4 Raman fingerprint of DNA hybridisation on graphene 53

4.1 Introduction 53

4.2 Materials and Methods 60

4.3 Results and Discussion 61

4.4 Summary 72

Chapter 5 Effect of graphene on DNA hybridisation 73

5.1. Introduction 73

5.2. Materials and methods 75

5.2.1 UV Analysis 76

5.2.2 UV-Vis Statistical Analysis 76

5.2.3 X-ray diffraction (XRD) Analysis 77

5.3. Results and Discussion 77

5.3.1 UV analysis 77

5.3.2 XRD analysis 91

5.4 Summary 92

Chapter 6 Geometric interpretation of current-voltage measurements 94

6.1 Introduction 94

6.2 Materials and Methods 97

6.2.1 Fabrication of ssDNA/graphene nanocomposites 97

6.2.2 Hybridisation of DNA and current-voltage measurements 99

6.2.3 Integration of current-voltage measurements 101

6.3 Results and discussion 102

6.3.1 Current-voltage characteristics 102

6.3.2 Electronic transport at the DNA-graphene interface 109

6.3.3 Geometric interpretation of current-voltage measurements 114

6.4 Summary 116

Chapter 7 Conclusions and recommendations 118

7.1 Conclusions 118

7.2 Recommendations 120

References 121

Appendix A: Design of a label-free ssDNA probe 166

Appendix B: List presentations at conferences, seminars and workshops 167

Appendix C: List of articles in peer-reviewed journals 169

List of Figures

Figure 2.1 Bibliometric survey analysis, for the year 1977–2016, on data provided in Scopus SciVerse of publications related refereeing to the keyword biosensor 15

Figure 2.2 Bibliometric survey analysis, for the year 1977–2016, on data provided in Scopus SciVerse of publications related the keyword biosensor in various scientific fields..... 16

Figure 2.3 Bibliometric survey analysis, for the year 1985–2016, on data provided in Scopus SciVerse of publications related to DNA biosensors..... 18

Figure 2.4 The schematic illustration of the underlying concept in DNA hybridisation biosensors (Adapted from Du et al., 2012) 19

Figure 2.5 Schematic representation of hybridisation of complementary nucleotide bases in a probe-target duplex. Nucleotide bases, adenine, cytosine, thymine and guanine are represented by letters A, C, T, and G, respectively (Adapted from Wolcott, 1992) 21

Figure 2.6 Bibliometric survey analysis, for the year 1985–2016, on data provided in Scopus SciVerse of publications related to graphene-based DNA..... 27

Figure 2.7 The schematic illustration of the basic structural units of DNA. A= Adenine, C= Cytosine, G= Guanine, T= Thymine, P= Phosphate group (Adapted from Wolcott, 1992) 29

Figure 2.8 Macroscopic illustration of DNA adsorption and desorption on graphene (Adapted from Du et al., 2012)..... 31

Figure 2.9 Bibliometric survey analysis, for the year 1985–2016, on data provided in Scopus of publications related to different types of transduction methods in DNA biosensors .. 38

Figure 2.10 Bibliometric survey analysis over the period of 1977 to 2016, on data provided in Scopus of publications and patents related to DNA biosensors 47

Figure 4.1 Raman spectrum of CVD-grown pristine graphene 61
Figure 4.2 Raman spectrum of (a) CVD-grown graphene, and (b) graphene upon self-immobilisation of a 26 bp ssDNA probe 63
Figure 4.3 Raman spectrum of (a) ssDNA probe-coated graphene, and (b) ssDNA-coated graphene after hybridisation with a complementary 26 bp DNA strand. N-type doping is evidenced by the red shift of the G peak 66
Figure 4.4 Raman spectra of (a) ssDNA probe-coated graphene, and (b) ssDNA-coated graphene after hybridisation with a 26 bp triple-base mismatched DNA strand. P-type doping is evidenced by the blue shift of the G peak 68
Figure 4.5 Raman spectra measured at different areas on. (a) Pristine CVD-grown graphene. (b) ssDNA-coated graphene, (c) ssDNA-coated graphene that is hybridised with complementary ssDNA target, and (d) ssDNA-coated graphene that is hybridised with triple-base mismatch ssDNA target substrates 71
Figure 5.1 The UV-Vis absorbance spectra monitored between the 200 and 300 nm range at room temperature of (a) CVD-grown pristine graphene, (b) of ssDNA probe-coated graphene, (c) ssDNA probe-coated graphene when hybridised with a complementary ssDNA target, and (d) ssDNA probe-coated pristine graphene when hybridised with a triple-base mismatched ssDNA target 79
Figure 5.2 UV-Vis absorption spectra of (a) dsDNA formed in solution, (b) dsDNA after removal from the graphene surface 84
Figure 5.3 UV-Vis absorption spectra of several samples of DNA (duplex of ssDNA probe and complementary target strands) after removal from the graphene surface 86
Figure 5.4 X-ray diffraction pattern of (a) CVD-grown graphene, (b) ssDNA probe-coated graphene, and (c) ssDNA probe-coated graphene when hybridised with complementary and (d) triple-base mismatch strands 92

Figure 6.1 Schematic of simple fabrication of the graphene based DNA hybridisation sensing device; (a) represents graphene/SiO_2/Si, (b) graphene/SiO_2/Si with the silver testing pads on two contact points, and (c) is the complete ssDNA/graphene/SiO_2 awaiting Hybridisation 98

Figure 6.2 Schematic of the experimental system for two configurations of the ssDNA/graphene/SiO_2/Si sensor; (a) illustrates the resistors in parallel configuration while (b) illustrates the resistors in series configuration. 100

Figure 6.3 Schematic illustration of the label-free electronic detection of DNA hybridisation using graphene (Adapted from Du et al., 2012) 101

Figure 6.4 Electronic responses of the ssDNA/graphene/SiO_2/Si sensor before and after hybridisation. The graphs demonstrate the Current-Voltage curves for the ssDNA/graphene/SiO_2/Si sensor configured in (a) parallel and (b) series. ssDNA/graphene/SiO_2/Si is the device 103

Figure 6.5 The Current-Voltage plot in the positive voltage (0 to 1 V) region of the ssDNA/graphene/SiO_2/Si sensor in the series configuration 105

Figure 6.6 Current-Voltage Measurements Fitted with Diode Equation $I = ISexp\ qV\eta kT\text{-}1in$ the forward bias. Circled regions show the depletion region. 108

Figure 6.7 Gate voltage dependent resistivity of CVD-grown pristine graphene, ssDNA probe-coated graphene, ssDNA probe-coated graphene when hybridised with a complementary ssDNA and ssDNA probe-coated graphene is hybridised with triple-base mismatched ssDNA for (a) Parallel and (b) Series configurations..... 110

Figure 6.8 General trend observed in Gate voltage shifts of ssDNA probe-coated graphene when hybridised with a complementary ssDNA and ssDNA probe-coated graphene is hybridised with triple-base mismatched ssDNA in both parallel and series configurations 113

Figure 6.9 General trend observed in Power of the device, sDNA probe-coated graphene, when hybridised with a complementary ssDNA and ssDNA probe-coated graphene is hybridised with triple-base mismatched ssDNA in both parallel and series configurations 116

Figure A0.1 Jalview Kalign (version 2.03) alignment of CDC19 gene sequences in ClustalW format identifying the conserved sequence region across 28 S.cerevisiae strains found in SGD..... 166

List of tables

Table 3.1 List of the base sequences of the target DNA, ssDNA/probe, and mismatch DNA strand 51

Table 4.1 Variation of Raman characteristics of graphene due to different effects 55

Table 5.1 SPSS results of Multivariate Test[a] 88

Table 5.2 Statistical data obtained from Pairwise Comparison of samples 90

Table 6.1 The gate voltage measured in Volts (V) at the Dirac point for CVD-grown pristine graphene, ssDNA probe-coated graphene, ssDNA probe-coated graphene when hybridised with a complementary ssDNA and ssDNA probe-coated graphene is hybridised with triple-base mismatched ssDNA 112

Table 6.2 The Power measured in Watts (W) at the Dirac point for CVD-grown pristine graphene, ssDNA probe-coated graphene, ssDNA probe-coated graphene when hybridised with a complementary ssDNA and ssDNA probe-coated graphene is hybridised with triple-base mismatched ssDNA 115

Nomenclature

A - Adenine

AFM - Atomic force microscopy

bp - Base pair

C - Cytosine

C=C – Carbon-Carbon double bond

cGMPs - Pharmaceutical current good manufacturing processes

C-O - Carbon-oxygen bonds

CVD - Chemical Vapor Deposition

DFT - Density functional theory

DNA - Deoxyribonucleic acid

dsDNA – double stranded deoxyribonucleic acid

ELISA - Enzyme-linked immunosorbent essay

Tris-EDTA - Trisaminomethane-ethylenediaminetetraacetic acid

FDA - Food and drug administration

FET - Field-effect transistor

FRET - Fluorescence resonance energy transfer

FT-IR - Fouriertransform infrared spectroscopy

FWHM - Full width at half maximum

G - Guanine

GFET - Graphene field-effect transistor

GO - Graphene oxide

HF - Hartree-Fock

HPOG - Highly oriented pyrolytic graphite

I- Electric current

I_S - Reverse bias saturation current

k - Boltzmann constant

M - Molarity

MOSFET - Metal oxide semiconductor field effect transistor

MP - Møller-Plesset perturbation theory

n-π* - n to pi star

P – Power

PAT - Process analytical technology initiative

PCR - Polymerase chain reaction

PO_3^{-4} - Phosphate groups

q - Electron charge,

R&D - Research and development

RFID - Radio frequency identification

RGO - Reduced graphene oxide

RNA - Ribonucleic acid

Si – Silicon

SiO_2 - Silicon dioxide

ssDNA - single-stranded deoxyribonucleic acid

SPSS - Statistical package for the social sciences

Temp – Temperature

T - Thymine

TEM - Transmission electron microscopy

UV-Vis - Ultraviolet–Visible spectroscopy

V - Voltage across the diode

vdW - van der Waals

V_g - Dirac point's back gate voltage

XRD - X-ray diffraction

η - Ideality factor,

π – pi

π-π - pi-pi

Chapter 1 Introduction

In this chapter, a statement of the research problem is presented with examination of its scope and potential contributions of this work. Furthermore, a rational motivation for this study is presented. The benefits of this research in the development and refinement of label-free graphene-based sensors are outlined from both the fundamental and commercial perspectives.

1. 1 Background and motivation

Biosensors have found employment as devices for analytical tasks in applications ranging from general medical diagnostics, through process control, to defence and security (Bora *et al*., 2013; Vigneshvar *et al*., 2016). Biosensors involve the amalgamation of a biological sensing molecule and a non-biological transducer (Thevenot *et al*., 2001). The amalgamation of the biological molecules with suitable transducers such as nanomaterials converts these simple transducers into powerful analytical instruments or devices (Turner, 2013). The biological molecule-nanomaterial amalgam that is commonly investigated in biosensor development is Deoxyribonucleic acid (DNA)-graphene amalgam.

A vast number of biosensors that have used DNA-graphene amalgam in detecting DNA hybridisation for different applications have been reported (Tjong *et al*., 2014; Zhang and Hu, 2014; Wang *et al*., 2011). These reports look into improving and/or circumventing one or more of these challenges associated with biosensor development: (a) Cost affordability, (b) manufacturing feasibility, (c) efficiency of sensing mechanism, (d) performance (detection limit and dynamic range), and (e) reproducibility (Gooding, 2002; Drummond *et al*., 2003). Therefore, efforts are geared towards the development of affordable bio-sensing instruments or devices that offer convenient, rapid and accurate analysis. However, these devices often require the use of sophisticated high-throughput laboratory based analytical machines and

techniques. The inexpensive instruments or devices enable simple on-field analysis and are mass produced (Turner, 2013). The biological recognition event, DNA hybridisation on graphene, in DNA-graphene based sensors can be converted into a readable output signal via electrochemical/electrical, mass-based, and/or optical, modes of detection (Hahn et al., 2005; Karamollaog˘lua *et al*., 2009; Kerman *et al*., 2004; Passamano and Pighini, 2006).

Optical methods involve the use of labels and dyes to facilitate detection, thus resulting in expensive biosensors. Nonetheless, optical methods still have a strong place in research and as a principal research and development (R&D) monitoring technique (Turner, 2013). Despite being able to qualitatively and quantitatively measure label-free DNA hybridisation at short response times in a sensitive and direct manner, mass-sensitive signal transduction methods have neither really found a niche in neither the R&D nor practical application (Turner, 2013; Karamollaog˘lua *et al*., 2009). Electrochemical and/or electrical transduction methods have experienced tremendous growth and are currently dominating the field of biosensors both in fundamental academic research and application driven commercial arena (Turner, 2013). Electrochemical/electrical transduction of DNA hybridisation allows for detection approaches that are facilitated by labels such redox-active labels and label-free electrochemical/electrical transduction (Gooding, 2002; Hvastkovs and Buttry, 2010).

The most common approach used for electrochemical transduction of DNA using graphene is label-free. The most common and most promising type label-free electrochemical/electrical sensors that have been recently explored in DNA hybridisation detection schemes are Graphene field-effect transistors (GFET) (Green and Norton, 2015). Graphene is an enticing sensor material for field-effect transistors (FET) sensors due to its ambipolar nature (Geim and Novoselov, 2007) and its biocompatibility to DNA (Green and Norton, 2015). Using graphene in FET sensors requires no prior sensor or DNA functionalisation. GFET is

sensitive to the pi-pi (π-π) stacking of nucleobases of the DNA molecule which then alters the electronic response of the DNA GFET. It is this biocompatibility and sensitivity that is responsible for the DNA adsorption on the graphene surface in these DNA GFET devices (Green and Norton, 2015).

Non-covalent bonds governs the interaction between DNA and graphene [Gowtham *et al*., 2007; Varghese *et al*., 2009; Lee *et al*., 2013). Due to the positively charged nature of the carbon making up the graphene and structural uniformity of the negatively charged hydrophilic single-stranded DNA (ssDNA), the reliable self-assembly between the two becomes inevitable irrespective of the length and nucleobase constituents of the probe nucleotide sequence (Oliveira Brett and Chiorcea, 2013; Drummond *et al*., 2003). Onto the surface of graphene, ssDNA probes is reversibly and non-specifically adsorbed. This adsorption is characterised by non-covalent spontaneous self-assembly of DNA on graphene (Lucarelli *et al*., 2008; Tang *et al*., 2011). On the graphene surface, the ssDNA probe molecule is not entirely enclosed and can subsequently bind to complementary DNA targets upon hybridisation. So, in the proposed sensing mechanism for DNA sensing graphene devices, is that upon hybridisation with its target ssDNA, the interactions between the ssDNA probe and graphene is weakened as the initial DNA adsorption onto the graphene surface is reversed. Similar to DNA adsorption, DNA desorption from the graphene is prompt and highly efficient. Following desorption, the ssDNA probe and its complementary target ssDNA hybridise and form a double-stranded (ds) DNA duplex (Gooding, 2002; Green and Norton, 2015; Oliveira Brett and Chiorcea, 2013; Tang *et al*., 2011). Despite the vast theoretical understanding of individual mechanisms of DNA adsorption and desorption on graphene involved in GFET sensors (Lin et al., 2013; Dong et al., 2010), the introduction of DNA in GFET sensors presents other challenges that further complicate the detection scheme. For example, the non-covalent nature of the π–π stacking and electronic primary

interactions between DNA and graphene, changes the structure and electronic properties of graphene through mechanisms such as buffer effects, doping, chemical/electrostatic gating, and induced dipoles (Mohanty and Berry, 2008). Furthermore, graphene is known to disrupt the structure of folded DNA (Liu *et al*., 2011; Husale *et al*., 2010; Wu *et al*., 2014).

Despite proof of concept in the demonstrations of application of GFETs that possess impressive DNA detection limits, the interaction between graphene and DNA in such devices is poorly understood (Dong *et al*., 2010; Lin *et al*., 2013). This poor understanding of the interactions between graphene and DNA has resulted in discrepancies in observed electronic signals associated with adsorption of DNA on graphene and as a consequence, an uncertainty regarding the origin of observed electronic responses of DNA GFET reported in the literature. This ambiguity hinders the following: 1) reproducibility, stability and standardisation of DNA GFET; 2) Improvement of the performance of DNA GFET; 3) development of novel DNA hybridisation detection schemes for DNA GFET devices; and 4) realisation of multi-property characterisation of DNA GFET devices (Green and Norton, 2015).

On the experimental side of label-free DNA-graphene based electrochemical/electrical biosensors, there has been a limited study of the interactions involved between graphene and DNA. On account of the poor understanding of DNA-graphene amalgams and seldom reported electronic DNA-sensor graphene platforms that address this challenge, in this study, the principal sensing mechanism of label-free electrochemical DNA hybridisation devices is explored. The study was attempted to identify the influence of DNA hybridisation/bio-modification on graphene's electronic and structural properties, also identified is the influence of graphene on the nature of DNA.

1.2 Research questions

The following research questions were posed in order to achieve the above-mentioned goal of the study:

- What is the effect of DNA adsorption and DNA desorption upon hybridisation on graphene's electronic properties?
- What is the effect of graphene on the structural conformation of DNA during DNA immobilisation on graphene and DNA desorption upon hybridisation?
- Can an electronic output signal observed during the monitoring and analysis of DNA hybridisation on graphene be benchmarked against the properties of graphene and DNA structural conformations?

1.3 Aims and objectives of the study

The aim of this study was to develop a label-free DNA/graphene-based electrochemical DNA hybridisation sensor, as well as evaluate and benchmark its output electronic signal as a function of the effect of DNA on graphene's electronic properties. In addition, the study sought to understand the effect of graphene on the nature of DNA conformations.

Based on chemical vapour deposition (CVD)-grown graphene, a simple DNA-graphene electronic based sensing device was fabricated for electronic detection of DNA hybridisation. On the same platform empirical evaluations of interaction between DNA and graphene were conducted whereby:

- Graphene electronic and structural fingerprints due to DNA adsorption and DNA desorption upon hybridisation were investigated using Raman spectroscopy.
- Fingerprints due to graphene on DNA structure and conformation during DNA immobilisation on graphene and DNA desorption upon hybridisation were

investigated using Ultraviolet–Visible (UV-Vis) spectroscopy and X-ray powder diffraction (XRD).

- DNA hybridisation on graphene was monitored and analysed through current-voltage measurements using two device configurations.
- The current–voltage characteristic as were converted into an easy to read parameter that holistically encompasses the electronic events and DNA morphological changes during DNA hybridisation of this sensing device.

1.4 Thesis layout

Chapter 1 describes the problem statement and presents a rational motivation for this study. It begins with an overview of the field graphene-based biosensors for label-free detection of DNA detection. It later outlines the need for these type of sensing devices and presents the main challenge that hinders the development and refinement of label-free graphene-based sensors at the fundamental and commercial standpoint. The research aim, objectives and structure of the thesis are also outlined in this chapter.

Chapter 2 reports in greater detail biosensor concepts and critically reviews previous studies reported in literature for a more in-depth understanding of context, scope, terminology and significance of the remainder of this study.

In chapter 3, the common experimental details and materials employed in all the subsequent chapters in this study are described.

Chapter 4 reports a background, materials used and methods undertaken to study the effect of DNA self-immobilisation and subsequent DNA hybridisation on Chemical Vapor Deposition (CVD) grown graphene using Raman spectroscopy. The Raman spectra are presented, discussed and then summarised.

Chapter 5 presents a background, materials used and methods that were involved in studying nature of DNA molecules adsorbed on graphene and their changes in conformation upon hybridisation. The results of the Ultra-Violet (UV) absorption and XRD measurements results are presented, discussed and then summarised.

Chapter 6 describes the deciphering of electronic charge transfer events and conformational changes in DNA structure that occur in the DNA-graphene interface into an easy to read electronic signal. It also reports the conversion current-voltage measurements into a parameter that describes DNA adsorption, nature of DNA and DNA morphological changes during DNA hybridisation in a standardised form.

Chapter 7 outlines the contributions and limitations of the study. It also highlights critical areas for future research.

Chapter 2 Literature review and state of the art

In this chapter, biosensor concepts and critical review of previous studies reported in literature for a more in-depth understanding of context, scope, terminology and significance of the remainder of this thesis are discussed.

2.1 Background

2.1.1 Consumer Expectation

Over the years biotechnology applications have been widely used in bioprocesses in food and beverages, pharmaceutical, medical diagnostics and wastewater treatment industries (Kingsbury, 1987; Richards, 1991; Ludwig *et al.*, 1995; Jobling and Gill, 2004). In view of the fact that biological processes are complex and dynamic with continuously changing physicochemical conditions. To ensure reliability and obtain good quality products, bioprocess needs to be controlled and monitored (Carloni and Turner, 2011; Schugerl, 2001). This is particularly important in bioprocesses used in the food and beverages and pharmaceutical industry in order to assure the consumer/patient of the quality and safety of the products produced.

Incessant occurrences of food scares and scandals has become a battle that requires the world's attention. Consequently, fields involved in product authentication are burdened with the responsibility of preventing possible, newly emerging, and pre-existing product scares and scandals. Due to consumer awareness of these continuous occurrences of food borne outbreaks/scandals, consumers have expectations (Berg, 2004; Chambers and Melkonyan, 2010; Heilig, 2003). Inasmuch as a consumer yearns for assured safety and authenticity in a product prior and subsequent to its release to the supply chain, assurance in time of crisis is also required by the public. That is, should there be any; (a) unexpected case of a scare and/or

scandal post entry of the product in the supply chain, or (b) a product is found to contain unauthorised components after it was assessed as safe, the public requires assurance that the product or product component of concern will be rapidly detected, traced and attributed to the source before it spreads and becomes a basis of panic to the public (Angulo and Gil, 2007; Verbeke and Ward, 2006; Zach *et al*., 2012). It is therefore, the consumer's expectation that post-marketing product safety assessment surveillance is treated with importance that is equivalent to that placed on pre-market evaluation of potential risks (Schilter and Constable, 2002).

Recognising this need, in 2003 a Process Analytical Technology (PAT) initiative was launched by the United States' Food and Drug Administration (FDA) launched (FDA, 2004). PAT is aimed at managing and controlling product quality from the raw materials throughout the production line to the final product using novel advanced analytical process techniques. The PAT framework encourages the subsequent use of real-time information obtained regarding the critical quality attributes product information obtained through monitoring and control process to authenticate and ensure product quality (FDA, 2004; Junker and Wang, 2006).

2.1.2 Product Authenticity

An authentic product is defined as a product whose compositional integrity concurs with the product's provenance and process of production as specified on the product's name, brand and ingredients (Dean *et al*., 2006; Heilig, 2003; Murphy *et al*., 2010; Robinson and Clifford, 2012). Product authentication involves the classification and analytical discrimination of

authentic products from non-authentic samples. In this regard, the following have been explicitly addressed in literature:

- The reduction of product borne incidences through strategic risk management tools and product safety regulation systems in the production chain (Walls and Buchanan, 2005).
- Implications that different product scandals have on the integrity of product safety regulation systems (Pei *et al*., 2011) and potential effect they could have the trade (Song and Chen, 2010; Yapp and Fairman, 2006).
- The development of novel methods of authenticating different products (Jaakola *et al*., 2010; Popping, 2002; Primrose *et al*., 2010; Reida *et al*., 2006).

Since products are classified by stringent parameters that describe traits relating to the origin and background of the product. Authentication of products is vigorous and often times involves the verification of legitimacy of claims made by the manufacturers about the composition and purity of the product in question. Therefore, testing of products strongly relies heavily on the use of technological and analytical techniques to critically discriminate products into their respective categories.

2.2 Analysis of Product Samples

2.2.1 Technology based techniques

Technology in product authentication is used to discriminate samples through innovative tracking and tracing systems. These technologies range from radio frequency identification

(RFID) systems to barcode labels. As long as the tag is on the product's package, these systems will automatically document in real-time, information about the flow of products in the supply chain and its movement in globalised distribution channels (Bardaki *et al*., 2011; Hong *et al*., 2011). However, it is not sufficient to only have information about the location of the product in the supply chain. For a comprehensive post-marketing product safety assessment surveillance, information about the components of the product needs to be collected and validated. Irrespective of the products' location, the characteristics of its constituents have to be ascribed back to their source (Kruse, 1999; Loureiro and Umberger, 2007). Therefore, the demand for sensitive analytical techniques/devices that are reliable, cheap, fast, and can be used on-site is growing (Ahmed, 2002). It is essential that these on-field analytical techniques/devices allow for;

- Authentication of the product through specific identification of traits of its different components, and
- Direct traceability by communicating of background information about the product's specific raw material.

Fields involved in product authentication are aware that an accentuation of post-marketing product safety assessment surveillance to importance that is equivalent to that of pre-market evaluation of potential risk could potentially provide a holistic view into the authentication of products. As a result, several sophisticated analytical techniques commonly referred to as conventional techniques have been developed and proposed as highly crucial methods of monitoring the authenticity and quality of products. Chromatography and Spectroscopy are examples of these highly recommended techniques (Costa *et al.*, 2012; Luthy, 1999). However, ambiguous results can be obtained using these techniques as similar products can be produced by different organisms (Costa *et al*., 2012; Luthy, 1999). To authenticate

products unambiguously, particularly plant and animal based products, analytical techniques based on qualitative and/or quantitative analysis of foreign and characteristic traits specific to the source-organism are attractive alternatives. Therefore, Cellular and Molecular Biology techniques which are either protein- or DNA-based are the preferred alternatives when it comes to checking the authenticity of products derived from plants and/or animals (Ahmed, 2002; Luthy, 1999; Shrestha *et al*, 2010).

2.2.2 Cellular and molecular biology techniques

2.2.2.1 Protein-based techniques

Protein-based techniques are of either electrophoretic and immunoassay origin (Luthy, 1999). The most popular protein-based techniques used to detect proteins are western blot and enzyme-linked immunosorbent essay (ELISA). Their subjectivity is reduced through automation (Dooley, 1994). However, the reliability of the techniques is restricted by the inherent low threshold levels of proteins. Proteins are thermodynamically unstable and heat liable (Costa *et al.*, 2012; Luthy, 1999; Shrestha *et al*, 2010). Moreover, protein-based techniques can be ambiguous since organisms of different species can share phenotypic properties. The probability of this occurring is increased by genetic diversity. For example, genes with small differences in nucleotide base sequences can code for proteins with identical amino acid sequences thus resulting in proteins coded for by different genes possessing identical structures and functions (Dooley, 1994; Luthy, 1999). In such cases, it becomes difficulty if not impossible to discriminate proteins produced by the target organism from those of a non-targeted organism. Therefore, analytical techniques that are based on targets whose detection is independent of gene expression are more attractive (Dooley, 1994).

2.2.2.2 Nucleic acid-based techniques

Nucleic acid-based analytical techniques are independent of gene expression. These techniques recognise nucleic acids as unique molecules. The presence of nucleic acids in products is taken advantage of in product authenticity investigations. The application of nucleic acids is mainly established in basic research. The use of nucleic acids in analytical techniques allows for exploitation of species or genus specific genotypic signatures of any organism with detectable genomic material. Genotypic signatures range from a promoter or terminator, to a gene itself, transgenic or not. Detection of genotypic signatures is used for in various fields including environmental and health surveillance. Surveillance of this calibre is practically achieved through a probe, a defined nucleic acid fragment. A nucleic acid probe is an identified single stranded sequence of nucleotide bases. Through specific and complementary binding to a target sequence of nucleotides, it is used to detect and identify target nucleic acids in a mixture of nucleic acids (Richards, 1991; Wetmur, 2008; and Wolcott, 1992). Since all organisms theoretically have unique sequence of nucleotide bases, probes targeted at recognising a specific nucleic acid region in the nucleotide base sequences of any living organism can be produced. The target sequence of nucleotides is usually of recognisable genotypic properties unique to genus or species. Nucleic acid probes can either be Deoxyribonucleic acid (DNA) or Ribonucleic acid (RNA). RNA requires gene expression to occur, consequently DNA is more attractive as it is independent of gene expression.

DNA-based analytical techniques bring to light the obscure link between product safety, quality and genomic signatures (Luthy, 1999). The DNA thermo-stability comparative to that of proteins reinforces DNA's suitability in authentication methods. Furthermore, DNA is highly selective and specific thus making it an effective target in DNA-based analytical

techniques that authenticate plant and animal based products. Using DNA, genetically modified organisms can be reliably discriminated from their non-genetically modified counterparts (Costa *et al*., 2012; Luthy, 1999).

To date, DNA-based analytical technique that are most established, sensitive, qualitative, quantitative, and that allow for accurate DNA detection, are based on real time polymerase chain reactions (PCR). DNA sequences of target genes that uniquely specific to an organism can be recognised through PCR-based techniques (Davison and Bertheau, 2005; Hanh *et al*., 2005). These involve amplification of trace concentrations of DNA in addition to specific identification of DNA sequences using primers (Davison and Bertheau, 2005). Southern blot analysis, gel electrophoresis, commercial DNA sequencing, and restriction digestion and analysis are among a few on a vast list of laborious and expensive techniques through which identification of DNA sequences is achieved. Furthermore, well-equipped laboratories with experienced and trained investigators are required to optimise results from PCR-based techniques (Karamollaogˇlua *et al*., 2009; Passamano and Pighini, 2006; Wua *et al*., 2009). Without a doubt, DNA-analysis for purposes ranging from healthcare to food safety, was revolutionised by the development of PCR (Hanh *et al*., 2005; Luthy, 1999). However, the development of innovative high-throughput, miniaturized, cheap and extremely rapid on-field analytical devices that are easily operated by individuals without any laboratory training or experience is equally if not more revolutionary (Hanh *et al*., 2005; Karamollaogˇlua *et al*., 2009; Nugen and Baeumner, 2008; Passamano and Pighini, 2006). These analytical devices are biosensors and bioelectronics.

2.2.3 Biosensing technologies

The first mention and illustration of a form of a biosensing technology was by Professor Leland C. Clark in 1956. Despite this early illustration of such a technology, the definition and proof of concept of Biosensors occurred only in the 1970s (Clark and Lyons, 1962; Mascini, 2006; Vigneshavar *et al*., 2016). From a Scopus bibliometric analysis of literature related to biosensors depicted in Figure 2.1, the number of publications on biosensors has increased tremendously over the last 41 years. From this bibliometric data it is also observed that research in the field of biosensors peaked in the year 2015 with work published in a wide range of scientific fields (Figure 2.2).

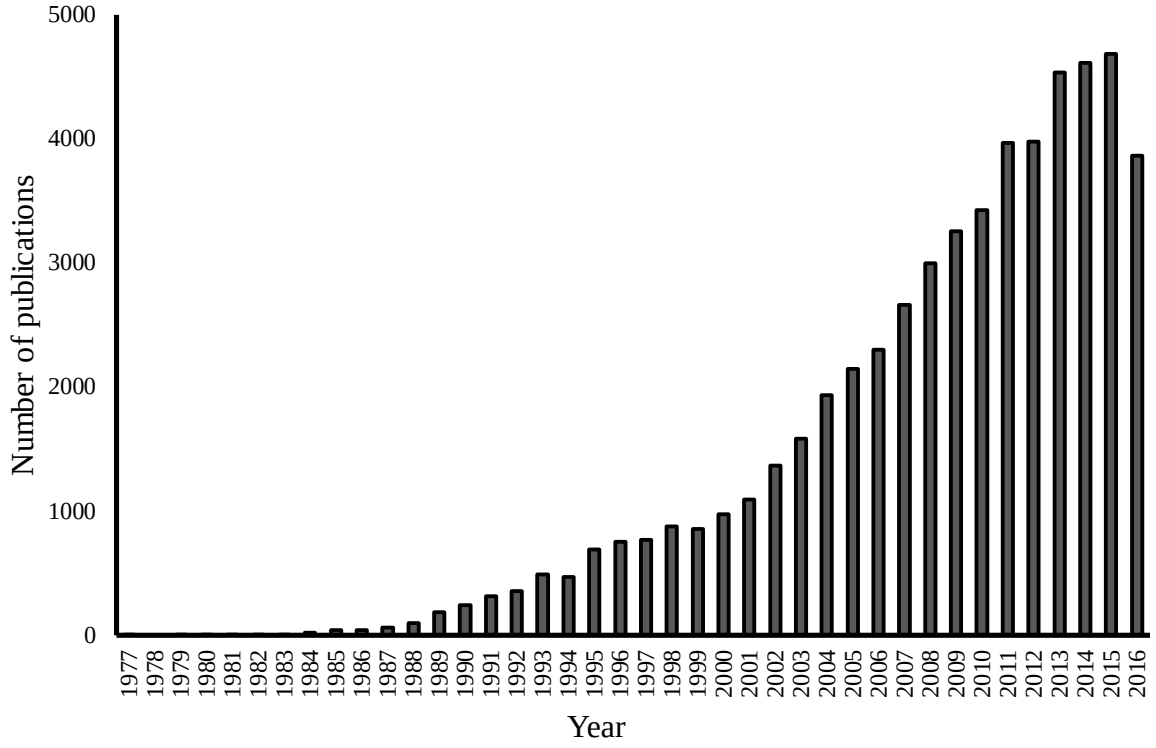

Figure 2.1 Bibliometric survey analysis, for the year 1977–2016, on data provided in Scopus SciVerse of publications related refereeing to the keyword biosensor

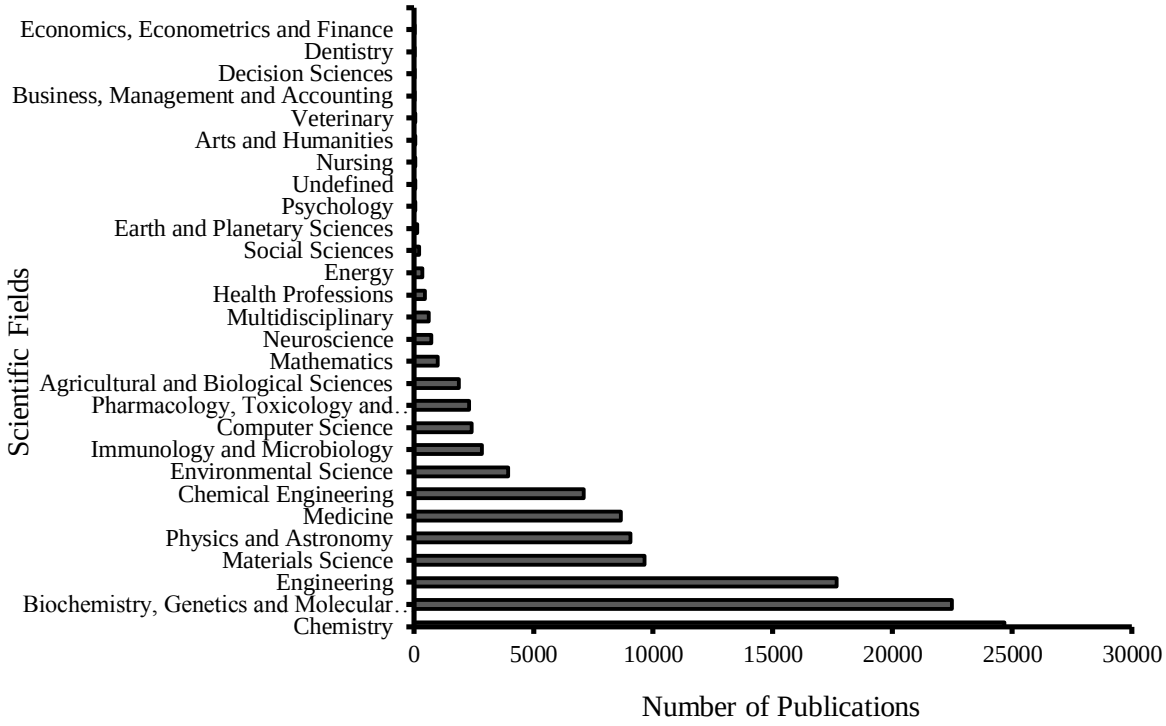

Figure 2.2 Bibliometric survey analysis, for the year 1977–2016, on data provided in Scopus SciVerse of publications related the keyword biosensor in various scientific fields

Biosensors are described at their most basic form as self-contained analytical devices that consists of a support material with a bioreceptor/probe bound to it. The bioreceptor/probe is immobilised as a bio-recognition layer onto the support. Binding of the bioreceptors onto the supports is made possible by the biocompatible nature of the support materials. This bio-recognition layer is responsible for the detection and specific binding of the target analyte while a transducer converts the corresponding biological reaction due to the interaction between the bioreceptor in the bio-recognition layer and its specific target analyte into a detectable and measurable signal which can be used to qualitatively screen for the target

analyte (Thevenot *et al*., 2001; Vo-Dinh, 2004; Mascini, 2006; Wang, 1999). Therefore, the basic working principal of biosensing devices is intimate coupling of bioreceptors and biocompatible support materials that transduce the bio-recognition even into various signals (Wang, 2000). In the following sections of this work, recent advances and trends in the areas of bioreceptors, biocompatible materials and different transduction methods used in biosensors will be reviewed.

2.2.3.1 Bioreceptors

Biosensors are classified based on the type of bioreceptor, support and subsequent nature of the biological recognition event. They are categorised into affinity- or biocatalytic-based biosensors. Components of organisms ranging from proteins and nucleic acid to an entire microorganism are used as bioreceptors form different kinds of bio-recognition layers. Biocatalytic sensors primarily utilise immobilised proteins as bioreceptors. On the other hand, nucleic acids and antibodies are utilised as bioreceptors in affinity-based biosensors (Thevenot *et al*., 2001; Vo-Dinh, 2004; Wang, 1999). Enzymes are also used as bioreceptors but typically not as actual bioreceptor instead as a label (Velusamy *et al*., 2010). Due to the aforementioned DNA stability, independence of DNA to gene expression and DNA self-recognition properties, bio-recognition layers composed of DNA have attracted attention in modern microarray and biosensing technologies. In spite of the many applications that biosensors can be designed for in various platforms (Nugen and Baeumner, 2008), growing interest in fundamental research and commercial development of biosensing technologies is on affinity-based biosensors that utilise nucleic acids, in particular DNA (Teles and Fonseca, 2008; Wang et al., 2013). DNA biosensors have revolutionised genetic analysis before the

21st century, and developments of DNA biosensors has been rising since as depicted by the number of publishing in this subject over years in Figure 2.3 (Wang, 2000).

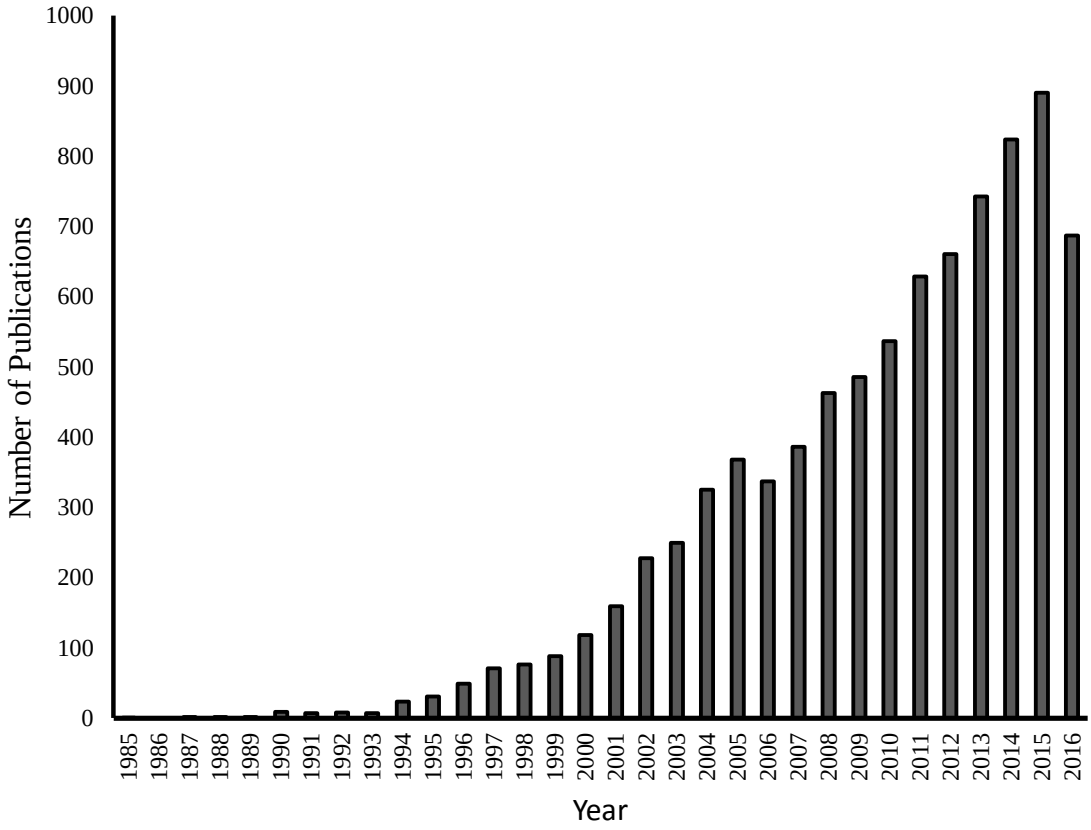

Figure 2.3 Bibliometric survey analysis, for the year 1985–2016, on data provided in Scopus SciVerse of publications related to DNA biosensors

In these types of sensors, DNA hybridisation is the biological recognition event hence the term DNA hybridisation biosensors (Figure 2.4). Immobilisation of a single-stranded DNA probe onto support materials such as silicon (Wang *et al*., 2012) gold (Lockett *et al*., 2008), and graphene (Du *et al*., 2012), enables sequence specific detection of DNA hybridisation by these sensors.

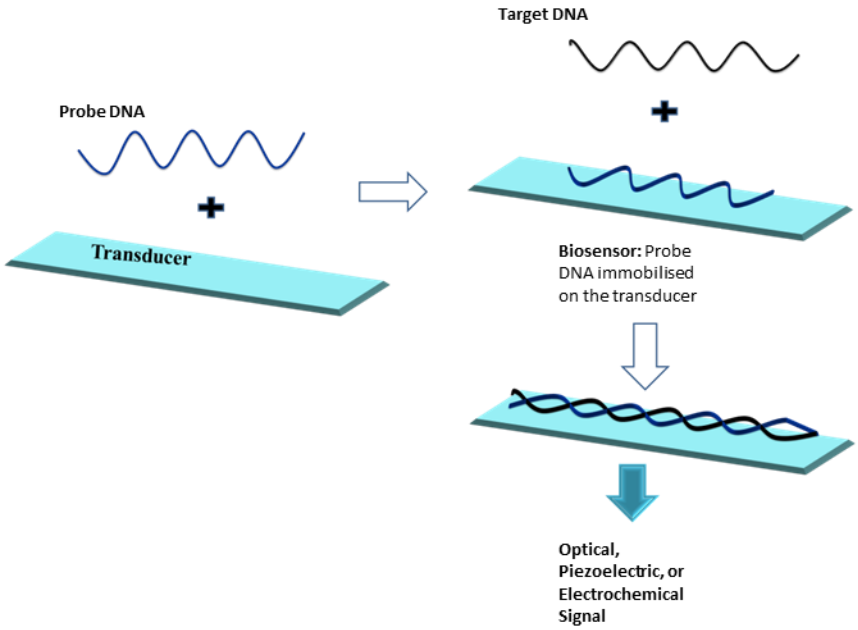

Figure 2.4 The schematic illustration of the underlying concept in DNA hybridisation biosensors (Adapted from Du *et al*., 2012)

2.2.3.1.1 Strategy in designing DNA probes

To date, there is no reported unified approach to follow when designing a probe of interest especially for application in biosensing technologies. Nevertheless, in designing an ideal probe, the only reported requirements that need consideration are that: (1) probe nucleic acids hybridises specifically and selectively to the target sequence nucleic acids; (2) probe must not self-hybridise nor should the probe hybridise to non-target sequence nucleic acids in a sample mixture of nucleic acids and; (3) the non-target cells should not have the targeted sequence of nucleic acids (Abd-Elsalam, 2003). The function of the target sequence nucleic acids or the identity of the target is not essential, provided that the choice of target sequence is of significance to the research study in question. Depending on the intended application of the device a probe can be designed to identify and bind to: nucleic acids specific to a genera,

species, or species of organisms, and conserved gene or conserved fragment of a gene in a species (Kingsbury, 1987; Wolcott, 1992).

In general, a probe is a short single-stranded (ss) strand of DNA with lengths ranging from 10 to 10000 base pairs (bp). A minimum of 20 bp of the nucleotide bases are required for statistical uniqueness (Wolcott, 1992). The recommended length of a probe for biosensor applications ranges from 15-50 bp (Gooding, 2002), while the most common probes used in electrochemical sensors is 15-40 bp (Wolcott, 1992; Wang, 1999). This recommendation is supported by the fact that short probes are effective in rapid stable hybridization with the target sequence at high rates than the longer probes (Wolcott, 1992). Furthermore, it has been shown that probes that are shorter than 15 bp lead to a reduction in sensor sensitivity, while probes with larger numbers of base pairs result in the lack of response by the sensor (Goda *et al*., 2013). It should be noted that the base composition of DNA probes does not necessarily have a significant influence on the sensitivity of the sensor but differences in base sequence could lead to variation in response signal thus providing the sensor its selectivity and specificity feature (Drummond *et al*., 2003). The sequence information of the probe can be derived using wide variety of bioinformatics tools (Abd-Elsalam, 2003) and produced using either cloning strategies or automated chemical synthesis of oligonucleotide. Automated chemical synthesis of oligonucleotide is the most convenient method of probe sequence production (Richards, 1991).

2.2.3.1.2 Principles of DNA

Since the description of the structure of DNA by Watson and Crick in 1953, unique properties of DNA have revolutionised both biological sciences and fields that find biological

concepts valuable (Wolcott, 1992; Jobbling and Gill, 2004). It is the ability of a single-stranded DNA (ssDNA) to form duplexes through hybridisation of ssDNA to another ssDNA of complementary nucleotide bases that makes application of DNA probes so prominent. To form probe-target duplexes, the same concept of hybridisation of complementary nucleotide bases (Figure 2.5) to form the Watson and Crick' DNA coiled double helix structure is applied (Trevors, 1985; Ludwig *et al*, 1995). Hybridisation is made possible due to the specific nature of DNA.

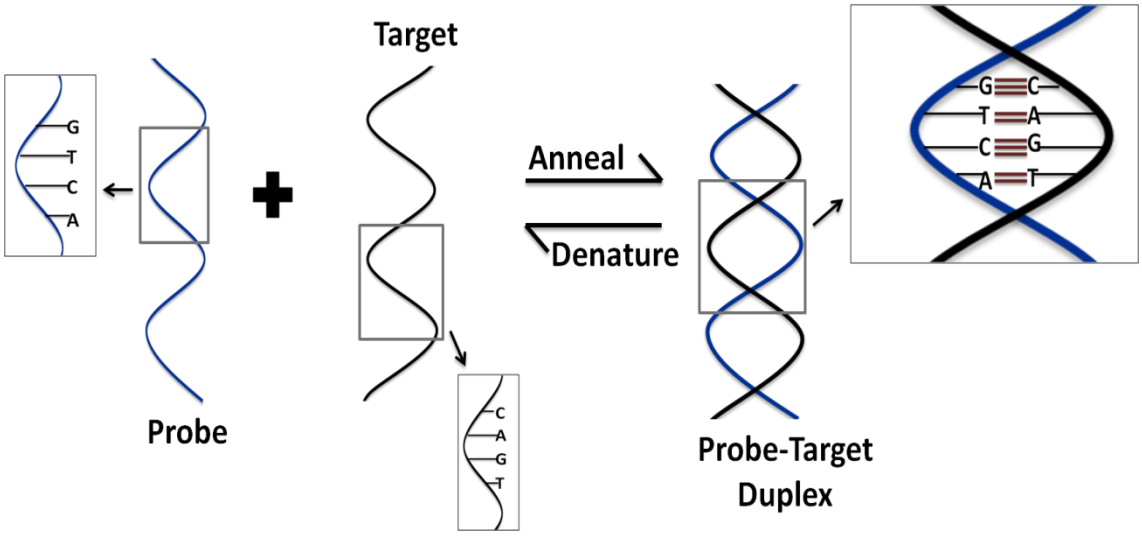

Figure 2.5 Schematic representation of hybridisation of complementary nucleotide bases in a probe-target duplex. Nucleotide bases, adenine, cytosine, thymine and guanine are represented by letters A, C, T, and G, respectively (Adapted from Wolcott, 1992)

Specificity and selectivity of the probe to the target nucleotide base sequences is determined by hydrogen bond formation between the probe and target nucleotide base sequences in which two hydrogen bonds connect adenine (A) and thymine (T) and nucleotide bases,

guanine (G) and cytosine (C) are connected by three hydrogen bonds (Wolcott, 1992). In DNA probe technology, these physical properties are manipulated in such a way that the probe or target is thermally or chemically separated if not initially single stranded (Wong *et al*, 1990; Ludwig *et al*, 1995: Sacca and Niemeyer, 2011). Under appropriate hybridisation conditions a stable probe-target duplex is formed. Hybridisation is dependent on the temperature, pH, ionic strength, and DNA concentration (Kingsbury 1987; Wong *et al*., 1990; Dooley, 1994; Wang *et al*, 1997; Ludwig *et al*, 1995). Appropriately changing aforementioned conditions can reverse annealing of the probe and target to form the probe-target duplex to denaturing of the probe-target duplex (separation of the probe form target) or vice versa (Dooley, 1994; Go *et al*., 2006; Dandy *et al*., 2007; Finche *et al*., 2007). Probes can be used in several different hybridisation formats generally classified into those that employ a solid phase whereby the probe is attached to a solid support of some sort and liquid phase hybridization reaction where neither probe or target are support bound (Richards, 1991).

2.2.3.2 DNA biocompatible support materials

The semiconductor industry based on silicon has an already well-established microelectronics technologies linked to it. The recognition of traditional semiconductors such as silicon as potential support material in modern DNA microarray and biosensing technologies simply takes advantage of these existing microelectronic technologies. Moreover, the transition of silicon into a DNA immobilisation substrate is made possible by its flexible surface chemistry, great optical and morphological properties (Wang *et al*., 2012).

Detection of DNA hybridisation has been successfully achieved using silicon. Generally in silicon-based DNA hybridisation sensors, DNA immobilisation is achieved through covalent chemisorption and/or biospecific affinity interactions of the DNA molecule onto functionalised silica substrates (Wang *et al*., 2012; Lee *et al*., 2013; Hoyle and Bowman, 2010). Covalent coupling and bioaffinity interactions tends to preserve the bioactivity of the DNA. To achieve such high affinity covalent coupling and bioaffinity interactions, modification of the DNA molecule prior to immobilisation on the substrate is required. Typically this involves the use of DNA oligonucleotides that are amine-modified oligonucleotide, Cy3- and Cy5- labelled oligonucleotide probes (Gifford *et al*., 2010; Hoyle and Bowman, 2010, Wang *et al*., 2012).

Unlike silica and silicon substrates, gold substrates are not limited to optical DNA hybridisation signal transduction monitoring and analysis systems (Lockett et al., 2008). Despites the fact that gold is chemically inert, DNA can be immobilised on bulk or nanoparticle gold surfaces through chemisorption and biospecific interactions that are compatible with other modes of signal transduction monitoring systems such as mass-based, and/or electrochemical signal (Hanh *et al*., 2005; Karamollaogˇlua *et al*., 2009; Kerman *et al*., 2004; Passamano and Pighini, 2006).

In recent years, carbon-based materials such as carbon nanotubes and graphite (Allen et al., 2010; Geim and Novoselov, 2007; Novoselov at al., 2004; Rao *et al*., 2009) are among widely explored non-traditional semiconducting materials to be transducers. (Fu and Li, 2010; Novoselov *et al*., 2004). These carbon allotropes are biocompatible and possess a wide potential window accordingly permitting label-free detection of DNA hybridisation detection that is highly selective and specific (Fu and Li, 2010; Du *et al*., 2012).

Due to the distinctly unique thermal conductivity (~ $4.8x10^3$ to $5.3x10^3$ W/mK) superlative structural strength (~ 40 N/m), and incredible electronic flexibility of graphene (Balandin *et al*., 2008; Geim, 2009; Neto *et al*., 2009; Novoselov *et al*., 2004; Geim and Novoselov, 2007) as opposed to all the other carbon allotropes; graphene and graphene related materials are currently explored and used worldwide in biosensor and electronic devices as suitable biocompatible DNA immobilisation platform. Since its first discovery in 2004, this simple sp^2 hybridized planar monocrystalline carbon structure has earned its discoverers, Novoselov and Geim, a nobel prize. Graphene has been shown to be the first of any atomic thin material to exhibit thermodynamic stability under ambient conditions whilst maintaining its continuous honeycomb network nature (Novoselov *et al*., 2004). Adding to and corroborating Novoselov *et al*,(2004) initial findings, this flexible two dimensional material has been reported to exhibit novel optical, mechanical, ballistic electron transport, thermal conductivity, and electronic properties (Allen *et al*., 2010; Balandin *et al*., 2008; Neto *et al*., 2009; Geim and Novoselov, 2007; Lee *et al*., 2008; Rao *et al*., 2009; Stampfer et al., 2008). As a result, graphene is by far the most versatile transducer as it can be used in electrical and electrochemical (Chen *et al*, 2010; Dong *et al*., 2010; Mohanty and Berry, 2008; Zhou *et al*., 2009), optical (Dong *et al*., 2010; He at al., 2010; Jang *et al*., 2010; Lu *et al*., 2009a; Xie *et al*., 2009) and other transduction schemes for DNA detection in variety of medical, environmental and industrial diagnostic applications(Feng *et al*., 2011; Heller at al., 2006; Lu et al., 2010).

The first and perhaps the most crucial step in achieving the necessary result in analytical applications involving detecting DNA hybridisation using graphene through various novel schemes, is the synthesis of high quality graphene with no residual defects (Du *et al*., 2012). To date the fastest and most reliable method used to effectively produce graphene of the highest quality is the micro-mechanical exfoliation method first invented by Novoselov *et al*.,

(2004). Although most successful graphene synthesis method, mechanically exfoliating highly oriented pyrolytic graphite (HOPG) using an adhesive tape is difficult to control and not scalable. Therefore, other methods of graphene synthesis have been developed. These methods include chemical synthesis of graphene, epitaxial growth of graphene on silicon carbide (SiC) (Berger et al., 2006; Emstev et al., 2009) and chemical vapor deposition (CVD) of hydrocarbons on metal substrates (Li et al., 2009; Reina et al., 2009; Sutter et al., 2008). These methods are yet to be made feasible for large-scale production of high quality graphene since they typically produce highly modified, low quality graphene (Zhang *et al*., 2014).

In fact, majority of graphene based sensors developed to date do not use graphene at its purest form. Graphene related materials such as graphene nanocomposites, reduced graphene oxide (RGO), graphene oxide (GO) and few-layered graphene oxide sheets are increasingly explored and subsequently reported as a sensitive and selective suitable platforms for graphene based transduction of DNA hybridisation. Although its detailed structure is not elucidated in detail in literature, GO is hydrophilic graphene layered flakes that consists of epoxy (C-O-C), carboxyl (-COOH) and hydroxyl (-OH) oxygenated functional groups randomly located on the edges and basal graphene surface (Dikin *et al*., 2007). This chemically functionalisation of graphene makes the resulting GO more biocompatible and easily modified for application in any desired application particularly biomedical/ biological related applications. Due to the polarity and ionizability of the oxygen-containing functional groups on GO, GO is hydrophilic in nature thus allowing for easy GO dispersion in water and wider range polar organic solvents (Dikin et al., 2007; Compton and Nguyen, 2010; Eda et al., 2008).

Although these devices are low cost, rapid highly sensitive and selective DNA sensors which demonstrated low detection limits, the majority of these devices use GO and not graphene.

Understandably so GO has improved biocompatibility compared to pristine graphene. Nonetheless GO presents' toxicity problems in biological/ biomedical applications. One study reported that of all graphene material, GO was the most toxic when dispersed in the lungs of mice. GO was found to be toxic unlike pristine graphene (Duch *et al*., 2011). Ahmed and Rodriques, (2013) recently corroborated this in activated sludge where GO was found to have an acute toxic effect that lead to oxidative stress and entrapment of bacterial cells. This reduced the microbial community metabolic activity, biogeochemical cycles of carbon, nitrogen, phosphorous) and ultimately deteriorating the waste water treatment process. It is worth noting that in this study the toxic effect of GO was observed at GO concentration range of 50-300 mg/L (Ahmed and Rodriques, 2013). The hydrophobic nature of pristine graphene makes it insoluble in aqueous solutions and as a result prone to large aggregation. On the other hand, GO is soluble in aqueous solutions. Recently, the stability and mobility of GO nanoparticles in soil, groundwater and surface water was studied. It was observed that GO nanoparticles were less stable and highly mobile particularly in surface waters (Lanphere, et al., 2014). Although shown to have diminutive impact in ground water, due to these toxicological effects and mobility of GO nanoparticles the use of GO raises safety concerns. Bioaccumulation of GO could disrupt the ecosystem and result in human health consequences for individuals exposed to GO. In biosensor development and commercialization, the safety of the sensing device is very important. This is particularly important in DNA hybridisation detection as it has tremendous potential opportunities to be marketed and commercialised for use in various biological/biomedical technologies.

The development of graphene-based DNA biosensors only started a few years after the 2004 discovery of graphene (Novoselov at al., 2004; Geim and Novoselov, 2007). As depicted in bibliometric data in Figure 2.6, the first publications that made reference to the use of graphene in DNA biosensors were published in 2008. Since then graphene-based DNA

biosensors have been explored every year. Detection of DNA hybridisation using graphene based sensors depends primarily on successful immobilisation of the single-stranded (ss) DNA probe as the bioreceptor onto the graphene transducer to form controllable ssDNA probe-graphene nanocomposites. The immobilisation of DNA on the support transducer material is crucial in the development of DNA-based microarray and biosensing technologies as it can impact on the quality of detection of DNA. Immobilisation of the probe should in all possible efforts maintain the inherent complementary affinity of the probe for its specific target DNA but yet be predictable and precise (Malmqvist, 1993; Lucarelli *et al*., 2008; Tang *et al*., 2011).

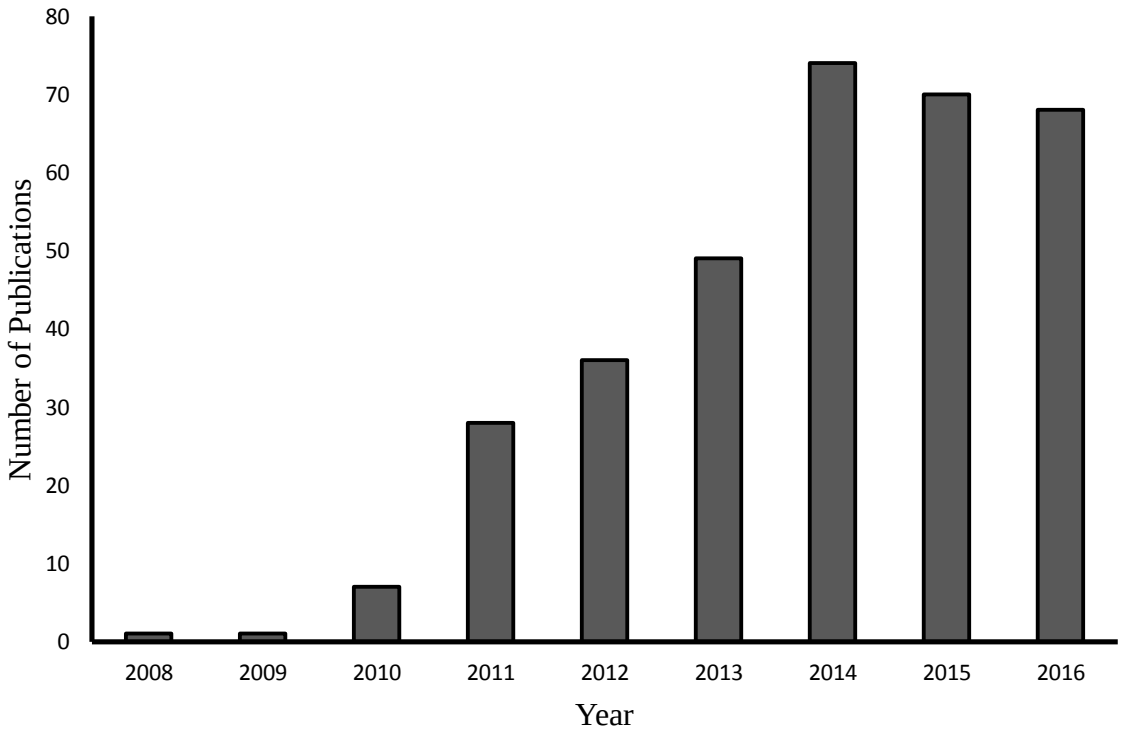

Figure 2.6 Bibliometric survey analysis, for the year 1985–2016, on data provided in Scopus SciVerse of publications related to graphene-based DNA

Other innovative approaches of DNA immobilisation on the graphene surface such as covalent linkage and affinity binding have been explored. However, adsorption namely spontaneous self-assembly is the simplest immobilisation approach of label-free ssDNA probes most successful and specific to graphene and its derivatives (Oliveira Brett and Chiorcea, 2003). See Lucarelli *et al.*, (2008) for a detailed review of immobilisation approaches most appropriate and specific for other electrodic materials. Onto the solid/crystalline surface of graphene, ssDNA probes are reversibly and non-specifically adsorbed. This adsorption is characterized by non-covalent spontaneous self-assembly (Lucarelli *et al.*, 2008; Tang *et al.*, 2011; Malmqvist, 1993). Adsorption of the ssDNA probe oligonucleotide in the buffer (in the solution it is prepared in sterile deionised water or buffer solution, namely trisaminomethane-ethylenediaminetetraacetic acid (Tris-EDTA) buffer) results in the formation of self-assembled monolayer/film of the ssDNA probe (adsorbate) on the surface of the graphene (adsorbent). As depicted in Figure 2.7, the atomic structure of the ssDNA probe is basically a phosphate-deoxyribose sugar backbone held together by 3'-5' phosphodiester bonds that consist of a phosphate groups (PO_3^{-4}) at the 5' end and the deoxyribose sugar ($C5H_{10}O_4$) at the 5' end and 3' end, respectively (Wolcott, 1992).

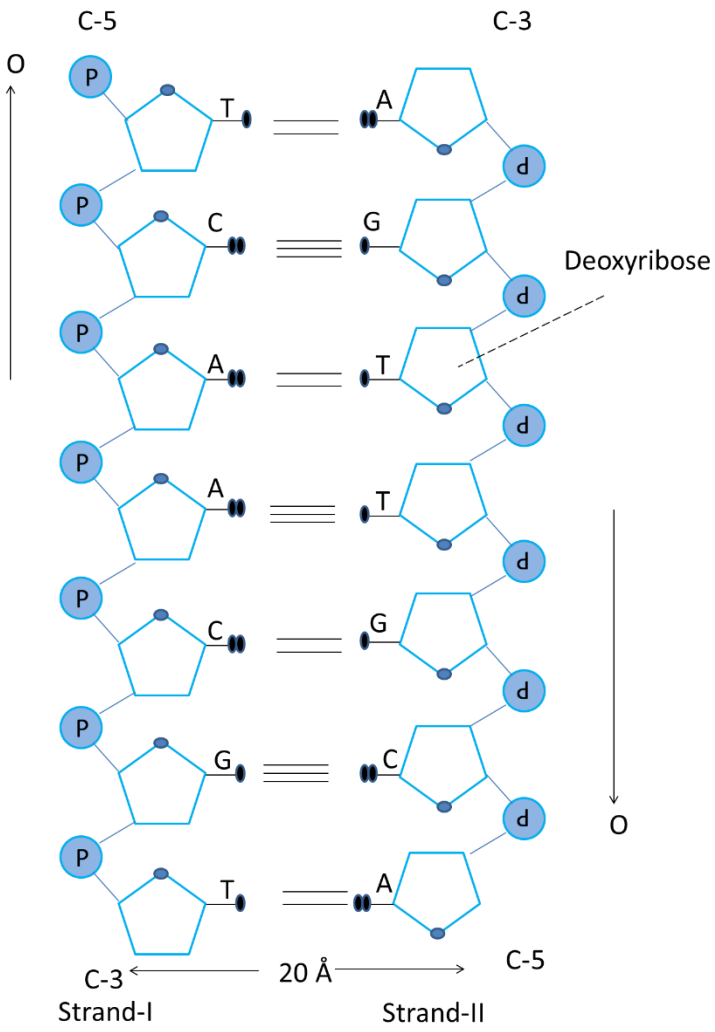

Figure 2.7 The schematic illustration of the basic structural units of DNA. A= Adenine, C= Cytosine, G= Guanine, T= Thymine, P= Phosphate group (Adapted from Wolcott, 1992)

Due to the strong affinity of the phosphate group to the graphene substrate, to form the self-assembled monolayer of helical ssDNA probes on the graphene surface, chemisorption of the phosphate groups (PO_3^{-4}) on the 5' end of each of the DNA probes with the graphene carbon atoms occurs. (Gooding, 2002; Oliveira Brett and Chiorcea, 2003; Kerman *et al*., 2004; Lee *et al*., 2008; Tang *et al*., 2010). Theoretical simulations predict the ssDNA probe molecule to possibly be geometrically perpendicular to the graphene surface when phosphate groups are then anchored onto the surface (Aliofkhazraei et al., 2016; Zhou, 2015). On the graphene

surface, the ssDNA probe molecule is not entirely enclosed and can subsequently bind to complementary DNA targets upon hybridisation. In fact upon hybridisation with its target ssDNA, the interactions between the ssDNA probe and graphene is weakened as the initial DNA adsorption onto the graphene surface is reversed. Similar to DNA adsorption, DNA desorption from the graphene is prompt and highly efficient. Following desorption, the ssDNA probe and its complementary target ssDNA hybridise and form a double-stranded (ds) DNA duplex (Gooding, 2002; Oliveira Brett and Chiorcea, 2003; Kerman *et al*., 2004; Lee *et al*., 2008; Tang *et al*., 2010; Du *et al*., 2012; Ngo *et al*., 2013).

Studies exploring the detailed mechanisms employed by ssDNA to bind to graphene are limited (Gowtham et al., 2007). As a result, aspects concerning binding mechanisms and; (2) quantification of the exact type and relative strength of DNA-graphene interactions that exist within ssDNA probe-graphene nanocomposites are not well understood (Oliveira Brett and Chiorcea, 2003; Tang et al., 2010). Nonetheless, it has been shown through DNA interactions with the graphene layer on the surface of highly ordered pyrolytic graphite, that ssDNA and graphene may be bound together by means of pi (π) base stacking, van der Waal interactions, hydrophobic interactions, electrostatic interactions, and hydrogen bonding while others have suggested that DNA interacts with graphene via weakly attractive dispersion forces induced by molecular polarisability (Oliveira Brett and Chiorcea, 2003; Gowtham *et al*., 2007; Lee *at al*., 2013).

Thermodynamic and kinetic studies of: (1) the structural DNA conformation changes that occur to the ssDNA probe and its nucleobases when immobilised on graphene; and (2) behavioural changes that ssDNA probe-graphene nanocomposites undergo to exert the necessary response signal in various novel platforms revealed that spontaneous self-assembly immobilisation of ssDNA probes involves physisorption of the individual DNA nucleobases

onto the graphene surface (Akca et al., 2011; Das et al., 2008; Gowtham et al., 2007; Varghese et al., 2009). In this case, theoretical simulations predict the ssDNA probe molecule to lay flat parallel to the graphene surface as depicted in Figure 2.8 (Aliofkhazraei et al., 2016; Zhou, 2015).

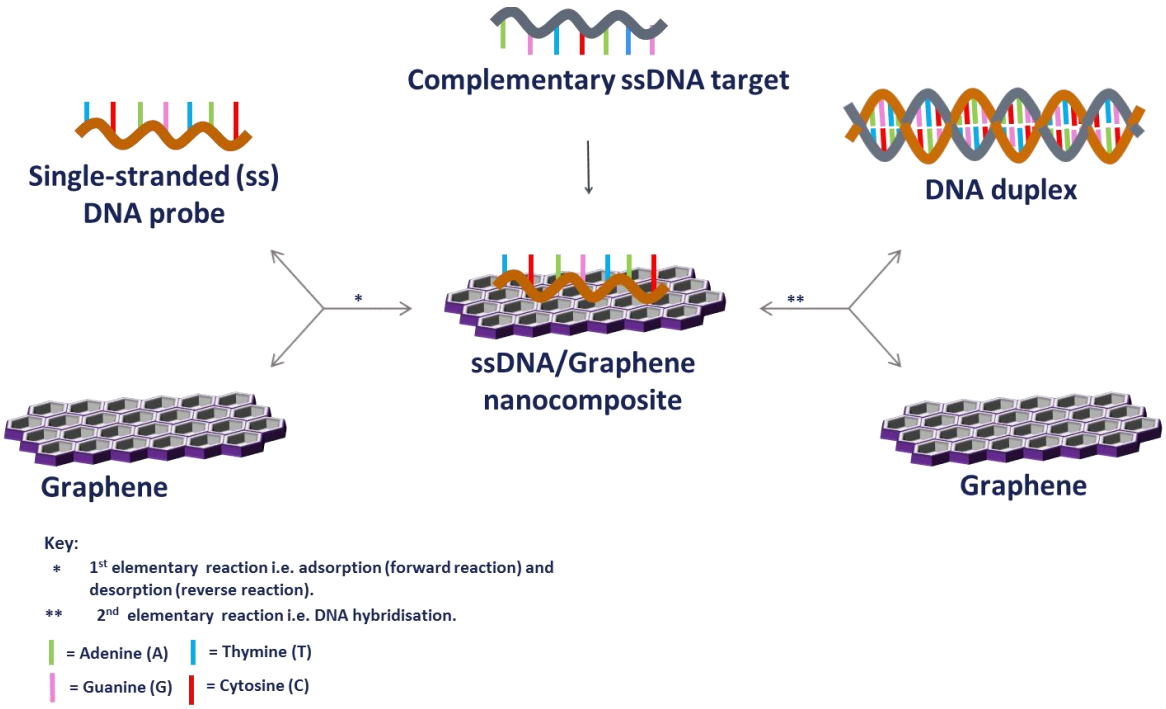

Figure 2.8 Macroscopic illustration of DNA adsorption and desorption on graphene (Adapted from Du et al., 2012)

Previous theoretical and experimental studies have been published separately approximating and calculating nucleobase interaction with graphene and its derivatives including carbon nanotubes by assuming π base stacking, van der Waal interactions, hydrophobic interactions, and hydrogen bonding (Das *et al.*, 2008; Gowtham *et al.*, 2007; Nandy *et al.*, 2012; Varghese *et al.*, 2009). However, electrostatic interactions have not been considered interactions which

determine DNA nucleobase interactions with graphene (Akca *et al*., 2011; Nandy *et al*., 2012)

Some of these theoretical models using first-principles density functional theory (DFT), plane wave pseudopotential local density approximation and ab-initio quantum chemical Hartree–Fock method coupled to the second–order Møller–Plesset perturbation theory frameworks and calculations have shown that during this physiosorption, the nucleobases guanine (G), adenine (A), thymine (T), cytosine (C), and uracil (u) [uracil in RNA] bind to graphene with similar equilibrium configurations. However, their binding energies scale in the following hierarchical order: G>A~T~C>U. (Gowtham *et al*., 2007; Mukhopadhyay et al., 2010; Varghese *et al*., 2009). However, theories based on van der Waal (vdW) interactions report the following hierarchy of nucleobase binding with graphene; (G>A~T>C). Overall vdW theoretical calculations supported by experimental studies such as isothermal titration (micro) calorimetry conclude that the overall trend of nucleobase-graphene interaction energy is: G>A>T>/<C when solvation effects are accounted for or taken into consideration (Das et al., 2008; Gowtham *et al*., 2007; Varghese *et al*., 2009). Theoretical and experimental models based on vdW interaction being the dominating interactions have efficiently explained with not only the nucleobase-graphene/carbon nanotube binding energies but also managed to account for some geometrical observations made especially in carbon nanotubes.

However, findings of a most recent study show that during immobilisation the DNA molecule adopts two distinct conformations that appear to be in total disagreement with the known interactions models predicted to be involved in DNA-graphene interactions (Acka *et al*., 2011). Using projective measurements of nucleobase-nucleobase interactions, Acka and colleagues, (2011) found that during immobilisation onto a graphene surface, within the DNA molecule the poly-A and C form spherical particles while the poly-T and G form elongated

networks. These findings, suggest the existence of competitive π stacking between DNA nucleobases-nucleobase and nucleobase-graphene. Furthermore, Acka *et al*., (2011) findings show no distinguishable involvement of hydrophobic interaction and do not support the previously predicted G>A>T>/<C hierarchy. Instead their findings lead them to suggest π stacking model that the purines, A and G bind to graphene with similar energies and pyrimidines, C and T also with similar binding energy interact with the graphene surface, (A~C, T ~G). In their structural and energetics studies via atomic molecular dynamics simulations, Mann and Pati, (2013) collaborated Acka *et al*., (2011) findings. Mann and Patti (2013), suggest π–π stacking nucleobase–nucleobase intra-molecular interactions being the ones responsible for maintaining the helical geometry of the DNA probe, while the inter-molecular π–π stacking nucleobase–graphene interactions playing a fundamental role in the adsorption of the single stranded DNA probe onto the graphene surface.

DNA and graphene interfaces used in a wide range of sensor technologies have been published. Traditionally, optical DNA-graphitic biosensors explored fluorescence resonance energy transfer (FRET) to exploit the ability of graphitic carbon to quench fluorescence properties of fluorophores when adsorbed on its surface and subsequent restoration of the fluorescence upon hybridisation with a complementary target (Kegan and Mccreery, 1994). DNA-graphene FRET biosensors have been used successfully to selectively detect both labelled (Jung *et al*., 2013; Liu *et al*., 2010) and non-labelled (He *et al*., 2010; Lu, *et al*., 2009a; Lu, *et al*., 2009b) complementary DNA strands. The use of fluorophores has been shown to enhance the devices sensitivity. However, this method of DNA detection on graphitic transducer surfaces such as graphene might affect the DNA probe's bioaffinity, increases complexity and cost of analysis (Lee, 2008; Özkumur *et al*., 2010). Therefore, despite graphene's compatibility with optical transduction modes of DNA hybridisation

detection, direct modes of detection such as label-free electronic/electrochemical transduction of DNA hybridisation are currently the most studied (Wu *et al.*, 2010).

Due the unique electron transfer properties of graphene and graphene related materials (Chen *et al.*, 2010), DNA-graphene hybrids are investigated in electrochemical/electrical sensors. In addition to label-free DNA hybridisation detection, electrical sensors offers rapid DNA hybridisation detection with single-base mismatch specificity and sensitivity as low as 0.1 pM of DNA (Bonanni and Del Valle, 2010; Dong *et al.*, 2010; Lin *et al.*, 2011; Wu *et al.*, 2010). The most common and promising type of label-free electrochemical or electrical sensors that are heavily explored are primarily, metal oxide semiconductor field effect transistor (MOSFET) and field-effect transistor (FET) devices (Green and Norton 2015). Graphene is an enticing construction materials for FET based devices. This is attributed to mainly to its ambipolar nature and biocompatibility to DNA hence using graphene in FET sensors requires no prior sensor or DNA functionalisation (Geim and Novoselov, 2007; Green and Norton, 2015).

In recent FET based devices, the output transduction observed is due to the electrical properties of label-free DNA oligonucleotide (Millan and Mikkelsen 1993; Bonanni and Del Valle, 2010). In such devices the actual label-free electrochemical or electrical detection of DNA hybridisation is achieved by monitoring the conductivity changes in graphene, where fluctuations in drain-source current-gate voltages of the graphene are measured (Torkel, 1959). From these current-gate voltage measurements, information on the carrier mobility and their corresponding carrier densities is extracted. The change in the current refers to characteristic differential responses of the DNA-graphene sensors' ability to chemically recognise and discriminate diverse and distinct molecular analytes in a sequence-dependent manner (Bo *et al.*, 2011; Dong *et al.*, 2010; Du *et al.*, 2012; Feng *et al.*, 2011; Lu *et al.*,

2010). Therefore, adsorption of ssDNA probe onto the graphene surface and desorption upon hybridising with complementary ssDNA target does not only result in the surface potential modulation but it is also the sensing scheme of FET based sensing technologies (Lin et al., 2011; Du *et al*., 2012).

Despite attempts to understand the theoretical principles involved in adsorption and desorption of DNA on graphene, little is known about the nature of DNA structure and conformation on graphene (Acka *et al*., 2011; Gowtham *et al*., 2007; Lin *et al*., 2013; Mukhopadhyay et al., 2010; Varghese *et al*., 2009). In FETs the introduction of DNA presents challenges that further complicate the sensing scheme. Buffer effects, doping, chemical/electrostatic gating, and induced dipoles could induce changes in graphene's electronic and structural properties thus affecting DNA detection and sensitivity (Kergoat *et al*., 2010; Mohanty and Berry, 2008). Furthermore, graphene has been reported to disrupt the structure of folded DNA (Husale *et al*. 2010; Liu *et al*., 2011; Wu *et al*., 2014]. Therefore, despite proof of concept demonstration of application of FET that are produced at low cost and possess impressive DNA detection limits, the exact cause of the commonly studied modulation in gate voltage observed in DNA graphene-based FET devices is unknown (Bonanni and Del Valle, 2010; Lin *et al*., 2013).

Consequently, in literature there are discrepancies in the reported observed shifts in gate voltage and perceived cause of the shifts (Chen *et al*., 2009; Dong *et al*., 2010; Lin *et al*., 2013). There are literature reports of DNA graphene-based FET devices that show large gate voltage shifts in both positive and negative potential directions. Recently, a group reported a significant positive shift in gate voltage observed upon DNA immobilisation on their FET based chemical vapour sensor. And they attributed this shift in the positive direction to a counteractive effect to overcome the induced negative field due to the negatively charged

nature of DNA's phosphate backbone (Kybert et al., 2014). Similarly, other previously published studies have demonstrated a negative potential shift of the gate voltage on DNA deposition on graphene (Chen *et al*., 2009; Wang *et al*., 2013). Dong et al. (2010). However, unlike previous studies that claimed the negative gate voltage bias to be due to electrostatic gating (Artyukhin *et al*., 2006), buffer effects (Chen *et al*., 2009) and ionic impurities masking (Chen *et al*., 2009; Wang *et al*., 2013), n-doping effect is an argument that was previously ruled out (Lerner et al., 2012). The n-doping effect caused by the π–π stacking of the electron-rich nucleobases was ruled out together with charge injection by Lerner *et al*., (2012) in a study performed on charged DNA strands of varied lengths tethered on graphitic surface in a FET sensor.

Negative voltage gate potentials have also been explained in literature to be due to mechanisms such as chemical doping by adsorbates (Lu *et al*, 2010b), n-doping (Yin et al., 2010) and p-doping (Mohanty and Berry, 2008). Lin *et al*. (2013), proposed recently that instead of using gate voltage to qualitatively monitor DNA hybridisation, using sheet resistance and carrier mobility could address the reported measurement inconsistencies. Lin and Co-workers (2013), claimed that electrical mechanisms involved in DNA graphene interactions did not occur consecutively but instead all three, that is, masking charge impurities, graphene doping and electrostatic occurred simultaneously. Inconsistencies in reported literature measurements are mainly due to the lack of in-depth understanding of interactions involved between DNA and graphene. But is also equally important to note that differences in design and composition of the device and analysed samples has a role in the current confusion (Green and Norton, 2015).

2.2.3.3 Transduction methods in DNA sensing

The most common and intensively explored mode of DNA hybridisation detection in biosensors is optical. It is highly selective and sensitive with detection limits as low as 10^7 biomolecules/cm^2 (Drummond *et al.*, 2003). Screening techniques that are based on measuring an output signal through photometric processes are employed in optical transduction. As a result, optical transduction of DNA hybridisation requires multifaceted and expensive instruments (Drummond *et al.*, 2003). The most common techniques which inherently require sophisticated instrumentation used to optically detect DNA hybridisation are fluorescence resonance energy transfer (FRET), reflectance spectroscopy, and Raman scattering and Fourier transform infrared (FTIR) spectroscopy (Velusamy *et al.*, 2010). These techniques are incompatible with the portable idealism that biosensors are required to possess (Gooding, 2002).

Therefore, other transduction methods such as mass-sensitive and electrochemical signal transduction have been explored. In mass-sensitive signal transduction, changes in physical mass or surface properties in the bio-recognition layer are monitored during the bio-recognition event (Drummond *et al.*, 2003). Mass-sensitive transductions using gold as a transducer support material have been reported to enable for a rapid label-free detection of DNA hybridisation in real-time (Karamollaog˘lua *et al.*, 2009; Passamano and Pighini, 2006). However, similar to optical transduction schemes, mass-sensitive signal transduction schemes involve the use multifaceted and expensive instruments (Drummond *et al.*, 2003). As a result they are not commonly used as depicted by the low number of publications relative to other transduction methods (Figure 2.9).

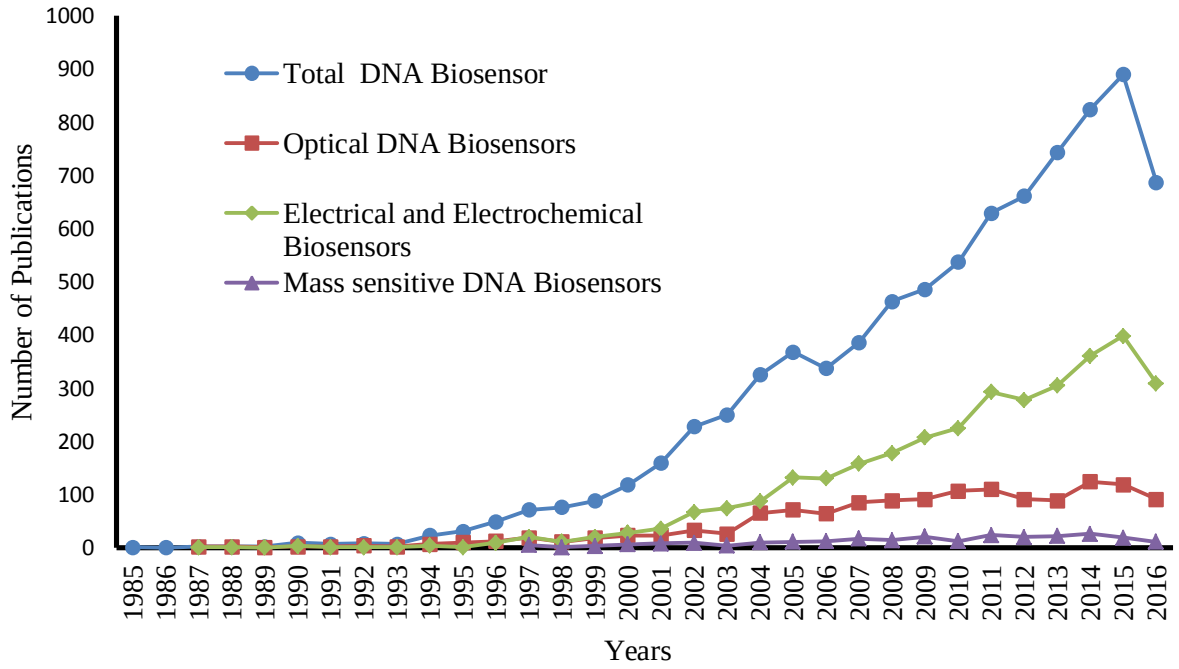

Figure 2.9 Bibliometric survey analysis, for the year 1985–2016, on data provided in Scopus of publications related to different types of transduction methods in DNA biosensors

On the other hand, biosensors that are based on electrochemical transduction of DNA hybridisation are cheap, easy to operate and maintain as they do not require the use of expensive and complex systems (Drummond *et al*., 2003; Gooding, 2002; Hanh *et al*., 2005; Hvastkovs and Buttry 2010; Kerman *et al*., 2004). In these biosensors, transduction of the bio-recognition event simply involves a direct transmission of electronic signal by the transducer. The type transducer that are typically used for direct transmission are semiconductors (Hanh *et al*., 2005; Hvastkovs and Buttry 2010; Kerman *et al*., 2004). In electrochemical transduction of DNA hybridisation can be achieved through two novel

approaches, redox active label assisted electrochemical transduction and label-free electrochemical transduction (Gooding, 2002; Hvastkovs and Buttry 2010).

The discovery of redox-active labels laid the groundwork for the development of innovative DNA hybridisation biosensors. In label-assisted electrochemical transduction, the ssDNA probes that forms the bio-recognition layer are chemically modified by covalently attaching redox active labels on their nucleotide bases (Gooding, 2002; Kerman *et al*., 2004). These labels can be incorporated during the synthesis of the oligonucleotides, or later added through enzymatic or chemical reactions. Redox active labels that are commonly used range from organometallics to nanoparticles. (Kerman *et al*., 2004; Labuda *et al*., 2010; Zhu *et al*., 2006). These redox active labels enable transduction by gauging the interactions between the DNA probes on the bio-recognition layer and their targets during DNA hybridisation (Gooding, 2002; Kerman *et al*., 2004). Transmission of electrochemical signal is distinctly conveyed by these labels both before and after hybridisation through selective changes in their oxidation-reduction potentials (Velusamy *et al*., 2010). Generally, a greater electrochemical signal intensity is reported for the redox label modified DNA probe before its interaction with a complementary target (Gooding, 2002; Kerman *et al*., 2004). The incorporation of redox active labels on the DNA probes, increases their specificity. Furthermore, by incorporating diverse labels on a number probes with diverse nucleotide base sequences, multiple analysis of targets can enabled (Kerman *et al*., 2004; Labuda *et al*., 2010; Zhu *et al*., 2006).

As result, commercialised technologies that are based on this type of redox-active transduction such as Sensor^{TM} and Genelyzer^{TM}, have been established and standardised. However, the covalent incorporation of redox labels in these technologies adds some complexity to the transduction scheme. Therefore making them not conform to the idealism that biosensors should be simple (Gooding, 2002; Kerman *et al*., 2004).

Therefore, label-free electrochemical transduction schemes are increasingly studied. Label-free electrochemical transduction is achieved through the direct and indirect use of unmodified DNA (Du *et al*., 2012). According to IUPAC standards, a probe is considered unmodified when it has no labels or when the labels are not covalently bound to the probe (Drummond *et al*., 2003; Labuda *et al*., 2010). The elimination of covalent incorporation of labels/indicators, simplifies the biosensor. In these label-free electrochemical biosensors, monitoring of DNA hybridisation is made possible through immobilisation of label-free or unmodified probes on a transducer with excellent electrochemical/electronic properties (Velusamy *et al*., 2010; Du *et al*., 2012). Therefore, label-free electrochemical transduction schemes are based on direct and/or indirect monitoring of changes in intrinsic electrochemical properties of the transducer during DNA hybridisation (Velusamy *et al*., 2010).

Electroactive noncovalent redox label are used for an indirect electrochemical detection of DNA hybridisation. Electroactive noncovalent redox labels are different from covalent redox active labels. Transmission of an electrochemical signal is achieved through the intercalation or binding of the noncovalent redox label to the double-stranded DNA duplex formed by the probe and its complementary target, accordingly specifically differentiating double stranded DNA duplexes from single stranded DNA structures (Drummond *et al*., 2003; Labuda *et al*., 2010). By measuring the noncovalent redox label's negative charge density using impedance and voltammetry, this differential electrochemical signal is monitored. Phenothiazine dye, and electrostatic ions such as the cationic $[Ru(NH_3)_6]^{3+/2+}$ and anionic $[Fe(CN)_6]^{3-/4-}$ complexes, and methylene blue are examples groove binders commonly used as noncovalent redox active labels in indirect label-free electrochemical DNA hybridisation transduction methods (Drummond *et al*., 2003; Labuda *et al*., 2010).

Akin to covalent redox label transductions schemes, the non-covalent redox label bound double-stranded probe-target DNA duplex also exhibit an electrochemical signal of greater intensity. This was proven consistent with previously reported literature in a recent study carried out by Siddiquee *et al*., (2010). In that study, an electrochemical DNA hybridisation biosensor to selectively and specifically detect a trichoderma harzianum related gene immobilised on a gold electrode was created. To observe the voltammetric transduction of DNA hybridisation, as the electroactive label, methylene blue was electrostatically bound to the probe on the gold surface and its voltammetric response upon formation of the DNA duplex was measured. The electrostatic responses of methylene blue were observed to be higher for the DNA duplex (Siddequee *et al*., 2010).

From literature it is therefore evident that detection of DNA hybridisation has been successfully achieved using gold substrates through optical, mass-based and electrochemical signal transduction monitoring and analysis systems (Lockett *at al*., 2008; Shimron *et al*., 2013). However, the transition of gold-based electrodes to direct electrochemical DNA hybridisation detection without using labels has been not successful. This is due to gold-based electrodes not possessing adequate electro-oxidation properties at positive potentials to detect electrochemical responses of unlabelled DNA. Moreover, the irreversible nature of electrochemical redox reaction in nucleobases prevents the reusability of DNA probes (Hvastkovs and Buttry, 2010; Labuda *et al*., 2010). As a result, for electrochemical DNA hybridisation biosensors that allows for reusability and improved electrochemical DNA detection limits while maintaining specificity and simplicity, non-traditional semiconducting transducer nanomaterials such as carbonaceous materials that possess controllable electronic and physical properties are explored (Fu and Li, 2010; Novoselov *et al*., 2004).

Direct label-free systems depend on intrinsic properties of DNA and its constituents. Properties exploited by these direct mechanisms are:

(1) DNA structural changes due to either the hydrophobic or polyanionic nature of nucleic acids. When tensammetric transitions occur in the DNA probe and its target DNA as they go from two single-stranded DNA strands to a double-stranded DNA duplex on the transducer, variations in conductometric, amperometric, potentiometric, and/or impedimetric responses are monitored and used as the electrochemical signal (Labuda *et al*., 2010; Velusamy *et al*., 2010; Xiang *et al*., 2007).

(2) The electrochemical activity of nucleic acids. To quantitatively and qualitatively display DNA hybridisation, electroactive nucleotide bases such as guanine and adenine are used. The ability of guanine and adenine to undergo redox reaction makes these nucleobases electrochemically active. The electrical current transportation properties of DNA are due to this electroactivity. Therefore, upon formation of the DNA duplex, the change in the electrical current of electroactive nucleotide bases can be examined and used as a quantitative measure of an electrochemical output response (Kerman *et al*., 2004; Labuda *et al*., 2010).

This type of signal monitoring and analysis is made possible by excellent electrical properties of carbonaceous materials. Among the different carbonaceous materials, the most popular biocompatible materials used in fundamental research and commercial development of DNA sensing technologies are graphene, carbon nanotubes and graphite.

2.3 Current limitations and Challenges of DNA biosensing technologies

Different transduction mechanisms and schemes have led to considerable successful development of biosensors in the academic arena with commercial potential to address multifarious applications in many fields (Mascini *et al*., 2001; Bora *et al*., 2013; Turner, 2013). In medical diagnostics, sensors are used to bio-medically detect infectious agents for both purposes of diagnostic and screening of diseases (Bora *et al*., 2013; Liao *et al*., 2006; Li *et al*., 2008; Wang *et al*., 2011). In other industries, electrochemical DNA hybridisation biosensors have been demonstrated to be useful and reusable devices for the environmentally analysis of pollutants (Domínguez-Renedo *et al*., 2010; Lucarelli *et al*., 2002; Wang *et al*., 1997) and testing for food authenticity in the food and beverage manufacturing industry (D'Souza, 2001; Nugen and Baeumner, 2008; Spadavecchia *et al*., 2005; Velusamy *et al*., 2010; Su *et al*., 2011; Bora *et al*., 2013). Potential of commercialisation of biosensors in various fields is tremendous. However, because of several technology challenges, commercialisation of biosensors has been slow (Bora *et al*., 2013; Turner, 2013).

DNA is relatively stable compared to proteins and its use in DNA hybridisation biosensors is considerably promising in providing cheap and rapid detection of specific fragments of DNA. Equally, DNA hybridisation biosensors and bioelectronics have limitations that need to be considered. One limitation is bridging the gap between experimental research and reality (Hanh *et al*., 2005). Many of the DNA hybridisation biosensors developed especially for application in food authentication are perfect for the clean-cut laboratory conditions (Nugen and Baeumner, 2008). Ideally, targets used in food authentication should preferably undergo very little if any alterations during processing of food products. However, in real-life environmental, biomedical and industrial fields, several factors that may affect the integrity

and quantity of DNA thus limit the effectiveness and reliability of DNA hybridisation biosensors (Luthy, 1999). These factors include:

Storage of sample- for example ineffectual traceability and authentication of certain food products, namely refined oils, may arise when the samples are not fresh. DNA in certain old food samples is prone to damage caused by oxidation (Costa *et al*., 2012). In other cases when poor quality storage of the DNA containing sample can lead to depurination of the DNA (Elsanhoty *et al*., 2011).

Sample preparation- Since these biosensors are generally nanoscale, sample size in the range of microlitres is at maximum necessary for adequate testing (Ahmed, 2002; Nugen and Baeumner, 2008). For instance, due to food matrix, obtaining sample sizes that allow for optimum sensitivity is often a mission. Additionally, many of the DNA hybridisation biosensors that have been developed still require a preliminary polymerase chain reaction (PCR) step to be sensitive to traces of DNA or let alone detect specific nucleotide sequences (Hanh *et al*., 2005). Due to the sensitivity of PCR to inhibitors, extensive sample clean-up is mandatory. Sample clean-up in foods matrix such as those in peanut butter may prove difficult (Nugen and Baeumner, 2008).

Reproducibility and natural integrity of the DNA after purification- For an effective application of all the DNA-based analytical methods discussed in this paper, good quality DNA of great quantity must be available. Accordingly, DNA prior to testing is extracted and purified. DNA extraction and purification methods often prove difficult with possible negative influence in DNA quality and quantity. For instance, the presence of DNA nuclease in food products like olive oil and environmental matter such as mud renders it difficult to extract high quantity DNA of high integrity (Luong et al., 2008; Costa *et al*., 2012; Xiu-Ling *et al*., 2008; Elsanhoty *et al*., 2011; Velasco-Garcia and Monttram, 2003).

Refining treatment and processing conditions- DNA-based methods can be affected by failure to detect trace concentrations of DNA in certain products. This can be caused by:

- *Conditions used in processing*- Pro-longed exposure of DNA to heat during thermal treatment and during refining degrade and fragment DNA consequently resulting in DNA of low Integrity. Moreover, pH variations (for example) and the use physical and chemical treatments during processing may randomly break DNA possibly reducing the fragment size of the target DNA sequence (Costa *et al*., 2012; Elsanhoty *et al*., 2011).
- *Condition in the final product*- food products derived from genetically modified organisms may have conditions unfavourable to the stability of DNA caused by the presence of media such as vinegar. Such extreme pHs may result in shortened DNA strands caused by hydrolytically degradation of 3, 5-phosphodiester linkages (Costa *et al*., 2012; Elsanhoty *et al*., 2011).

Reference samples- One major limitation of DNA-based analysis is their inability to completely determine unknown DNA sequences. A DNA sequence needs to be predicted or known in advance (Davison and Bertheau, 2005). Even in circumstances where target DNA sequence is known, an appropriate reference is required (Ahmed, 2002).References reduce the measure of uncertainty and form a basis for analytical method validation (Anklam, 1999; Ahmed, 2002; Wua *et al*., 2009). Due to intellectual property rights obtaining reference samples of some food products is at times impossible (Ahmed, 2002).

2.4 Future outlook

This review of literature has critically surveyed the state of the art, detailed biosensor concepts and discussed challenges and limitations in biosensor development from fundamental and commercial standpoints. Despite challenges and limitations discussed, the number of DNA biosensors patents relative to literature publications is higher (Figure 2.10). This enormous registration of patents serves as a model for future possibilities but it has overshadowed the actual commercialisation of biosensors and useful way to dealing with limitation and challenges reviewed. Patents may offer an important financial goal to drive development of biosensors, since the principal developer is not a fundamental scientific researcher, but a commercial company seeking to produce an efficacious device. However, it shifts the dynamics of the biosensors development process towards isolating DNA sensing platforms rather than having a comprehensive understanding of interactions involved in the bio-recognition event and developing innovate methods of evaluations that can produce consistent output signals regardless of the experimental set-up and conditions used.

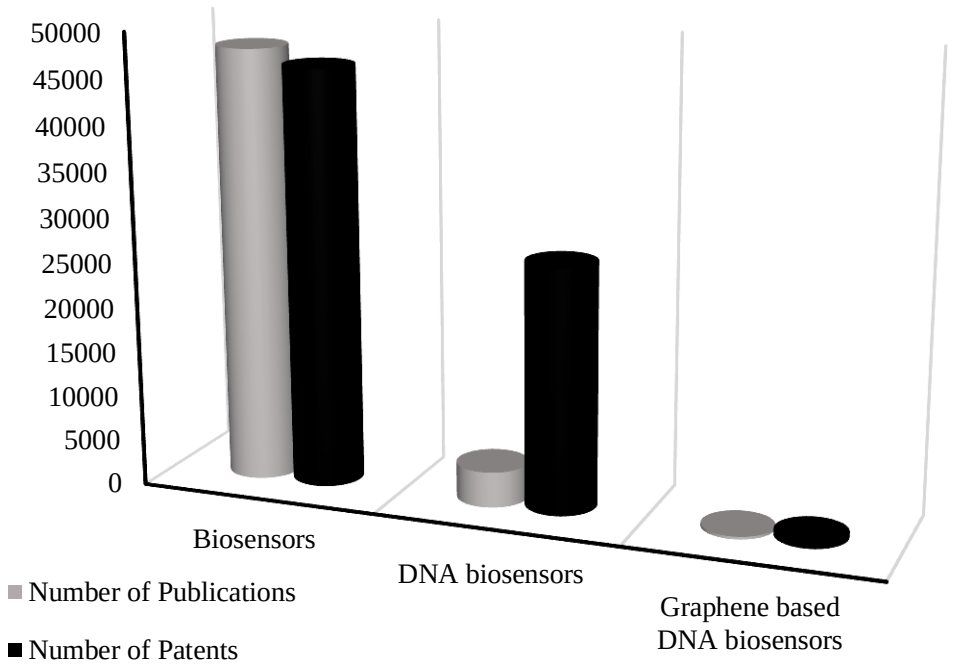

Figure 2.10 Bibliometric survey analysis over the period of 1977 to 2016, on data provided in Scopus of publications and patents related to DNA biosensors

In the development of DNA biosensor technologies, progress has been made, but only a few have reached the biosensor market (Bora *et al.*, 2013). Reported biosensors are developed and their operation demonstrated in clean-cut laboratory set ups using short oligonucleotides as model targets (Nugen and Baeumner, 2008; Zhang and Hu, 2014). This illustrates implications that a patent driven biosensor development process can have on scientific research. Studies and approaches that simulate and address problems that may arise in real sample conditions remain to be developed. To reach a level of commercialisation that will propel biosensor technologies towards the market, biosensors will require the use of a comprehensive highly accurate analytical parameter such as relative response factor than be used in conjunction with bio-sensing procedures to correct for impurities that can affect the output detection signal of the sensor. This could offer a unique opportunity to a precise

measurement of sensitivity and selectivity of the sensor for a given real sample relative to a standard laboratory clean-cut sample. Such an approach can be applied to existing biosensor technologies without compromising the novelty, accuracy and reliability.

Chapter 3 Experimental

In this chapter, experimental details and materials that are common to all the subsequent chapters are described.

3.1 Target region

In this study, a fragment of *CDC19* gene conserved in *Saccharomyces cerevisiae* is targeted for biosensor hybridisation. The *CDC19* gene encodes for pyruvate kinase that plays a role in glycolysis (Benjaphokee *et al*., 2012). The *in silico* 26-bp probe selection and design process was applied to a 235-bp fragment of the *CDC19* gene on chromosome 1 (from position 71914 to 72040 of the gene coding sequence). This 235-bp fragment of the *CDC19* gene from *Saccharomyces cerevisiae* strain S288C is conserved throughout all known CDC19 genes from all known *Saccharomyces cerevisiae* strains in the Saccharomyces Genome Database (SGD) (Appendix A). Given that the specific *Saccharomyces cerevisiae* strain used in this study is not known, the Conserved region of the *CDC19* gene was not only preferred in the probe selection but was used to design the probe in order to ensure specificity in hybridisation regardless of the strain *of S.cerevisiae* used.

3.2 Sequence Selection

In order to design a probe that specifically targets a fragment of the conserved region of a *CDC19* gene specific to *S.cerevisiae* species, first the nucleotide base sequence of the *CDC19* gene from one *S.cerevisiae* strain namely, *S.cerevisiae* S288C was derived. The source sequence of the *CDC19* gene used for probe design was derived from the Saccharomyces Genome Database (SGD) (http://www.yeastgenome.org). In order to select for a *CDC19*

gene-specific probe that is unique to all the strains of S.cerevisiae, the *CDC19* gene from *S.cerevisiae* strain S288C were aligned against all other *CDC19* gene sequences from known *s.cerevisiae* strains compiled by the SGD. This multiple alignment was performed with an EMBL-EBI bioinformatics algorithm, Kalign- Multiple Sequence Alignment, using the default parameters. The input sequences of the CDC19 gene from all S.cerevisiae strains were also derived from SGD. From the multiple alignment results, a short region conserved throughout all yeast strains was then used to design a perfect match 15mer- 40mer oligonucleotide ssDNA probe. A number of possible perfect match 15mer-40mer oligonucleotide *CDC19* gene-specific probes were designed using PrimerQuest, an online Integrated DNA technology (IDT) SciTool (http://eu.idtdna.com/Scitool.application/PrimerQuest). PrimerQuest basic default parameters were used.

PrimerQuest provided a series of possible probes. Using UNAFold the secondary structure was confirmed and the hybridisation of these short oligonucleotides was predicted (SantaLucia, 1988; Zuker, 2003). Although the short oligo sequences were predicted to have more than one possible confirmation, the sequence which yielded the least probe penalty number and had low energy structures was chosen. In the probe generated by PrimerQuest, random mismatches was introduced to generate a control DNA that will determine the specificity of the probe. Random introduction of mismatches was done by assigning non-complementary nucleotide base compositions for; Adenine (A), Cytosine (C), Thymine (T), and Guanine (G). Penultimate mismatches were chosen instead of terminal mismatches as they provide high discriminatory power as demonstrated though reported nearest-neighbour model (SantaLucia and Hicks, 2004; Batcheor-McAuley *et al.*, 2009). From the conserved 235-bp fragment, the selected a 26-base ssDNA probe, its target complementary DNA (i.e. target 26 base fragment of the conserved region of the *CDC19* gene sequence), triple-base

mismatch DNA and a non-complementary DNA strands are shown in Table 3.1. Unless otherwise stated, these are the oligonucleotide used in this work.

Table 3.1 List of the base sequences of the target DNA, ssDNA/probe, and mismatch DNA strand

	Sequence
Complementary Target DNA	5'-TGGTGTCCAAAGCAATGGCCAATGGT-3'
Probe (ssDNA)	5'-ACCATTGGCCATTGCTTTGGACACCA-3'
Mismatched DNA strand	5'-TGGGGTCCAAAGTAATGGCCACTGGT-3'

3.3 DNA strands preparation

All designed oligonucleotides i.e. target DNA, ssDNA/probe, and mismatch DNA strands were used without modifications and commissioned from Inqaba Biotechnical Industries (Pty) Ltd (South Africa). Before use, the concentration of as-per received oligonucleotide were adjusted to 100pmol/µL ($1x10^{-6}$ M) according to manufacturer's specifications. Sterilized NaCl-Tris EDTA (TE) buffer (1 M NaCl, 10 mM Tris-HCl, 1 mM EDTA, pH 8.0) was used to make the stock solutions.

3.4 Graphene samples

The monolayer graphene samples used in this study were purchased from Graphene Laboratories Inc. (New York, United States of America). The as-purchased samples were synthesised by Graphene Laboratories Inc. (New York, United States of America) using the CVD method on a copper foil (Li *et al.*, 2009a) and received as-deposited on p-type degenerately doped on a silicon wafer (Si) with a 285 nm silicon dioxide (SiO_2) layer (Li *et al.*, 2009b; Liang *et al.*, 2011).

3.4 DNA self-immobilisation and hybridisation on graphene

A 1 µL solution of 1 µ M ssDNA probe (Tris-EDTA buffer, 10mM tris, 1 mM EDTA, pH 8.0) dropped cast onto the CVD-grown graphene and allowed to self-immobilise at ambient temperature thus forming a graphene-based DNA detecting platform. DNA hybridization reaction was conducted by dropping 1 µL solution of 1 µM concentration of target DNA solution (Tris-EDTA buffer, 10mM tris, 1 mM EDTA, pH 8.0) on the ssDNA coated graphene's recognition surface and kept the reaction to air-dry at ambient temperature. For hybridisation with triple-base mismatch sequences, the same procedure as mentioned above was applied. After each hybridisation reaction, the samples were washed with Tris-EDTA buffer (10 mM tris, 1 mM EDTA, pH 8.0), followed by nuclease free water and then the graphene was reused. Each of these reactions were performed three or more times for statistical significance and accuracy in measurements. To analyse the products formed after hybridisation, hybridisation reaction were performed as aforementioned, but then removed by washing with 4 mL Tris-EDTA buffer (10 mM tris, 1mM EDTA, pH 8.0) from the graphene surface and analysed separately from graphene. Solution-phase hybridisation of equimolar (1 µM) concentration of µL ssDNA probe and µL complementary ssDNA target was performed in a solution of (Tris-EDTA buffer, 10 mM tris, 1 mM EDTA, pH 8.0) at room temperature.

Chapter 4 Raman fingerprint of DNA hybridisation on graphene

Herein, the effect of DNA self-immobilisation and subsequent DNA hybridisation on the electronic structure of CVD-grown graphene using Raman spectroscopy is reported. The analysis of Raman peak frequency shifts, intensities and widths characteristic to graphene was carried out after self-immobilisation of ssDNA and hybridisation with complementary and mismatched ssDNA strands on CVD-grown graphene. The results were critically compared with literature on Raman investigation of graphene when interacting with different adsorbates to reach logical conclusions regarding the effect of DNA adsorption and DNA desorption on graphene's characteristic structural and electronic properties.

4.1 Introduction

Since its discovery by Geim, et al. (2007), graphene has been a subject of extensive investigation (Geim *et al*., 2007; Neto *et al*., 2009). This is due to its unique properties such as exceptional optical absorption (Nair *et al*., 2008), high electron mobility at room temperature (Mayorov *et al*., 2011), and high thermal conductivity (Balandin, 2011; Chen *et al*., 2012). Given these mechanical, optical and electronic properties (Novoselov *et al*., 2005; Geim, 2009), a densely packed single-atom-thick layer of densely sp^2-bonded carbon atoms has, therefore, become a promising material of choice for next generation sensors (Novoselov *et al*., 2012; Sarkar *et al*., 2014), nano-devices (Yang *et al*., 2011), flexible, ultrathin membranes (Eda *et al*., 2008; Yu *et al*., 2010), nanocomposites (Li *et al*., 2009; Williams *et al*., 2008) and various conductive and transparent electrodes (Wang *et al*., 2008; Bae *et al*., 2010). The use of graphene in both fundamental and application-based investigations is further merited by the ability to fabricate easily transferable large surface area graphene at low cost using chemical vapor deposition (CVD) method (Reina *et al*., 2008; Li *et al*., 2009; Novoselov *et al*., 2012).

There are several methods through which the properties and quality of graphene are characterised for various fundamental and practical applications (Ferrari, 2007). Optical microscopy has been used mainly for identification of the graphene-containing region on the oxidised silicon substrates (Novoselov *at al*., 2004; Novoselov *et al*., 2005). Atomic force microscopy (AFM) and transmission electron microscopy (TEM) are used to check graphene thickness, and definitively identify fold or wrinkles graphene samples (Novoselov *at al*., 2004; Novoselov *et al*., 2005; Ferrari *et al*., 2006). However, Raman spectroscopy remains as a widespread 'go-to' tool used to characterise graphitic/carbon materials (Ferrari and Robertson, 2004; Ferrari, 2007). Raman spectroscopy uses a monochromatic laser to identify the vibrational modes that correspond to unique chemical, electronic, and structural properties of the analysed sample matter. The position, width and intensity of these Raman vibration modes make it possible to identify unknown materials, differentiate materials and quantify material composition (Gardiner, 1989). Raman spectroscopy is a fast, reliable, sensitive, non-contact, high resolution and non-destructive method that requires no sample preparation to measure the degree of changes in the electronic structure of graphene (Ferrari, 2007; Saito et al., 2008).

Raman has become an integral part of graphene-related research and provides a wide range of information regarding the electronic and structural properties of graphene in various conditions (Ferrari, 2007). In such studies the position, width and intensity of major Raman vibrations modes for graphene investigated are the defect activated D peak (~1360 cm^{-1}) due to sp^2 carbon atoms Breathing modes; vibrational modes of E_{2g} phonon at the Brillouin zone centre, G peak observed at ~1560 cm^{-1}; and the phonons at K+Δk points in the Brillouin zone involving 2D (~2700 cm^{-1}) (Ferrari *et al*., 2006). Raman fingerprints of graphene due to the effects of disorder (Saito *et al*., 2011), number of layers of graphene (Yang *et al*., 2011; Ferrari *et al*., 2006; Ferrari and Basko, 2013), thermal conductivity

(Calizo *et al*, 2007), covalent functionalisation (Niyogi *et al*., 2010; Dat *et al*., 2008), substrate thickness (Yoon *et al*., 2009; Wang *et al*., 2012), lattice strain (Mohiuddin *et al*., 2009), hydrogen intercalation (Melios *et al*., 2009), doping (Casiraghi, 2009; Das et al., 2008; Ferrari, 2007) among others, have been reported in literature. For instance, G peak position, shape of the 2D peak and I_{2D}/I_G ratio are used to fingerprint the number of layers of graphene (Ferrari *et al*., 2006; Gupta *et al*., 2006; Ni *et al*., 2008). D peak intensity is used to characterise the amount of disorder present on graphene (Saito *et al*., 2001; Saito *et al*., 2011). The position of G and 2D peaks have been used to characterise thermal conductivity (Calizo *et al*., 2007a; Calizo *et al*., 2007b; Balandin *et al*., 2008; Jauregui *et al*., 2010). Table 4.1 shows variations of graphene Raman fingerprints with each of the aforementioned effects.

Table 4.1 Variation of Raman characteristics of graphene due to different effects

Effect	Parameters	References
No Effect (Pristine Graphene) Prominent G and 2D peak, 2D peak twice the size of G peak	D peak (1360 cm^{-1})* -Not always present - Activated by defects in the sp^2 carbon lattice	Ferrari *et al*., 2006
	G peak (~1560 cm^{-1})*	
	2D peak (~2700 cm^{-1})* -Always present -Doesn't require defects for activation	
Disorder Size of D peak directly proportional to the amount of disorder present	D peak (1350 cm^{-1}) -Intensity increases - Related to disorder induced by a phonon	Saito *et al*., 2001 Saito *et al*., 2011
	D´ (1620 cm^{-1}) -Intensity increases	
	D+G (2940 cm^{-1}) -Intensity increases	
Number of Graphene	G peak - smaller red shifts	

Layers Position, size and shape of 2D peak are the main features used for characterisation of number of layers	2D peak -Upshifts (higher frequency shift) -Wider FWHM increases - intensity decreases (intensity is independent of the number of layers)	Ferrari *et al*., 2006 Gupta *et al*., 2006 Ni *et al*., 2008
Thermal conductivity (Increase in temperature)	G peak -Red shift	Calizo *et al*., 2007a Calizo *et al*., 2007b Balandin *et al*., 2008 Jauregui *et al*., 2010
	2D peak -Red shifted	
Charged Impurities (no contacts, charge due to substrate, adsorbates, water) Shifts in Raman parameters	G peak -Shape sometimes asymmetric -Significant upshift -FWHM decreases (never smaller than 6 cm^{-1})	Casiraghi *et al*., 2007
	2D peak -Small upshift -2D stiffening with increasing G peak position	
	D peak -Dependent on disorder present	
Electrical/Chemical Gating (top and back gating) Changes in G peak position and FWHM	Electron and hole doping, G peak: - Upshifts - Sharpens and FWHM decreases	Lazzeri and Mauri 2006 Pisana *et al*., 2007
	For hole doping 2D peak: - Position increases For electron doping 2D peak: - Position softens	Yan *et al*., 2007 Das *et al*., 2007

*Position of these peaks is dependent on the energy/wavelength of the used excitation laser. Positions cited are from a 514nm excitation laser.

There has been much interest in the biocompatibility of graphene to DNA. Physisorption and chemisorption of DNA molecules on graphene are employed to fabricate complex integrated devices such as graphene-based field effect transistors (FET) for biosensing purposes (Mohanty and Berry, 2008; Zhang *et al*, 2010)**.** The DNA molecules on graphene serve as a bio-recognition layer, which is an indispensable element of all DNA sensing devices. Therefore, an important issue for study in graphene-based DNA devices and sensors is the interaction of DNA adsorbates with electrons in graphene (Zhang and Hu, 2014). An interesting phenomena originating from DNA and its importance in; understanding the DNA-graphene interface, rational design and optimisation of DNA-graphene-based diagnostics devices have led to extensive theoretical studies of the interaction between graphene and DNA (or nucleobases) (Gowtham *et al*., 2007). Density functional theory (DFT), Hartree-Fock (HF) and a second order Møller-Plesset perturbation theory (MP) have been used to extensively investigate the interaction of the individual DNA nucleobases with graphene and their binding energy (Varghese *et al*., 2009; Rad *et al*., 2016; Gholami *et al*., 2016).

These theoretical studies found that nucleobases are physisorbed onto graphene surfaces; and presented a significant step in understanding the binding energy order in which the individual DNA nucleobases are bound onto the graphene surface (Akca et al., 2011; Das et al., 2008; Gowtham et al., 2007; Nandy et al., 2012; Varghese et al., 2009). Binding energies of both single-stranded (ss) and double-stranded (ds) DNA were also studied by Alshehri *et al*. (2013) using classical applied mathematical modelling and found that ssDNA molecules had a greater affinity to graphene than dsDNA molecules. This was further corroborated through experimental exploration of DNA and graphene interactions using graphene-based fluorescence resonance energy transfer (FRET) biosensors. FRET-based DNA biosensors support physisorption to be made possible by strong π-π stacking

interactions between the hexagonal carbon cell structure of graphene and the aromatic parts of nucleobases in DNA (Lu *et al*., 2009; Jang *et al*., 2010; Park *et al*., 2014; Wu *et al*., 2011; Lu *et al*., 2009). FRET-based platforms demonstrate ssDNA adsorption through fluorescence quenching mechanisms and indicate desorption in the presence of a complementary DNA strand on graphene and graphene-based materials by fluorescence induction/restoration (Lu *et al*., 2009; Wu *et al*., 2011; Park *et al*., 2014; Liu *et al*., 2016; Wang *et al*., 2016).

However, label-free graphene-based electrochemical biosensors and optical surface plasmon resonance biosensors have shown or proven sequence-specific detection of DNA and attributed the output signal to DNA hybridisation (Benvidi *et al*., 2015; Shushama *et al*., 2017). Despite continuously creating different DNA hybridisation platforms and demonstrating successful detection of DNA hybridisation, charge transfer during chemical and electronic interaction between graphene and DNA interfaces is lacking. DFT studies have already demonstrated that adsorption of DNA nucleobases on graphene and graphene-related surfaces changed the graphene's electronic properties due to charge transfer between nucleobase and graphene substrates (Vovusha *et al*., 2013; Vovusha *et al*., 2015; Gholami et al., 2016; Rad *et al*., 2016).

This electron transfer between DNA and graphene is what causes the sensing behaviour, particularly in label-free electrical/electrochemical DNA hybridisation sensors. The formation of DNA/graphene nanocomposites is assumed to cause local changes in structural and electronic properties of both graphene and DNA during their amalgamation (Tjong *et al*., 2014). Charge delocalisation properties of graphene have been applied in scanning tunnelling spectroscopy (STS) and gated nano-pore experiments for fast, inexpensive and direct DNA sequencing (Branton *et al*., 2008; Ahmed et al., 2012).

However, how DNA physisorption and chemisorption affect the electronic and structural properties of graphene is in its infancy and poorly understood (Mohanty and Berry, 2008; Zhang *et al*, 2010; Premkumar and Geckeler, 2012; Zhang and Hu, 2014).

It has been suggested that organic molecules may modify the electronic structure of graphene, resulting in changes in electrical properties of graphene (Dong *et al*., 2009). In literature, only two studies were found that reported Raman frequency shifts in G and 2D peaks of graphene peaks that result due to interactions with DNA.

- Lin et al. (2010) reported on the role of charge transfer and carrier transport modulation of graphene by 24 base single-stranded hetero-oligonucleotides (polyATCG) fragments. Upon immobilisation of the DNA strands on graphene, these authors reported a $2cm^{-1}$ shift to higher frequencies in the G peak and a shift of about 1 cm^{-1} to lower frequencies in the 2D peak.
- Reuven et al. (2013) where the authors monitored the degree of interaction of graphene nanoribbons with 20 base single stranded homo-oligonucleotides (polyA, polyC, polyG, and polyT), hetero-oligonucleotide (polyAT and polyGC), double-stranded plasmid (circular) and Herring sperm (linear) DNA. These authors reported a 14 cm^{-1} shift of the G peak to lower frequencies and no significant shift in the 2D peak upon immobilisation of the DNA strands.

As far as could be ascertained, this study is the first to report on the electronic structure of graphene as it uniquely evolves (during hetero-DNA hybridisation) and is altered as a result of DNA interaction with graphene**.** It is important from both fundamental and practical applications standpoint that the influence of DNA on structural and electronic properties of graphene is understood. In this study, Raman fingerprints are reported on graphene as a function of graphene, DNA interaction and DNA hybridisation. Raman characterisation of

interactions between DNA and Raman could potentially offer a non-destructive reliable method for spatial and temporal monitoring of DNA hybridisation on graphene locally, and the possibility to selectively and specifically detect base sequence-specific hybridisation. In this study, the electronic sensitivity of monolayer graphene and high-resolution Raman spatial measurements were used to identify and define novel graphene parameters that evolve during DNA self-immobilisation and hybridisation on graphene.

The effect of DNA self-immobilisation and subsequent DNA hybridisation on CVD-grown graphene was investigated using Raman spectroscopy. The ssDNA self-immobilised on CVD-grown graphene were hybridised with DNA strands of different base sequences (complementary and triple-base mismatch strands). Self-immobilisation of ssDNA and its hybridisation with complementary and mismatched ssDNA strands are shown to affect the structure as well as the electronic properties of the CVD-grown graphene as evidenced by the measured Raman spectra. Moreover, it is shown that Raman spectroscopy can be sufficiently used to fingerprint differences between graphene and samples of graphene coated with DNA adsorbates and DNA clusters of specific base sequences.

4.2 Materials and Methods

Raman spectroscopy was used to identify the CVD-graphene monolayers as well as the Raman peak position shifts upon immobilisation of the ssDNA probe and after hybridisation of ssDNA probe on top of the CVD graphene with complementary and triple-base mismatch strands. The unpolarised Raman spectra we measured with a Renishaw spectrometer at 514 nm. To collect the backscattered light from the samples, a working distance objective of x100 was used. A low excitation power of 1.2 mW for the 514 nm line of argon laser was used as a

precaution to avoid any local heating effects in the samples. For wavenumber calibration, the silicon peak at around 977 cm^{-1} (longitudinal optical (LO) mode) was used as a reference.

4.3 Results and Discussion

In an effort to elucidate the effect of DNA self-immobilisation and subsequent DNA hybridisation on electronic properties of CVD-grown graphene, a Raman study of the vibrational modes during the interaction of DNA and graphene was performed. Shown in Figure 4.1 is the Raman spectra of the pristine CVD-grown graphene and ssDNA probe-coated sample. 2D, G and D peaks are observed at around 2683 cm^{-1}, 1587 cm^{-1} and 1347 cm^{-1}, respectively, in pristine CVD-grown graphene. The intensity of the G peak is about half that of the 2D peak. The I_{2D}/I_G ratio is 2.02 for this monolayer graphene before self-immobilisation of ssDNA probe.

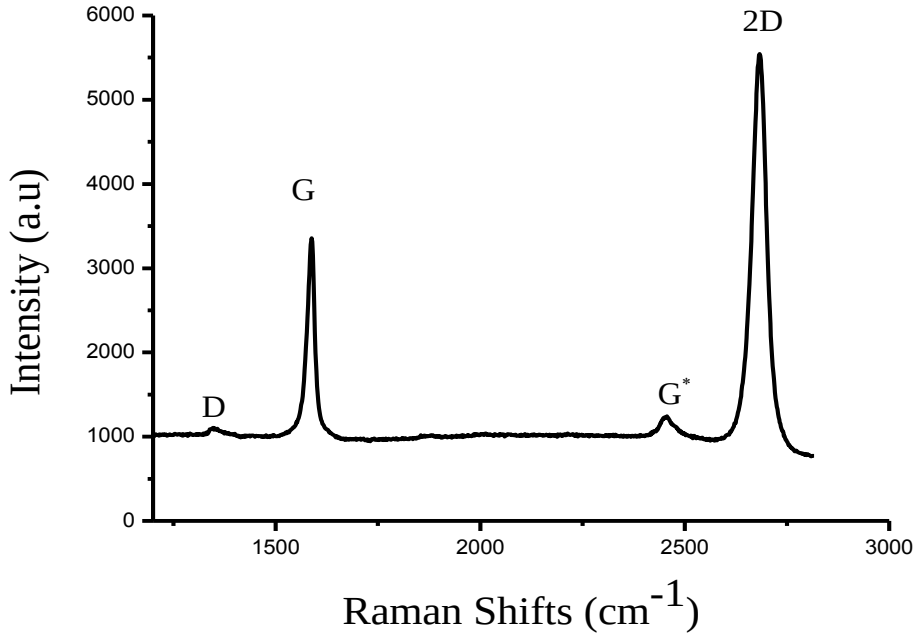

Figure 4.1 Raman spectrum of CVD-grown pristine graphene

The 2D, G and D peaks, are the typical Raman peaks characteristic of monolayer graphene. In monolayer graphene spectrum, for an excitation laser wavelength 514 nm, the D peak is observed at around 1350 cm^{-1}, G peak is observed between 1585 to 1587 cm^{-1} and 2D peak at around 2683 cm^{-1}. The D peak, defect or disorder peak, which is characteristically absent or weak in high-quality graphene, is due to out of plane A_{1g} breathing vibrations mode from sp^3 bonded carbon atoms in graphene samples. The G peak observed is associated with in-plane E_{2g} vibration mode due to sp^2 hybridised carbon atoms in the graphene sheet. The 2D peak, an overtone of the D peak, present regardless of the presence of defects (Ferrari *et al*., 2006; Ferrari, 2007; Das *et al*., 2008; Casiraghi, 2009; Niyogi *et al*., 2010; Wang *et al*., 2012; Paulus *et al*., 2013). The small D peak observed in the spectrum of CVD-grown pristine monolayer graphene indicates the high quality of the graphene sample used in this study. The defect-free graphene sample is further confirmed by the ratio I_{2D}/I_G of 2.02 (Das *et al*., 2008; Casiraghi, 2009). It is noted in this study that a clear G^* peak (which is a D and D' combination peak) is observed in pristine graphene at around 2450 cm^{-1}.

After self-immobilisation of ssDNA probe on the CVD-grown graphene, a drastic change in the intensities of the 2D, G, and D peaks was observed as revealed in Figure 4.2. While the 2D peak remains in the same position (2683 cm^{-1}) and the prominent feature of the Raman spectrum (besides the silicon peak at around 977 cm^{-1}), its intensity reduced drastically. The D peak disappeared and this observation is accompanied by the disappearance of the D + D" peak. The ratio of I_{2D}/I_G becomes 2.69 as compared to I_{2D}/I_G ratio of 2.02 in pristine graphene before self-immobilisation ssDNA probe. In ssDNA probe-coated graphene, the intensity of the G peak reduced drastically and was observed at 1585 cm^{-1}, which is 2 cm^{-1} red shift from the CVD grown pristine graphene.

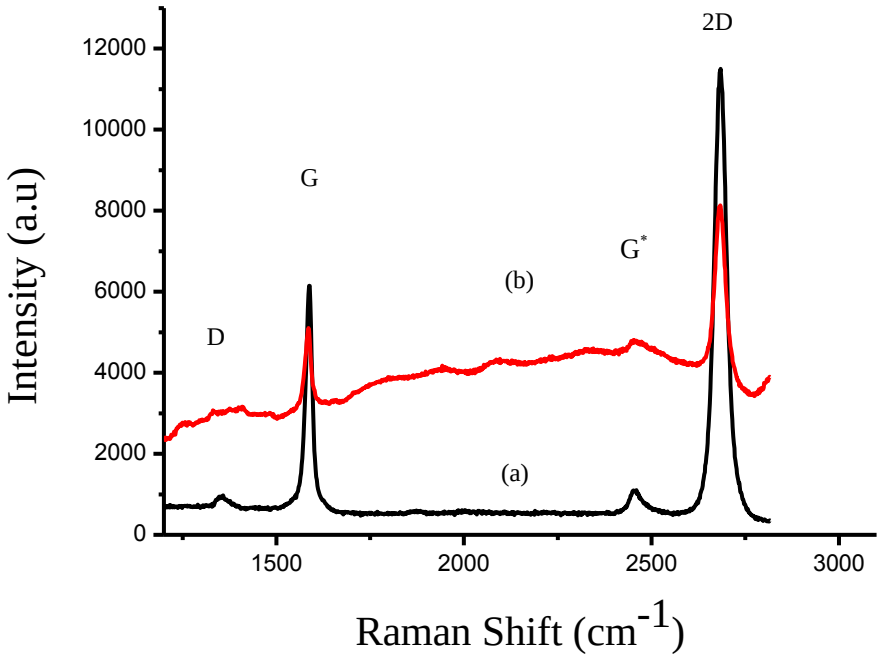

Figure 4.2 Raman spectrum of (a) CVD-grown graphene, and (b) graphene upon self-immobilisation of a 26 bp ssDNA probe

A change in the intensity of the 2D, G, and D peaks after self-immobilisation of the ssDNA on the graphene was expected as graphene can be perturbed by adduct transfer interaction (Reuven et al., 2013). The position and intensity of these peaks are reported in literature to be highly sensitive to factors such as temperature (Calizo *et al*., 2007a; Calizo *et al*., 2007b; Balandin *et al*., 2008; Jauregui *et al*., 2010), doping (Casiraghi, 2009; Das *et al*., 2008; Ferrari, 2007), substrate thickness (Yoon *et al*., 2009; Wang *et al*., 2012), number of graphene layers (Ferrari *et al*., 2006; Gupta *et al*., 2006; Ni *et al*., 2008) and strain present in the sample (Mohiuddin *et al*., 2009). The monolayer graphene had defects (Figure 4.1) but disappeared when coated with ssDNA. A lack of the defect activated Raman D peak on graphene has been reported on defect-free graphene (Ferrari *et al*., 2006; Ryu *et al*., 2008;

Elias *et al*., 2009; Niyogi *et al*., 2010). This disappearance of the D peak graphene upon self-immobilisation reveal the existence of an interaction between ssDNA and graphene. It further suggests that the hydrocarbons of the ssDNA must have filled/incorporated into the defective gaps on the graphene. Zan et al. (2012) reported similar behaviour in the presence of additional hydrocarbons, where gaps in graphene sheets were filled, in a reknitting process.

At atomic layer resolution, the Raman G peak intensity and position have been utilised in numerous studies to give insight regarding doping effects and determination of thickness of graphene layers in samples that are less than four layers thick (Ferrari *et al*., 2006; Ferrari and Basko, 2013). A red shift of the G peak is typical of n-type doping of graphene (Pisana *et al*., 2007). The G peak red shifting upon interaction with ssDNA shows that the ssDNA nucleobases behave as an electron donor to graphene. This corroborates theoretical predictions that the negatively charged sugar-phosphate backbone of ssDNA drive electrostatic interactions with graphene (Lin *et al*, 2010). It is also reported that the reduction of the intensity and red shift of the G peak position is associated with bond softening in graphene as the layers of graphene increases (Miyamoto *et al*., 2010). These findings suggest a similar behaviour upon self-immobilisation of the ssDNA probe on the graphene thus indicating a formation of a π–π stacking and electronic interactions driven chemical bonding between graphene and ssDNA (Mohanty and Berry, 2008).

Analysing the peak intensity ratio of the 2D and G peaks, the ratio I_{2D}/I_G after self-immobilisation of the ssDNA on the graphene increased on average to 2.69 as compared to the initial 2.02. This increase in the I_{2D}/I_G further supports the restoration of graphene defects by DNA. Changes in intensity and position of the 2D peak have been observed primarily in studies that evaluated the graphene quality and properties as the function of the number of layers (Yang *et al*., 2011; Kalita *et al*., 2011; Jung *et al*., 2009; Jung *et al*., 2010). In these

studies, 2D peak characterisation method depends not only on peak position but also on the shape of the peak (Yang *et al*., 2011; Kalita *et al*., 2011; Jung *et al*., 2009; Jung *et al*., 2010). This is contrary to the findings of this study where the shape and symmetrical nature of the 2D peak remained the same as function of ssDNA immobilisation. However, comparable reduction in 2D peak intensity has been reported in literature during the investigation of doping effects of various material on graphene, whereby as the doping increases, the 2D peak intensity decreases (Jung *et al*., 2009; Mohiuddin *et al*., 2009). Therefore, the observations from this study do not only confirm a mere charge transfer between DNA and graphene, but also show that this interaction between graphene and electron-donating ssDNA could also lead to self-healing of graphene by DNA. However, this is not within the scope of this study.

Figure 4.3 shows is the Raman Spectra of ssDNA probe-coated graphene when hybridised with a complementary ssDNA thus forming a perfectly matched DNA duplex coated CVD-grown graphene. In ssDNA probe-coated graphene, the 2D and G peaks were observed at 2683 cm^{-1} and 1585 cm^{-1}, respectively. The D peak was not observed. Upon hybridisation of ssDNA probe-coated graphene with the complementary ssDNA to form perfectly matched DNA duplex coated CVD-grown graphene, the 2D peak disappeared and a small D peak re-appeared at 1349 cm^{-1}. This observation is accompanied by another appearance of a small peak at about 1488 cm^{-1}. The G peak was observed at 1580 cm^{-1}, which is red shifted by 5 cm^{-1} from ssDNA probe-coated graphene. This points to either the formation of stronger bonds or crosslinking of the DNA to graphene or by the emergence of uniaxial strain due to DNA hybridisation (Cullity and Weymouth, 1957; Jung et al., 2010; Lin et al., 2010; Mohiuddin *et al*., 2009).

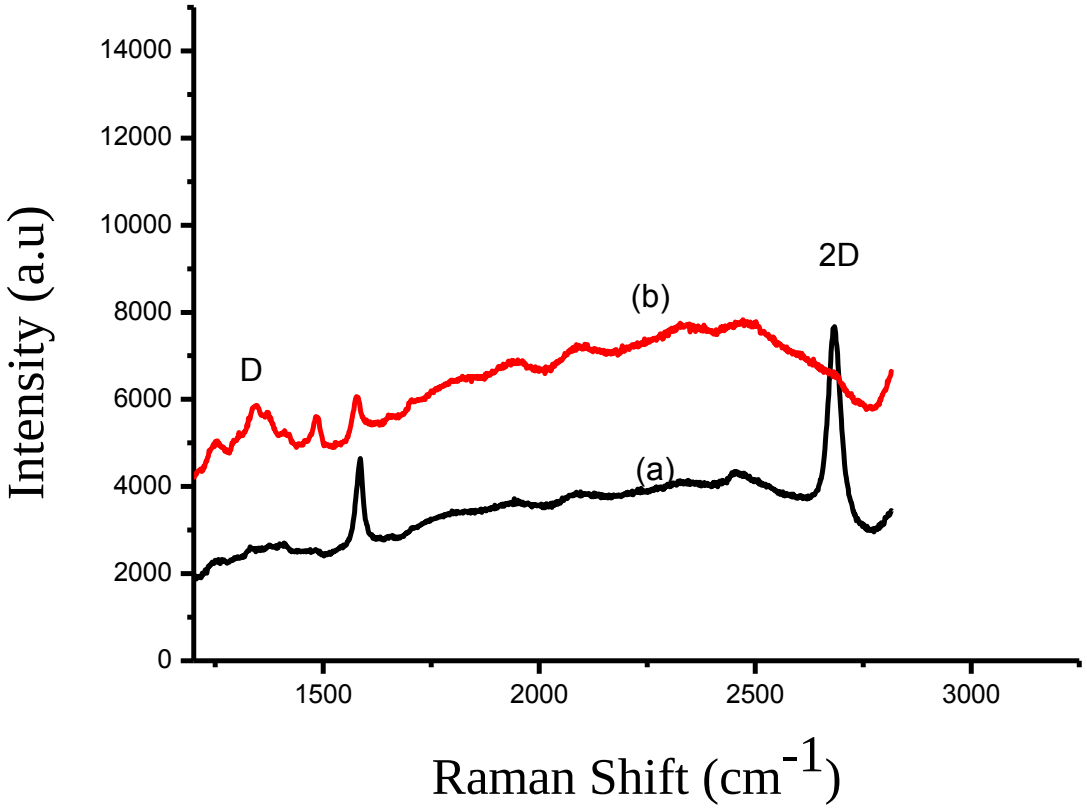

Figure 4.3 Raman spectrum of (a) ssDNA probe-coated graphene, and (b) ssDNA-coated graphene after hybridisation with a complementary 26 bp DNA strand. N-type doping is evidenced by the red shift of the G peak

The recovery of the D peak suggests exposure of small defects on the graphene sample. It is an indication of an induced decrease in size of sp^2 domains in the basal plane of the graphene, possibly due to electronic and structural conjugation disruption of the graphene upon formation of the DNA duplex (Jung *et al*., 2010). Similar behaviours are reported during basal plane reactions such as hydrogenation and oxidation which chemically modify the lattice structure of graphene through the disruption of π-conjugation as sp^2 carbon atoms are converted to sp^3 carbon atoms (Ryu *et al*., 2008; Liu *et al*., 2008). Although reported to be always present in graphene, the 2D peak is absent, possibly due to a suppression of sp^2 hybrid

orbitals of the lattice of the graphene monolayer by the DNA duplex formed from the ssDNA and complementary target (Ryu *et al*., 2008; Liu *et al*., 2008). The intensity of the 2D peak is reportedly sensitive to doping and dependent on the ratio phonon scattering and total scattering. Therefore, its absence in this case could be due to doping effects due to charge transfer between graphene and dsDNA duplex formed during hybridisation.

The DNA duplex on graphene must have caused a highly electron-electron collision to the extent that the 2D peak intensity finally disappeared (Casiraghi, 2009). Moreover, suppression of the 2D peak could be attributed to the nature of the stacking of the DNA on graphene as this vibrational mode is sensitive to the stacking order of graphene along the C-axis (Ferrari *et al*., 2006; Gupta *et al*., 2006; Ni *et al*., 2008). Correspondingly, the lower frequency shift of the G peak upon hybridisation of the ssDNA graphene with its complementary target strand could be due to doping effects of dsDNA (Jung *et al*. 2009; Mohiuddin *et al*., 2009). The backward shift of G peak to low frequencies, could be attributed to bond softening in graphene and not electron or hole doping as that would lead to forward shift of the G peak position (Pisana *et al*., 2007; Lazzeri and Mauri, 2006).

Upon hybridisation of ssDNA probe-coated graphene with the triple-base mismatch ssDNA to form triple-base mismatched DNA duplex coated CVD-grown graphene, the D peak was still not observed. The G peak remains in the same position (1585 cm^{-1}) as in ssDNA probe-coated graphene Raman spectrum, but has a slightly reduced intensity (Figure 4.4). The reduced intensity of the G peak could be attributed to a reduction in the electron-transfer efficiency (Zhao *et al*., 2009). Mismatches in nucleotide base-pair stacks of DNA duplexes have been shown to alter the DNA structure and disrupt electron-transfer efficiency (Monk *et al*., 1987; Rueven *et al*., 2013). At 2685 cm^{-1}, a 2D peak was blue shifted from the ssDNA

probe-coated graphene by 2 cm^{-1}. As compared to 2.024 I_{2D}/I_G ratio in ssDNA probe-coated graphene, the ratio of I_{2D}/I_G decreased slightly to 1.531.

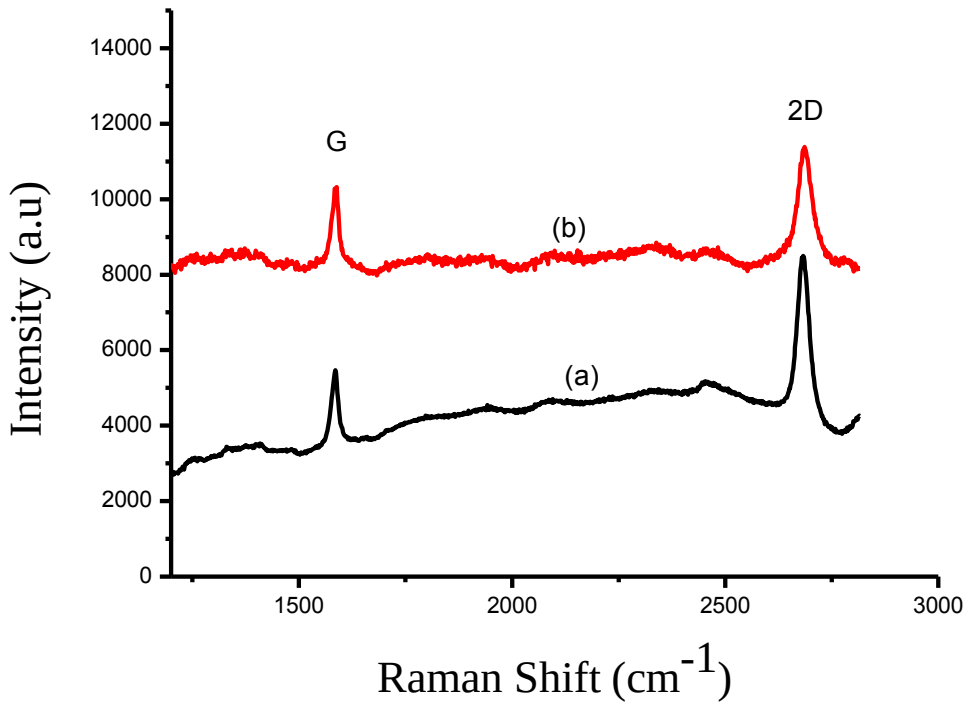

Figure 4.4 Raman spectra of (a) ssDNA probe-coated graphene, and (b) ssDNA-coated graphene after hybridisation with a 26 bp triple-base mismatched DNA strand. P-type doping is evidenced by the blue shift of the G peak

The absence of D peak after hybridisation with a triple-base mismatch DNA strand may not necessarily indicate a lack of significant disruptions in graphene carbon structure lattice. There could be insufficient structural defects for the activation of the D peak (Ferrari *et al.*, 2006). As in qualitative graphene studies, the variation in Raman characteristics could be attributed to charged impurities in the absence of the D peak (Casiraghi *et al.*, 2007). Therefore, the blue shift position and intensity reduction of the 2D peak may be associated to p-type (hole) doping of graphene opposed to electron doping (Das *et al.*, 2007). Such p-type

doping can be induced by chemical doping by the DNA adsorbates and/or water in the buffer used to prepare the DNA molecules (Schedin *et al.*, 2007). The selectivity of graphene in DNA detection can be seen by the difference in charge transfer as uniquely captured in the Raman spectra across DNA films (i.e. films of perfectly matched and triple-base mismatched DNA duplexes) formed upon hybridisation. This is evidenced by the recovery of the Raman D peak upon hybridisation with the complementary ssDNA and not upon hybridisation with a triple-base mismatched ssDNA. Furthermore, these results show that shifts of peak frequencies coupled to changes in intensities and widths of CVD-grown graphene Raman peaks can be used as fingerprint DNA interactions with graphene and DNA hybridisation the graphene surface. The observation reported in this study was consistent across the substrates as shown in Figure 4.5.

Several Raman spectra measured at several regions on pristine CVD-grown graphene, ssDNA-coated graphene, and ssDNA coated graphene that is hybridised with complementary and mismatched ssDNA, support that DNA interactions affect graphene uniformly (Figure 4.5). In Raman collected at different areas on the pristine CVD-grown graphene (Figure 4.5(a)) no significant differences were observed. Raman spectra collected for ssDNA probe-coated graphene at different areas is represented in Figures 4.5(b), and no significant difference was observed between the spectra. For the different areas on ssDNA coated graphene, the I_{2D}/I_G ratio is unaffected. Figure 4.5(c), represents the Raman spectra collected at different regions on ssDNA probe-coated graphene sample when hybridised with complementary target strands. The 2D peak is not observed in all areas. The G peak position and shift is constant across the film. Therefore, no significant difference was found between the spectra for ssDNA probe-coated graphene when hybridised with complementary target

strands. The Raman spectra at different areas in ssDNA probe-coated graphene when hybridised with triple-base mismatched target strand are represented in Figure 4.5(d), and no significant difference was observed, as the blue shift of the 2D peak is consistent across the substrate.

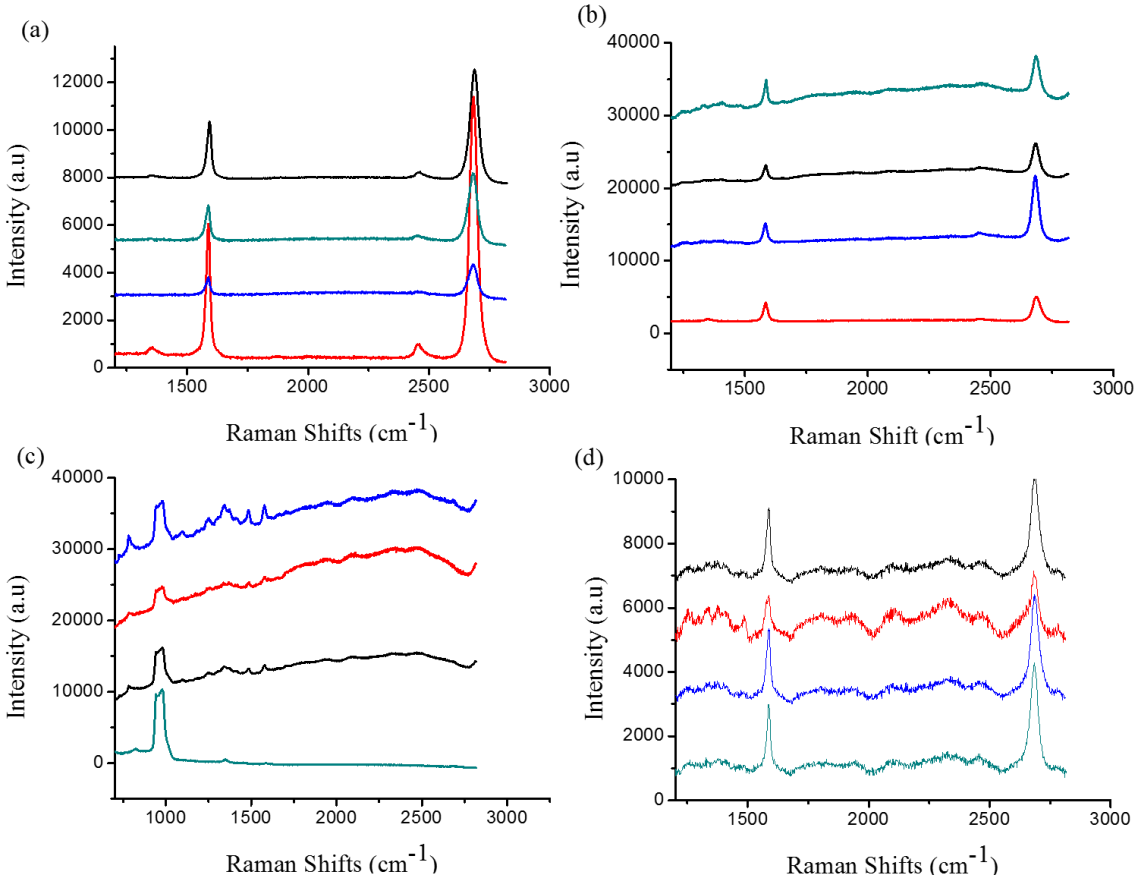

Figure 4.5 Raman spectra measured at different areas on. (a) Pristine CVD-grown graphene. (b) ssDNA-coated graphene, (c) ssDNA-coated graphene that is hybridised with complementary ssDNA target, and (d) ssDNA-coated graphene that is hybridised with triple-base mismatch ssDNA target substrates

4.4 Summary

The interaction of ssDNA with CVD-grown graphene and subsequent effect of DNA hybridisation reactions on structural and electronic properties of CVD-grown graphene were studied using Raman spectroscopy. Self-assembly of ssDNA and hybridisation reactions affect the electronic and structural properties of the CVD-grown graphene as indicated by their respective Raman spectra. This is evidenced by the difference in charge transfer characteristic of the CVD-grown graphene as uniquely captured in the Raman spectra upon interaction with ssDNA films. The disappearance of the small D peak, red shift of the G peak frequency and reduction of 2D peak intensity upon self-immobilisation of ssDNA is related to donor-acceptor interaction between graphene and ssDNA. After hybridisation with complementary and mismatched DNA targets on CVD-grown graphene, shifts in peak frequencies, changes in intensities and widths of CVD graphene characteristic Raman peaks were analysed. Doping of graphene by DNA clusters formed during DNA hybridisation was indicated by the shifts in the G and 2D peak positions. CVD-grown graphene is n-type doped during formation of a perfectly matched dsDNA, and p-type doped for triple-base mismatched dsDNA. It was found that changes in the Raman characteristics are distinct and demonstrate selectivity of graphene in DNA detection. This is a significant finding, which reconciles the variation of structural properties often found in perfectly matched and triple-base mismatched DNA duplexes. However, it should be noted that the use of Raman features that are characteristic to graphene only neglects possible effects that graphene could have on the structural properties of DNA. Therefore, it is recommended that the influence of graphene on the DNA is considered in subsequent studies and this can be investigated by fingerprinting of unique and distinguishable optical properties that are characteristic features of DNA polymers in solid-state films. Understanding the effects of graphene on DNA may pave the way to an in-depth investigating of DNA-graphene interfaces.

Chapter 5 Effect of graphene on DNA hybridisation

A novel UV-Vis spectroscopy technique for the label-free study of the interaction between DNA-graphene interfaces during DNA hybridisation on graphene is reported in this chapter. The tracking of the cooperative transitions of DNA from ssDNA to dsDNA (facilitated by Watson and crick base stacking in DNA molecules) was used to determine the effect of graphene on DNA self-immobilisation and subsequent desorption upon DNA hybridisation. The consistency of graphene's effect on DNA hybridisation, DNA duplexes formed during DNA hybridisation of the ssDNA probe on graphene with its complementary target DNA strand was also analysed after removal from the graphene surface.

5.1. Introduction

The relevance of DNA-graphene interfaces in the development of cheap, fast, reliable and sensitive on-field portable sensing micro-devices such as optical, mass-based, and/or redox/electrochemical biosensors as reviewed in chapter 2 necessitate an in-depth fundamental understanding of the binding and interaction between DNA and Graphene (Saleem, 2013; Turner, 2013). Currently, the field is focused on demonstrating practical analytical applications of various forms of DNA-graphene interfaces (Power and Morrin, 2013; Rahman et al., 2015). As a result, several applications in health care, molecular and cellular diagnostics and environmental sciences have demonstrated successful detection of nucleic acids using novel graphene-based sensors (Mohanty and Berry, 2008; Ratinac *et al*. 2010; Pumera, 2011; Liu *et al*., 2012; Tang *et al*., 2012). However, binding interactions between graphene and DNA are still poorly understood. As a result of this poor understanding, discrepancies have been observed in output signals of graphene sensing devices particularly, graphene field-effect transistors (GFET) based DNA sensors (Green and Norton, 2015).

Mohanty and Berry (2008), in their study of DNA transistor based on graphene for detection of bacterium, suggested that single-stranded (ss) DNA reliably and non-covalently self-assemble onto the graphene thus forming a film of DNA on the graphene surface. This occurrence could be attributed to the positively charged nature of the carbon making up the graphene and structural uniformity of the negatively charged hydrophilic single-stranded DNA. Later, Tang *et al.* (2010) showed that upon hybridisation of the ssDNA probe molecule with its complementary ssDNA, the interactions between the DNA probe and graphene is weakened as the ssDNA probe and its complementary target ssDNA hybridise to form a double-stranded (ds) DNA duplex. In a study of ssDNA of a varied number of bases, Wu et al. (2011) observed that shorter ssDNA strands are adsorbed tighter and more rapidly than longer DNA strands.

Despite poor understanding of atomic-level interactions between DNA and graphene, the believed principle of DNA detection on graphene was that graphene is biocompatible to ssDNA and does not bind dsDNA (Lucarelli *et al*., 2008; Lu *et al*., 2009; He *et al*., 2010; Tang *et al*., 2010; Tang *et al*., 2011; Liu *et al*., 2013). However, Pak et al. (2014) in an attempt to further understand the adsorption and desorption mechanisms on graphene, found that albeit ssDNA is preferentially bound on graphene; dsDNA does interact with graphene and is adsorbed on graphene with a lower affinity. While investigating the dynamic process involved during adsorption of ssDNA on a graphene-related substrate, Chen *et al*. (2014) found that due to electrostatic repulsion DNA did not lay flat but stood on the graphene surface. However, molecular simulations further exploration of DNA adsorption mechanisms on graphene found that it was dsDNA that stood on graphene and ssDNA lay flat on graphene surfaces (Zeng *et al*., 2015).

Regarding DNA-graphene interfaces and their application in DNA hybridisation detection schemes, it is thereby evident that it is critical that binding interactions between DNA and graphene during adsorption and subsequent desorption upon hybridisation are understood at an atomic level. However, equally critical is to understand how DNA is altered during DNA hybridisation on graphene (Sharma *et al.*, 2016). In chapter 4, it was shown that DNA adsorption and desorption on graphene has an effect on graphene's electronic and structural properties as evidenced by changes in Raman peak frequency and intensity of graphene characteristic features. In this chapter, the effect of graphene on DNA self-immobilisation and subsequent desorption upon DNA hybridisation is presented. Seeing that DNA polymers in solid-state thin-film have distinguishable and unique optical properties (Steckl *et al.*, 2011), the nature of DNA molecules adsorbed on graphene and their changes in conformation upon hybridisation was investigated on CVD-grown graphene using Ultraviolet-Visible (UV-Vis) spectroscopy and X-ray powder diffraction (XRD). Results from both UV-Vis and XRD measurements showed that the adsorption of ssDNA strongly influences the chromophoric structure of DNA as evidenced by the absence of the signature DNA absorbance peak at 260 nm in the presence of DNA. The findings of this work could help to clarify and expand on the knowledge of interactions between DNA and graphene particularly offer valuable insight into the effect of graphene on the conformation of DNA.

5.2. Materials and methods

Fabrication of ssDNA probe-coated graphene and DNA hybridisation reactions were performed as detailed in chapter 3, section 3.4.

5.2.1 UV Analysis

UV-Vis measurements absorbance at a specific range of wavelengths of CVD-grown graphene, ssDNA-coated graphene, and ssDNA-coated graphene when hybridised complementary and triple-base mismatched ssDNA targets were performed at room temperature using a UV-Vis spectrophotometer (Varian Cary 500). Background correction for solution analysis of DNA was performed using a 1 cm quartz cuvette filled with Tris-EDTA buffer as a blank. The UV-Vis absorbance curves were recorded for scanned wavelengths between the 200 nm to 300 nm range.

5.2.2 UV-Vis Statistical Analysis

All statistical analyses were performed using statistical package for the social sciences (SPSS) software on UV data that was converted into delimited text using Microsoft Excel 2010. Each of these reactions was performed and measured on the same continuous scale, that is, 200-300 nm and repeated three or more times for results verification and statistical analysis. Therefore, standard deviations and means were calculated using a one-way repeated measures analysis of variance (ANOVA) and contributions from both within- and between-experiment variations were included (Pallant, 2010). In this analysis, multivariate statistics was reported. According to Pallant, 2010, the multivariate statistics provided in the output is safer to inspect as it does not require satisfaction of the sphericity assumption. The heterogeneity of UV absorbance variation across the samples was reported using the most commonly reported multivariate test statistic, Wilks' Lambda (Pallannt, 2010, Pallant, 2013). The effect of size on the heterogeneity results was assessed by the statistic value of Partial Eta Squared, obtained from the multivariate test. Guidelines proposed by Cohen (1988) (0.01

= small, 0.06 = moderate, 0.14 = large effect) were used in this assessment. Each pair of samples were compared to indicate where the absorbance differences lie and this was performed using Bonferroni adjustment for pairwise comparisons (Pallant, 2010).

5.2.3 X-ray diffraction (XRD) Analysis

The phase changes and crystallography of CVD-grown graphene, ssDNA-coated graphene, and ssDNA-coated graphene when hybridised complementary and triple-base mismatched ssDNA targets were checked using X-ray diffraction (XRD). The analyses were carried out on the aforementioned samples on a 1 cm x 1cm silicon wafer (Si) with a 285 nm silicon dioxide (SiO_2) layer. The XRD diffractograms were examined and recorded with a Bruker D2 diffractometer (Cu Kα1 and 2 radiation).

5.3. Results and Discussion

5.3.1 UV analysis

5.3.1.1 Effect of graphene on DNA hybridisation

The UV-Vis absorbance spectra of CVD-grown pristine graphene, of ssDNA probe-coated graphene, ssDNA probe-coated graphene when hybridised with a complementary ssDNA target, and ssDNA probe-coated pristine graphene when hybridised with a triple-base mismatched ssDNA target were monitored between the 200 and 300 nm range at room temperature (Figure 5.1). The UV-Vis absorbance spectrum of pristine CVD-grown graphene shown in Figure 5.1 (a) exhibits characteristic features at about 212 nm, 235 nm and 257 nm. The main peak at 235 nm corresponds to pi to pi star (π-π*) transition of aromatic carbon-

carbon (C=C) bonds in graphene, while the shoulder at 257 nm is attributed to overlapping n to pi star (n-π*) and π-π* transitions in graphene (Vo-Dinh, 1989; Kemp 1991; Benesi and Hildebrand, 1949; Friedel and Orchin, 1951; Badertscher *et al*., 2009; Pretsch *et al*., 2009). Absorption peaks for graphene between 200 nm to 300 nm are expected as graphene contains aromatic carbon rings that have been demonstrated to absorb light across the ultraviolet range with minimum reflection of the incident light (Mak *et al*., 2008; Thongrattanasiri *et al*., 2012; He *et al*., 2014).

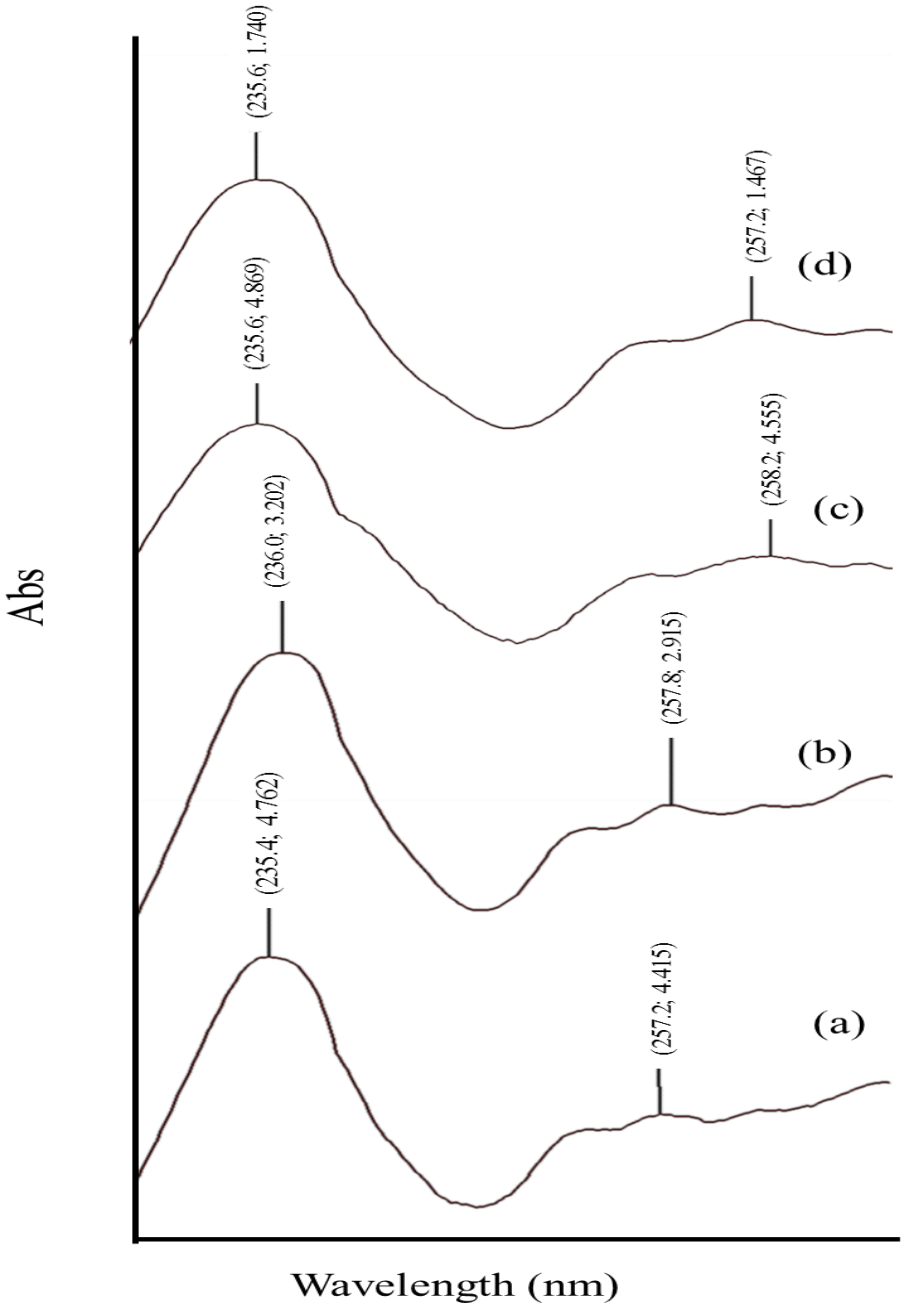

Figure 5.1 The UV-Vis absorbance spectra monitored between the 200 and 300 nm range at room temperature of (a) CVD-grown pristine graphene, (b) of ssDNA probe-coated graphene, (c) ssDNA probe-coated graphene when hybridised with a complementary ssDNA target, and (d) ssDNA probe-coated pristine graphene when hybridised with a triple-base mismatched ssDNA target

After self-immobilisation of ssDNA probe on the CVD-grown graphene, the absorption peaks and transmission intensities changed as shown in Figure 5.1 (b). In the absorption spectrum of ssDNA probe-coated graphene captured upon self-immobilisation of ssDNA probe on CVD-grown graphene, a maximum absorption peak corresponding to π-π* transitions of carbon-carbon (C=C) bonds red shifted less than 1 nm to 236 nm and the shoulder ascribed to overlapping n-π* (due to carbon-oxygen (C-O) bonds) and π-π* transitions in graphene remained at around 257 nm (Vo-Dinh, 1989; Kemp 1991; Benesi and Hildebrand, 1949; Friedel and Orchin, 1951; Badertscher *et al*., 2009; Pretsch *et al*., 2009). Furthermore, a lower absorption of about 32 % was seen in this absorption spectrum of ssDNA probe-coated graphene. It appears that the ssDNA probe-coated graphene behaves as an independently isolated species as evidenced by the sharp absorption peak at about 236 nm. However, the less than 1 nm bathochromic shift that leads to this peak at 236 nm is worth noting; it is similar to that observed as an indicative effect of substitution of electron donating group in aromatic compounds and π conjugation in aromatic compounds (Kumar, 2006). Therefore, this bathochromic shift could advocate formation C-O bonds between carbon atoms in graphene and oxygen atoms from phosphate groups (PO_3^{-4}) in the ssDNA probe (Lucarelli *et al*., 2008; Tang *et al*., 2011; Du *et al*., 2012; Ngo *et al*., 2013). The decrease in intensity of absorption is known as the hypochromism (Kumar, 2006).

In DNA, hypochromism occurs where the individual bases of the ssDNA on the graphene surface interact with one another in a significant way and therefore absorb less light (Tinoco Jr, 1960; Rhodes, 1961; Sinanoğlu, 1963; DeVoe, 1969; Pechenaya, 1975). The observed decrease in absorbance intensity in ssDNA-coated graphene in this study suggests that the nucleobases of the adsorbed ssDNA on graphene are enclosed either through intramolecular interactions of the bases on the DNA strand (Breslauer *et al*., 1986; Elstner *et al*., 2001; Gao *et al*., 2006) and/or the nucleobases are enclosed as a result of the ssDNA probe being tightly

bound on graphene (Tang *et al*., 2010; Liu *et al*., 2010; Wu *et al*., 2011). Nonetheless, the change in absorbance and transmission of light from nucleobases in DNA upon adsorption of ssDNA graphene provides useful insight. Similar to when hyporchromism is used as monitoring tool and indicator of cooperative transition characteristics of dsDNA in studies involving DNA melting and denaturing (Bhattacharya and Mandal, 1997; Kumar and Asuncion, 1993; Sweeney and Hennessey, 2002; Tautorov *et al*., 2008), hypochromic shift in absorbance intensity during adsorption of DNA on graphene can be used as indicator of successful ssDNA immobilization on graphene.

Shown in Figure 5.1 (c) is the absorption spectrum of ssDNA probe-coated graphene when hybridised with a complementary ssDNA thus forming a perfectly matched duplex coated CVD-grown graphene. In ssDNA probe-coated graphene a maximum absorption peak as was observed at around 236 nm. Upon hybridisation of the ssDNA probe-coated graphene with a complementary ssDNA strand target, a < 1 nm blue shift in the absorbance wavelength from 236 nm to 235 nm was observed with a 52% increase in transmittance. The observed 52% increase in absorption intensity indicates that upon hybridisation the ssDNA molecule on the graphene surface and the added complementary target DNA strand began to aggregate or associate into paired stacked bases (Lee *et al*., 2013; Tang et al., 2011; Du *et al*., 2012). However, this pairing of the stacks of aromatic chromophores in DNA on graphene resulted in the increase of absorption intensity in a manner contrary to the traditional DNA hyperchromicity effect during DNA hybridisation in solution (Tinoco Jr, 1960; Rhodes, 1961; Sinanoğlu, 1963; DeVoe, 1969; Pechenaya, 1975). Schweitzer and Kool (1995), reported the aromatic ring resonance of the nucleobases in dsDNA to be limited due to specific hydrogen bonding and subsequent hydrophobic effects between two complementary nucleobases. Consequently, it could be expected that the dsDNA has a decreased absorption as opposed to the increased absorbance observed in this study where upon hybridization the

complementary strands of DNA with protected nucleobase aromatic rings that do not readily absorb light (Sharma *et al*., 2016).

The findings of this study provide a different viewpoint of use of DNA hyperchromisim and hypochromism relating to the illumination of interactions between DNA and graphene. The < 1 nm wavelength blue shift of the maximum absorption peak suggests the restoration of the electronic conjugation of the graphene upon formation of the DNA duplex. This supports literature reports of the weakening of the interactions between the ssDNA probe and graphene upon DNA hybridisation thus reversing the initial DNA adsorption onto the graphene surface (Liu *et al*., 2010; Tan *et al*., 2012; Wu *et al*., 2012; Zhang *et al*., 2013). This observation shows that following desorption, the ssDNA probe and its complementary target ssDNA hybridise and form a double-stranded (ds) DNA duplex (Lee *et al*., 2013; Tang *et al*., 2010; Du *et al*., 2012; Ngo *et al*., 2013; Tang *et al*., 2011).

Shown in Figure 5.1 (d) is the absorption spectrum of ssDNA probe-coated graphene when hybridised with a complementary ssDNA thus forming a triple-base mismatched DNA duplex coated CVD-grown graphene. An absorption peak corresponding to π-π* transitions of carbon-carbon (C=C) bonds and the shoulder ascribed to overlapping n-π* (due to carbon-oxygen (C-O) bonds) and π-π* transitions in graphene were observed at around 235 nm and 257 nm, respectively (Vo-Dinh, 1989; Kemp 1991; Benesi and Hildebrand, 1949; Friedel and Orchin, 1951; Badertscher *et al*., 2009; Pretsch *et al*., 2009). Moreover, a 45 % decrease in absorption was observed. The < 1 nm hypsochromic shift from 236 to 235 nm observed is similar to that of ssDNA probe-coated graphene when hybridised with a complementary DNA strand. However, unlike when hybridised with complementary strand a decrease in absorption was observed when ssDNA-coated graphene was hybridised with a triple-base mismatch strand as was observed in self-immobilisation ssDNA on graphene. The < 1 nm

hypsochromic shift in wavelength suggests that DNA duplex was formed with the triple-base mismatch (Lee *et al*., 2013; Tang et al., 2011; Du *et al*., 2012). But the decrease in absorption suggests the formation of a different kind of duplex from that formed with a complementary strand and a possible further interaction of the mismatched regions with graphene. An increase in absorption for the formation of the triple-base mismatch duplex would be expected as it would contain regions of denatured loops at which the mismatched nucleobases are exposed and expected to absorb more light (Schweitzer and Kool, 1995; Reuven *et al*., 2013). However, the contrary observations reported in this study infer that the mismatched nucleobases at the denatured region of the dsDNA chain are not exposed. Instead the nucleobases at the denatured regions of the dsDNA chains could have further folded over and interacted with the graphene surface. Although not desired, this interaction with mismatched nucleobases is possibly facilitated by the adsorption of DNA duplexes on graphene as was found to occur at a lower affinity by Park et al. (2014).

5.3.1.2 Efficiency and consistency of the effect of graphene on DNA hybridisation

In order to assess the consistency of graphene's effect on DNA hybridisation, DNA duplexes formed during DNA hybridisation of the ssDNA probe on graphene with its complementary target DNA strand were analysed using UV-Vis spectroscopy after the removal of the DNA from the graphene surface. These products of solid-phase surface hybridisation were compared with the DNA duplex formed during solution-phase hybridisation (Figure 5.2). The UV-Vis spectrum of DNA duplex formed in solution (Figure 5.2 spectrum a) and ssDNA coated-graphene on graphene after hybridisation with the complementary strand as presented in Figure 5.1 (c) exhibits absorption peaks at 260 nm and 235 nm (with just a shoulder at around 260 nm), respectively. As previously known, free DNA displays strong absorption at

around 260 nm (Labarca *et al*., 1980; Wolfe *et al*., 1987; Xu *et al*., 1994). After the removal of the DNA duplex from the graphene surface and analysed (Figure 5.2 spectrum b), it exhibited a strong absorption at around 260 nm. This peak was covered by the strong absorption peak of graphene located at around 235 nm (Figure 5.1 (a)); thus absorption peak of DNA after removal from graphene appeared at around 260 nm.

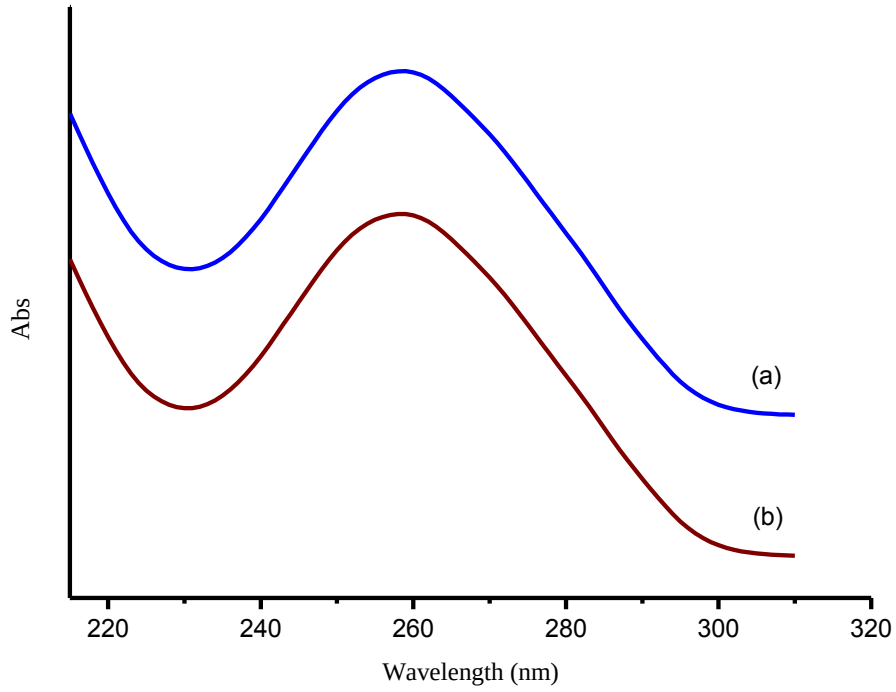

Figure 5.2 UV-Vis absorption spectra of (a) dsDNA formed in solution, (b) dsDNA after removal from the graphene surface

These results demonstrate that graphene has an effect on the DNA structure and/or suggests that DNA hybridization on graphene may not be efficient. DNA hybridization and/or formation of a dsDNA on graphene may have not completely occurred or detected, hence a

weak DNA peak at around 260 nm in the presence of graphene. The presence of graphene during DNA hybridisation hinders the formation of the complete DNA duplex, thus corroborating Levicky and Horgan (2005) analysis of DNA hybridisation at interfaces as being more complex and less favourable than that in solution. On surfaces, the efficiency of DNA hybridisation is affected by physicochemical limits that inhibit the accessibility of immobilised DNA probe to its target consequently limiting DNA duplex formation (Wong and Melosh, 2010; Zhang *et al*., 2012). Cases such as steric hindrances (Chen *et al*., 2009; Halperin *et al*., 2006) and electrostatic repulsion (Ge *et al*., 2003; Wong and Melosh, 2010) between immobilised DNA molecules on surfaces have been known to lead to the aforementioned decreased efficiency of DNA hybridisation on interfaces. Furthermore, it may be that DNA desorption from the graphene is not prompt and efficient; thus further corroborating Park *et al*. (2014) observations that dsDNA duplex can be adsorbed on graphene regardless of graphene being known to interact with ssDNA with high affinity.

This could be due to non-specific adsorption and desorption of DNA whereby ssDNA on the graphene surface does move away from the graphene surface and formed DNA duplex with its complementary strand but the formed DNA duplex further interacts with graphene thus affecting the efficiency of DNA hybridisation. Similar non-specifically adsorption of DNA molecules and effect on DNA hybridisation have been observed in curved surfaces of carbon nanotubes and gold nanoparticles (Cederquist and Keating, 2009; Wang *et al*., 2009; Yang *et al*., 2008). Although graphene is planar in structural nature, topological defects on graphene have been reported to lead to curvature of the local surface (Cortijo and Vozmediano, 2007). Therefore, such curvature of the graphene surface could have led to a decrease in efficiency of DNA hybridisation. Nevertheless, the consistency of the DNA duplexes formed on graphene was evaluated. Several UV-Vis spectra of the duplexes after removal from graphene were evaluated (Figure 5.3).

Overall, the absorption wavelength was observed to be around 260 nm in all the spectra. However, it is worth noting that differences in the spectra were observed in the absorption wavelength between the spectra, as seen in Figure 5.3 the maximum absorbance are not exactly observed at 260 nm. Although a small amount of differences in peak maximum is an acceptable systematic random error, these minor differences could suggest differences in the chromophoric structure of the duplexes formed on graphene (Stulz, 2016). Although DNA contains the same atoms, the configuration of theses atoms may be different thus resulting in different electronic structures hence the differences in maximum absorbance wavelength (Breslauer *et al*., 1986; Elstner *et al*., 2001; Kumar, 2006). Therefore, these differences in absorbance suggest a possible reason for the discrepancies reported in the literature on output signals of graphene-based DNA hybridisation sensors (Dong *et al*., 2010; Lin *et al*., 2013; Green and Norton, 2015).

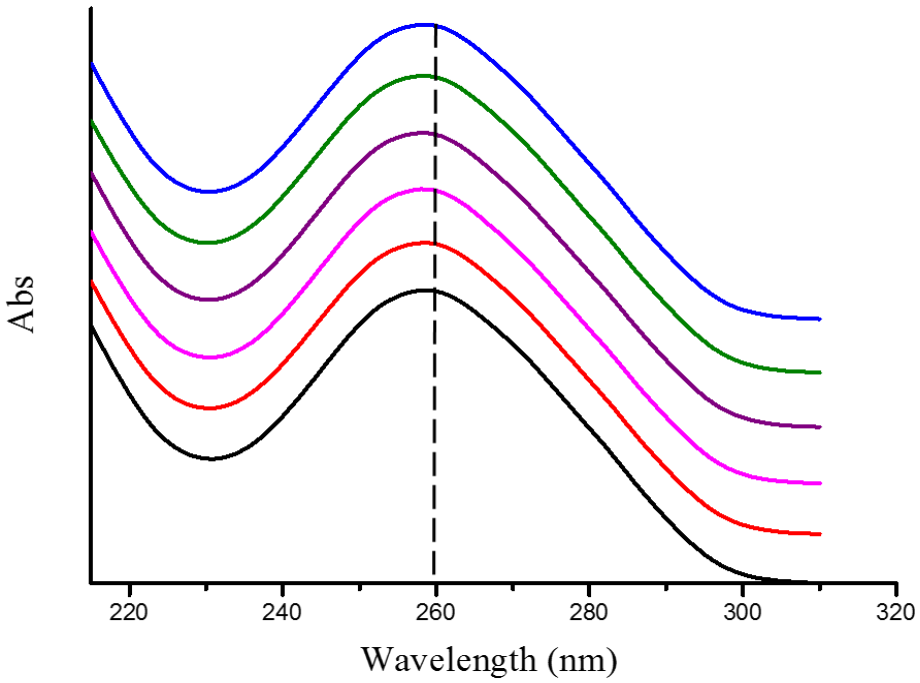

Figure 5.3 UV-Vis absorption spectra of several samples of DNA (duplex of ssDNA probe and complementary target strands) after removal from the graphene surface

5.3.1.3 Statistical analysis of UV data

A one-way repeated measures ANOVA was conducted to determine the heterogeneity of UV absorbance across CVD-grown graphene, ssDNA-coated graphene, and ssDNA-coated graphene when hybridised complementary and triple-base mismatched ssDNA targets. From the SPSS results depicted in Table 5.1, the heterogeneity of UV absorbance variation across the samples showed that there is sufficient evidence to conclude that there is a significant measurement difference between the experiments and/or over the four samples (Wilk' Lambda = 0.172, $F(3,636) = 1020$, $p = 0.000 < 0.05$). The effect of size on this result was found to be large (Partial Eta Squared = 0.828) based on Cohen (1988) guidelines.

Table 5.1 SPSS results of Multivariate Test[a]

Effect		Value	F	Hypothesis df	Error df	Sig.	Partial Eta Squared
Absorbance Samples	Pillai's Trace	0.828	1020.963[b]	3.000	636.000	0.000	0.828
	Wilks' Lambda	0.172	1020.963[b]	3.000	636.000	0.000	0.828
	Hotelling's Trace	4.816	1020.963[b]	3.000	636.000	0.000	0.828
	Roy's Largest Root	4.816	1020.963[b]	3.000	636.000	0.000	0.828

a. Design: Intercept

Within Subjects Design: Absorbance Samples

b. Exact statistic

F = F-statistic

df = degrees of freedom

Sig. = Significance values

Pairwise comparison (Table 5.2) showed that a significance differences ($p < 0.05$) exists between CVD-grown graphene and ssDNA-coated graphene; CVD-grown graphene and ssDNA-coated graphene when hybridised with a triple-base mismatched ssDNA target; ssDNA-coated graphene and ssDNA-coated graphene when hybridised with a complementary ssDNA target; ssDNA-coated graphene and ssDNA-coated graphene when hybridised with a triple-base mismatched ssDNA target; and ssDNA-coated graphene when hybridised with a complementary ssDNA target and ssDNA-coated graphene when hybridised with a triple-base mismatched ssDNA target. No significant difference ($p > 0.05$) was found between CVD-grown graphene and ssDNA-coated graphene when hybridised with a complementary ssDNA target. These results show that not only is DNA hybridisation taking place but the two duplexes formed when hybridised with a complementary ssDNA target and triple base mismatch are different.

Table 5.2 Statistical data obtained from Pairwise Comparison of samples

(I) Absorbance Samples	(J) Absorbance Samples	Mean Difference (I-J)	Std. Error	Sig.[b]	95% Confidence Interval for Difference[b]	
					Lower Bound	Upper Bound
1	2	0.300*	0.080	0.001	0.088	0.513
	3	0.042	0.069	1.000	-0.142	0.226
	4	1.952*	0.050	0.000	1.821	2.084
2	1	-0.300*	0.080	0.001	-0.513	-0.088
	3	-0.258*	0.082	0.010	-0.475	-0.042
	4	1.652*	0.065	0.000	1.481	1.823
3	1	-0.042	0.069	1.000	-0.226	0.142
	2	0.258*	0.082	0.010	0.042	0.475
	4	1.910*	0.054	0.000	1.768	2.053
4	1	-1.952*	0.050	0.000	-2.084	-1.821
	2	-1.652*	0.065	0.000	-1.823	-1.481
	3	-1.910*	0.054	0.000	-2.053	-1.768

Based on estimated marginal means

*. The mean difference is significant at the .05 level.

b. Adjustment for multiple comparisons: Bonferroni.

1 = CVD-grown graphene, 2 = ssDNA probe-coated graphene, and 3 = ssDNA probe-coated graphene when hybridised with complementary and 4 = triple-base mismatch strands

5.3.2 XRD analysis

XRD analysis was employed to characterise the crystalline/structural nature and conformational that occur during DNA immobilisation and DNA desorption on CVD-grown graphene upon hybridisation with different target DNA strands (complementary and mismatched DNA strands). The XRD pattern shown in Figure 5.4, namely the diffraction patterns of pristine CVD-grown graphene (Figure 5.4 a), ssDNA probe-coated graphene (Figure 5.4 b), and ssDNA probe-coated graphene when hybridised with complementary (Figure 5.4 c) and triple-base mismatch strands (Figure 5.4 d) exhibited a major peak doublet kα1 and kα2 at around 2θ = 82.7° corresponding to an inter-planer spacing (d spacing) of 1.35 Å. A diffraction peak at about 2θ = 73.4° for a d spacing of about 1.50 Å was also observed in all diffraction patterns. An exception in the diffraction pattern can be seen on the diffraction pattern ssDNA probe-coated graphene when hybridised with triple-base mismatch strand with an occurrence of several peaks between 2θ = 11° to around 2θ =40° (circled in Figure 5.4 d). This suggests that the triple-base mismatched duplex formed on graphene is different in composition and stoichiometry from the duplex formed with a complementary target (Cullity and Weymouth, 1957; Cullity and Stock, 1978).

A closer analysis of the kα1 and kα2 peak doublets across all the diffraction patterns (insert in Figure 5.4), showed a shift of kα1 and kα2 peaks to lower angle upon DNA adsorption and desorption on graphene. Change in chemical composition, change in stoichiometry and compressive stress have been reported in the literature to produce similar effects (Cullity and Weymouth, 1957). However, for DNA films on graphene, a strain effect is expected although the influence of chemical composition and stoichiometry cannot be excluded. Strain contributions are expected to be important in this case since it is known that during translocation of the DNA through graphene interactions between DNA nucleobases and

graphene has been known to cause strain. Whereby a pull in graphene is caused during bond formation between DNA and graphene and the pull is ended when bonds between DNA and graphene are broken (Schneider *et al.*, 2010; Wells *et al.*, 2012; Deamer *et al.*, 2016; Kundu and Karmakar, 2016; Heerema and Dekker, 2016). Therefore, the shift of kα1 and kα2 to lower angles could signify adsorption and desorption of DNA on graphene.

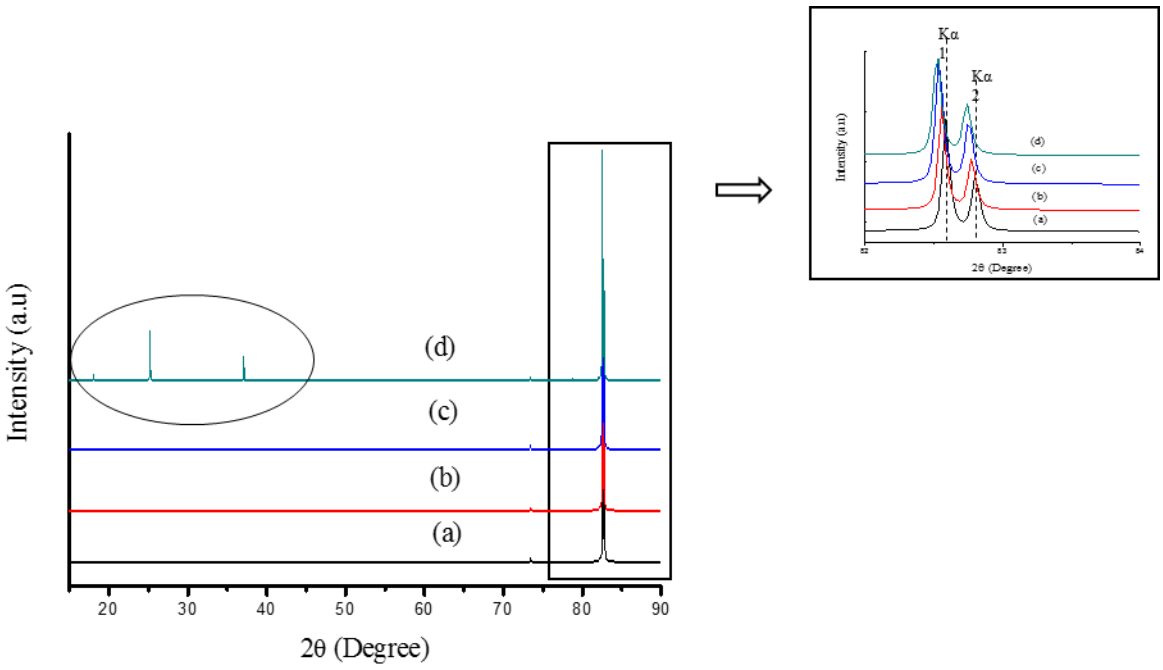

Figure 5.4 X-ray diffraction pattern of (a) CVD-grown graphene, (b) ssDNA probe-coated graphene, and (c) ssDNA probe-coated graphene when hybridised with complementary and (d) triple-base mismatch strands

5.4 Summary

The effect of graphene on DNA hybridisation was studied to enhance the understanding of the interactions between graphene and DNA in DNA-graphene interfaces. The bathochromic

shift that occurred upon adsorption of ssDNA probe on graphene and a hypsochromic shift in absorption wavelengths that accompanied hybridisation of ssDNA coated-graphene with complementary and triple-base mismatch target could be used as indicators of DNA adsorption and desorption on graphene, respectively. However, the observed increase and a decrease in absorption for hybridisation of ssDNA-coated graphene with a complementary and triple-base mismatch, respectively, suggest that graphene interacts differently with DNA duplexes that contain mismatches and those without mismatches. It was found that the denatured region of the dsDNA chain was not exposed instead further fold over and interaction of nucleobases in that region with the graphene surface occured. This was further corroborated by diffraction pattern complexities between $2\theta = 11°$ to around $2\theta = 40°$ in the XRD pattern of ssDNA-coated graphene when hybridised with a triple-base mismatch. The presence of graphene after desorption of DNA, therefore, can have an effect on the conformational nature of the DNA duplexes formed. Moreover, it can be concluded that the subsequent interaction of target DNA strands with ssDNA probe-coated graphene induces a change in absorbance and transmission of light from nucleobases in DNA thus making the ssDNA-coated graphene to act as a sensor system.

The effect of graphene on DNA hybridisation was observed through a comparison of solution DNA hybridisation with that of solid-phase graphene hybridisation. During DNA adsorption and desorption upon DNA hybridisation, graphene affects the chromophoric structure of DNA as evidenced by the coverage of the signature DNA absorbance wavelength peak at known to be at 260 nm. A peak at 260 nm was easily seen when DNA hybridisation of ssDNA and its complementary target strand was performed in solution in the absence of graphene. The results of this study provide a fundamental step towards understanding a) DNA interactions with graphene, B) effect of graphene on DNA structure and c) conformational changes of DNA that occur during DNA adsorption and desorption on

graphene. Therefore, the results could be instrumental to the optimisation of current graphene-based DNA sensing systems and development of innovative mechanisms of DNA adsorption and desorption on graphene that could potentially effect consistent output signal.

Chapter 6 Geometric interpretation of current-voltage measurements

In this chapter, a new method of representing electronic events and DNA conformational changes during DNA detection on graphene from current-voltage measurements is presented. The variability of this integrative approach and its ability to yield consistent easy-to-read electronic signals was investigated.

6.1 Introduction

The effects of DNA hybridisation reaction on structural and optical properties of CVD-grown graphene and that of graphene on DNA hybridisation were studied in Chapter four and Chapter five respectively. As reported in those chapters, during adsorption and desorption of DNA on graphene, distinct electronic charge transfer events and conformational changes in DNA structure occurred. The information provides a step towards better understanding of DNA-graphene interfaces, a fundamental phase in biosensor development (Saleem, 2013; Turner, 2013). However, the understanding of interactions in DNA-graphene interfaces does not make a biosensor. Therefore, in order to develop a cheap, fast, reliable and sensitive on-field portable sensing micro-device for DNA hybridisation detection, it is equally critical that electronic charge transfer events and conformational changes in DNA structure that occur in the DNA-graphene interface be deciphered into an easy-to-read electronic signal (Hahn *et al.*, 2005; Kerman, *et al*., 2003; Karamollaogˇlua *et al*., 2009; Passamanno and Pighini, 2006).

The Dirac point's gate voltage (V_g) from current-voltage measured characteristics is the output electronic signal typically used in studies that have demonstrated practical analytical

applications of various forms of DNA-graphene interfaces for selective label-free electrical detection of DNA hybridisation (Mohanty and Berry, 2008; Chen *et al*., 2009; Yin *et al*., 2012; Green and Norton, 2015). However, there has been discrepancies in the V_g between studies, causes of which have been reviewed in greater detail in chapter 1. In a study that utilised a DNA-based back-gated field effect transistors (GFET) in arrays of chemical vapour sensors, Kybert et al. (2014), observed a positive shift in V_g upon adsorption of single stranded DNA on graphene surface. A few years earlier, the same group had developed a liquid gated GFET and observed a shift towards the negative gate potential. The authors attributed this to chemical gating of the graphene (Lu *et al*., 2010). Dong *et al*. (2010), also reported negative shifts upon adsorption of DNA on a liquid gated graphene based field effect transistor for single-base specific detection of DNA hybridisation. These authors attributed this negative shift in gate potential to n-doping of graphene through its pi-pi interaction with electron rich aromatic rings of DNA nucleobases (Dong *et al*., 2010). Mohanty and Berry (2008), Lin *et al*. (2013), and Artyukhin *et al*. (2006) also reported negative shifts in the gate potentials and attributed the shift to p-doping, electrostatic gating and chemical gating, respectively. However, a study that experimentally quantified the electrostatic transduction mechanism using charged groups of varied lengths discounted doping and buffer effects as the cause of a shift of gate voltage toward negative potentials is reported by Lerner *et al*. (2012). In an attempt to address inconsistencies in output signal, after reviewing multiple experiments, Lin *et al*.(2013) claimed that the mechanisms (doping, electrostatic and chemical gating) to which various studies have attributed the V_g values and shifts to, do not occur separately but simultaneously. Green and Norton, (2015) speculated that these discrepancies in reported measurements could be attributed to differences in device design.

At this juncture, discrepancies as a result of differences in device design will be explored by studying current-voltage characteristics of the ssDNA-coated graphene (characterised in

Chapter 4 and Chapter 5) when configured into two distinct electronic circuit configurations. This could provide a new probable insight on the electronic transport at the DNA-graphene (i.e. biomolecule/nanomaterial) interface and the graphene-silicon (i.e. nanomaterial/substrate) interface during DNA hybridisation. However, due to inconsistencies in the measured V_g values and attributed detection mechanisms, a shift in V_g may not be a simple output electronic signal that can decipher electronic charge transfer events and conformational changes in DNA structure that occur in the DNA-graphene interface (Lin *et al*., 2013). The use of alternative parameters such as sheet resistance and carrier mobility instead of shifts in V_g has been proposed by some researchers (Lin *et al*. 2013, Green and Norton, 2015). As could be ascertained, there has been no reported advancements in this regard. It must be noted as an aide-mémoire that one of main attributes and specifications that founded the invention of a biosensors is that, skills required to operate them should be minimum (Hanh *et al*., 2005; Labuda *et al*., 2010).

Therefore, in bio-sensing technologies with a wide range of applicability, it is critical that the output signal is easy to read and understand (Passamanno and Pighini, 2006; Karamollaogˇlua *et al*., 2009). Individuals without laboratory training or any experience will have difficulty understanding mechanisms such as doping, electrostatic and chemical gating that are associated with the gate voltage. The veracity of the output signal signifying DNA adsorption and DNA hybridisation (desorption) is not questionable, as it is apparent that this measurable electronic signal is elicited by interactions between DNA and graphene in all reported studies (Green and Norton, 2015). Therefore, in the second part of this chapter, an alternative integrative approach that converts the current-voltage measurements into an alternative parameter that describes the physical DNA adsorption, nature of DNA and DNA morphological changes during DNA hybridisation in a standardised geometric manner is proposed.

6.2 Materials and Methods

6.2.1 Fabrication of ssDNA/graphene nanocomposites

The DNA hybridisation sensing device consisted of uniform large surface area (10 mm x10 mm) chemical vapour deposition (CVD) graphene films on a 285 nm thick SiO_2 layer on top of a Si substrate (Graphene Laboratories Inc. New York, United States of America) and a ssDNA probe. A millimetre-size graphene square and 285 nm SiO_2 thickness were chosen in this study in order to ensure simplicity of the device fabrication (without any need to use an optical microscope to ascertain the location of the graphene film). Conductive silver paint was used as testing pads. Silver paint pads paint were placed on two contact points on the edges of the graphene/SiO_2/Si to ensure that the electrodes are placed at the same position throughout the electronic measurement taking and to circumvent the electrodes damaging the graphene (Figure 6.1b).

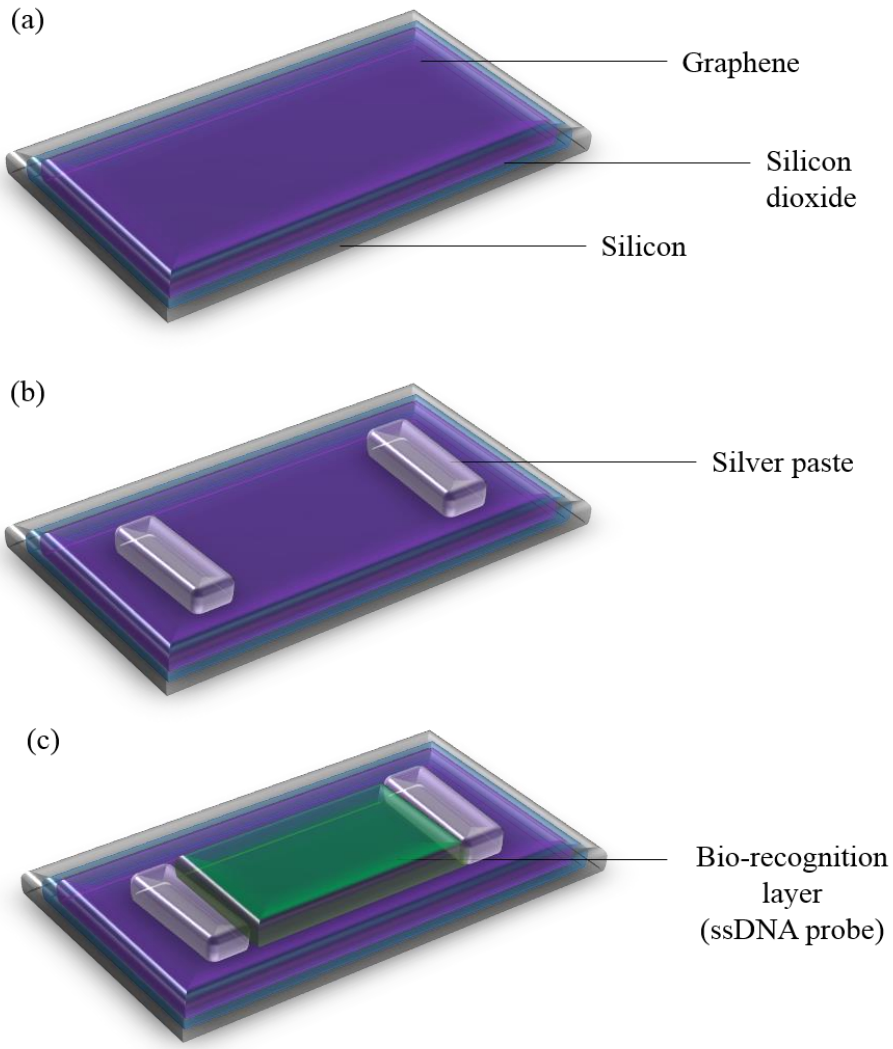

Figure 6.1 Schematic of simple fabrication of the graphene based DNA hybridisation sensing device; (a) represents graphene/SiO_2/Si, (b) graphene/SiO_2/Si with the silver testing pads on two contact points, and (c) is the complete ssDNA/graphene/SiO_2 awaiting Hybridisation

Onto graphene films (on SiO_2/Si substrates), a 1 µL solution of $1x10^{-6}$ M ssDNA probe in pH 8.0 10 mM TE buffer was dropped casted, and allowed to air dry for 30 minutes at ambient temperature. This was done to allow the ssDNA probe to bind to the graphene sheet and form a layer of ssDNA probe bio-recognition layer (Figure 6.1c). The ssDNA/graphene/SiO_2 all combined makes the DNA hybridisation sensing device which is herein denoted as ssDNA/graphene/SiO_2/Si.

6.2.2 Hybridisation of DNA and current-voltage measurements

In order to characterise the ssDNA/graphene/SiO_2/Si sensor, DNA hybridisation reactions were conducted and the electronic responses of the graphene were measured. Electrical contacts were provided by gold electrodes attached to the silver paint pads on the graphene film (Figure 6.1). The gold electrodes were placed directly on the graphene layer in order to make the gate electrical contact to the ssDNA layer. Two configurations of DNA hybridisation sensor i.e., resistors in series and parallel were tested (Figure 6.2). The series resistor configuration was achieved by separating the graphene layer into two layers separated by a space between them (Figure 6.2 (b)). To demonstrate the specificity and selectivity of the device, we quantitatively and qualitatively captured electrical responses of the ssDNA/graphene/SiO_2 upon hybridisation with $1x10^{-6}$ M of the target DNA and $1x10^{-6}$ M triple-base mismatch. In these experiments (in real time), the Current-Voltage behaviour of the device were monitored and recorded by a source measure unit (Hewlett Packard 4140B). The current measurements were carried out at room temperature in a potential range of -1 V to 1 V with a scan rate of 0.01 V/s^{-1}. Approximately, 200 current measurements were taken over the -0.1 V to 0.1V potential range. Ambient temperature was used to execute all experiments in an endeavour to keep the process as simple as possible. In order to remove the non-hybridized ssDNA, after each hybridisation, the graphene/SiO_2/Si was rinsed carefully several times with distilled water. It was then allowed to air dry and be re-used. Electronic detection of DNA hybridisation by the ssDNA/graphene/SiO_2/Si in this study depends predominantly on the successful immobilisation of the ssDNA probe to the graphene transducer and the inherent complementary affinity of the probe for its specific target DNA (Du *et al.*, 2012). Figure 6.3 illustrates the detection scheme of the sensor.

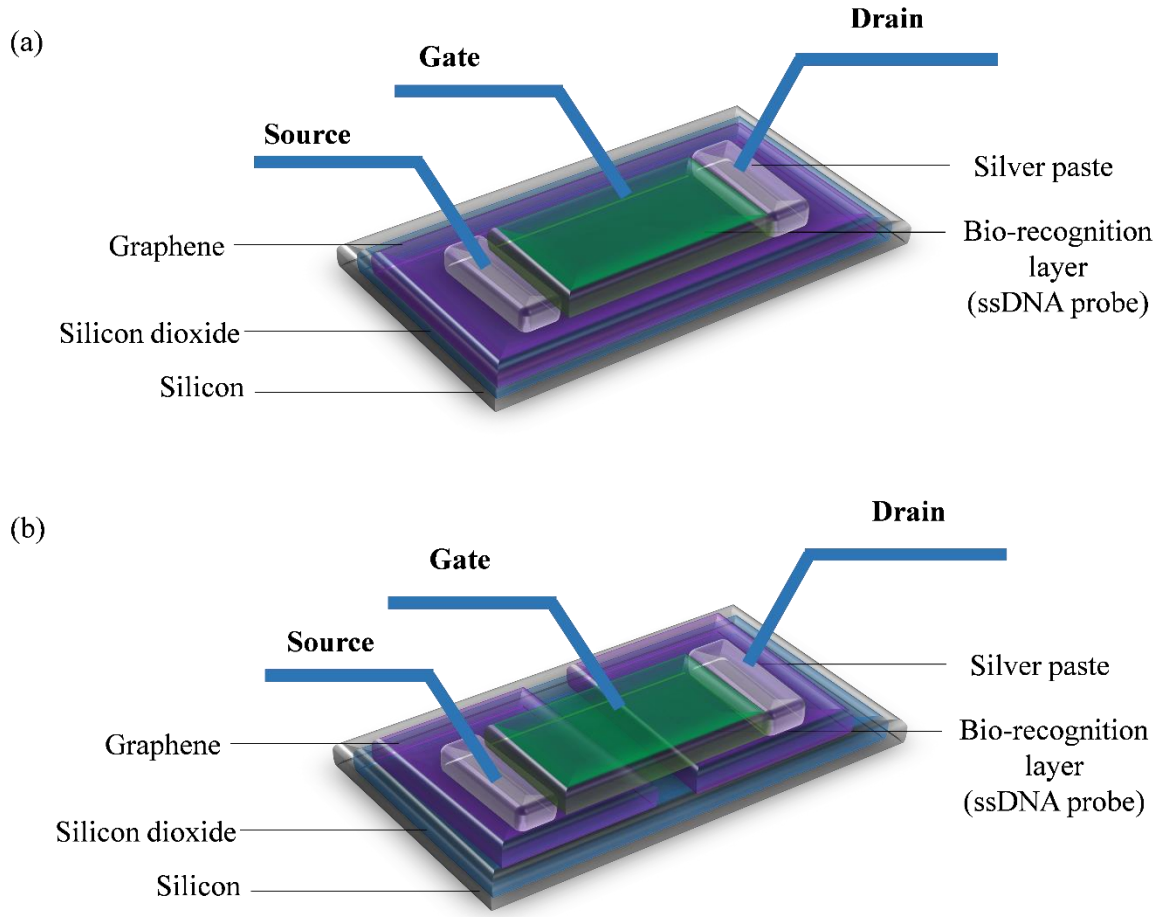

Figure 6.2 Schematic of the experimental system for two configurations of the ssDNA/graphene/SiO_2/Si sensor; (a) illustrates the resistors in parallel configuration while (b) illustrates the resistors in series configuration.

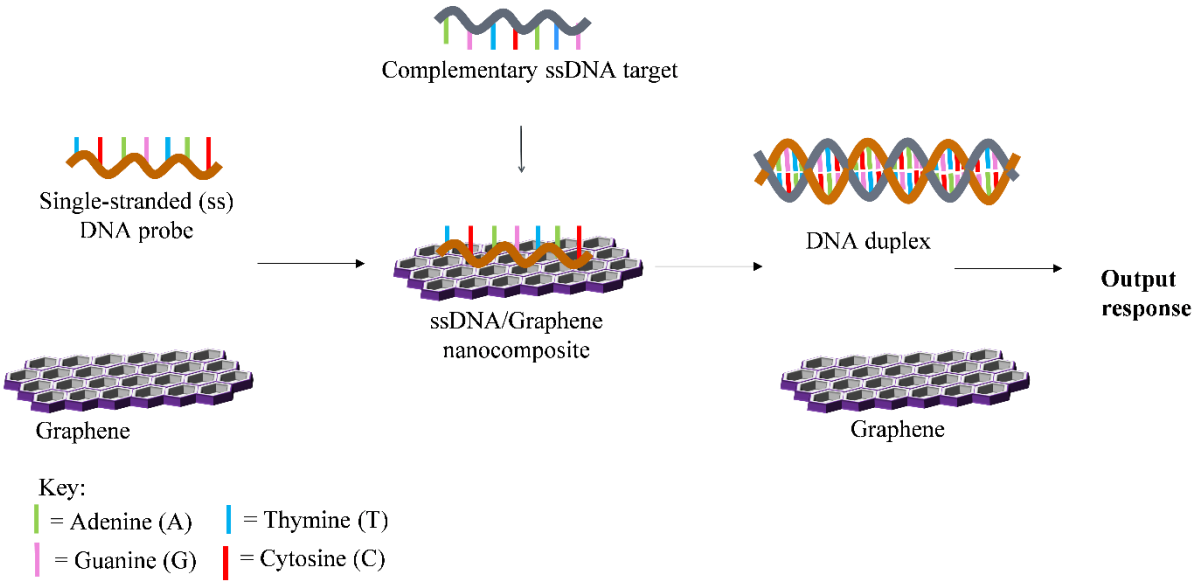

Figure 6.3 Schematic illustration of the label-free electronic detection of DNA hybridisation using graphene (Adapted from Du *et al*., 2012)

6.2.3 Integration of current-voltage measurements

Area under current-voltage curves [current= f (voltage)] was found through definite integration between the voltage = -1V and voltage =1V range. Computation of the area was performed on Microsoft Excel (2013) using Riemann sum approximation method (Abramowitz et al., 1966; Thompson *et al*., 2008). The area under the current-voltage curve signifies the magnitude of a quantity, Power (P), measured in watts (W) that relays the rate at which energy is transformed in a device.

6.3 Results and discussion

6.3.1 Current-voltage characteristics

The device, ssDNA/graphene/SiO_2/Si, exhibited a non-linear Current-Voltage response for both configurations before and after hybridisation (Figure 6.4a and b). This non-linear Current-Voltage characteristic behaviour suggests that the device is non-ohmic (Avouris *et al*., 1999; Lo *et al*., 2013). This asymmetric behaviour resembles a current-voltage relationship that is similar to that observed in diodes (Elbing *et al*., 2005; Grover and Moddel, 2012). From Figures 6.4, it can be deduced that the resistance of the as-described device before and after hybridisation with the complementary target, and triple-base mismatch increases as the voltage is applied in a dynamic constantly changing manner (Okahata *et al*., 1998; Cai *et al*., 2000). Nevertheless, the device configured in parallel (Figure 6.4 a) was observed to have low responsivity as no distinct difference was observed in the current of ssDNA/graphene/SiO_2 both before and after hybridisation with a complementary target DNA and the triple-base mismatch. The lack of response could be due to the transport of electrons through alternative pathways such as through the graphene (Merchant *et al*., 2010; Schneider *et al*., 2010; Postma, 2010). The device configured in series exhibited a higher responsivity (Figure 6.4 b).

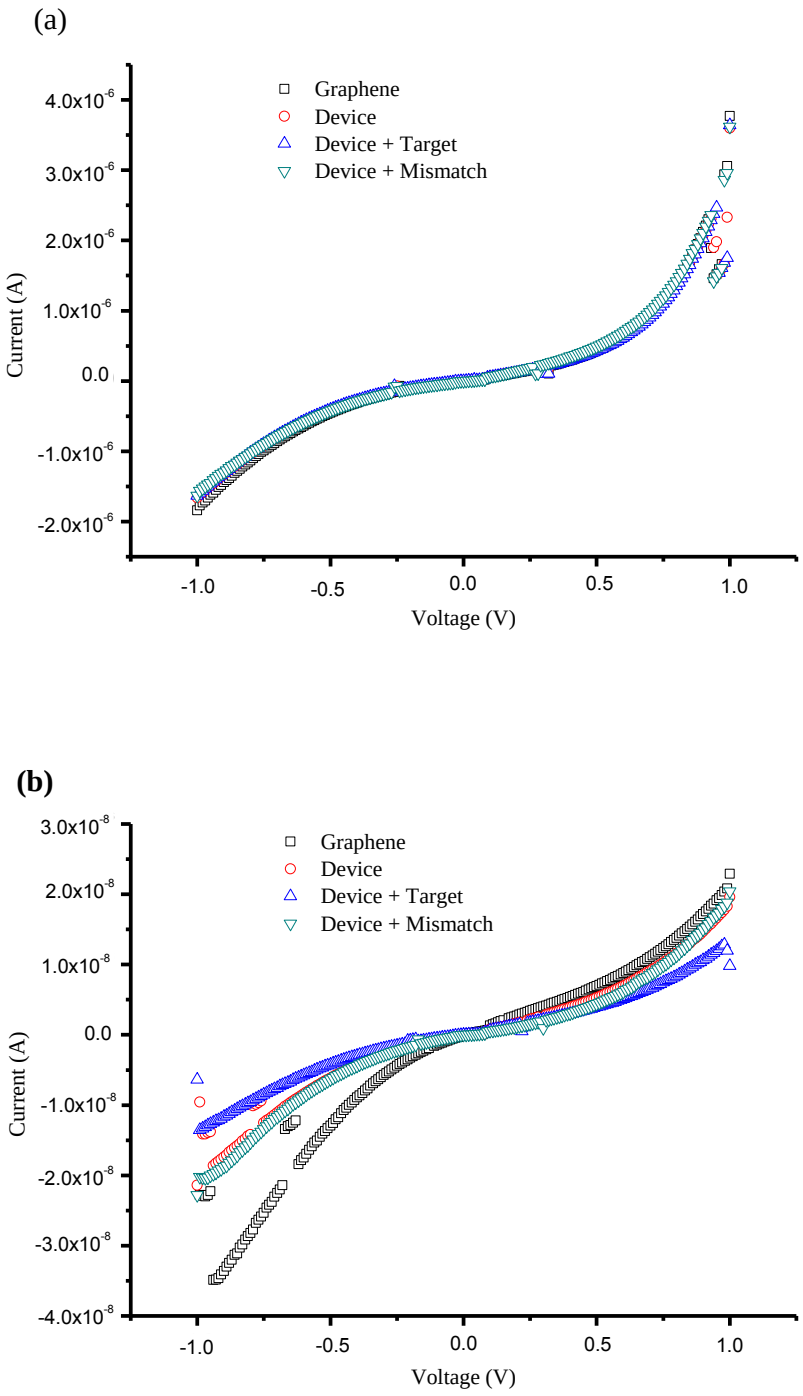

Figure 6.4 Electronic responses of the ssDNA/graphene/SiO_2/Si sensor before and after hybridisation. The graphs demonstrate the Current-Voltage curves for the

ssDNA/graphene/SiO_2/Si sensor configured in (a) parallel and (b) series. ssDNA/graphene/SiO_2/Si is the device

In the 0.4 V – 0.7 V range (Figure 6.5); upon hybridisation there is a significant decrease in the current responses in comparison with those of graphene and ssDNA/graphene/SiO_2/Si. It was perceived that the current of the ssDNA/graphene/SiO_2/Si decreased upon hybridisation with a complementary target. The reason for this could be attributed to DNA's excellent conducting properties (Dekker and Ratner, 2001). This decrease in the current indicates that the electron transfer rate was faster in ssDNA/graphene/SiO_2/Si but then decreased significantly when the device, ssDNA/graphene/SiO_2/Si, was hybridised with a complementary DNA strand (Lo *et al*., 2013). Although conflicting results have been reported regarding electronic properties of DNA (and the conductance of DNA is poorly understood), findings from this study are in agreement with reports on DNA possessing conducting properties (Braun *et al*., 1998; Yoo *et al*., 2001; Endres and Singh, 2004). If going by the suggestion Dekker and Ratner (2001) that DNA is a charge-carrying conductor with virtually no resistance, the decrease in current in this study suggests formation of dsDNA by the target DNA strand and the ssDNA probe on the bio-recognition layer of the graphene sensor. Due to the direct mathematical relationship between current and conductivity, formation of the dsDNA may have decreased the conductivity of the ssDNA/graphene/SiO_2/Si and dsDNA leaving the surface of the graphene as demonstrated in Figure 6.3. This would mean the DNA molecule no longer plays a role in facilitating electron transfer (Šponer *et al*., 2001; Xu *et al*., 2007).

When hybridised with the triple-base mismatch, it is observed that the current also decreased in comparison to the ssDNA/graphene/SiO_2/Si but was slightly higher than that observed for hybridisation with complementary target in the 0.4 – 0.7 V range (Figure 6.5). This infers an

increased conductivity, feasibly showing that ssDNA on the device did not hybridise fully with the triple-base mismatch. The DNA bases at the mismatched part of the dsDNA formed chain are not only exposed but those mismatched regions further folded over and are interacting with the graphene surface thus facilitating electron transfer (Dekker and Ratner, 2001; Šponer *et al.*, 2001; Xu *et al.*, 2007). The increased conductivity could also be due to possible field assisted charge injection that lowers the schottky barrier located at the silver paste and graphene contact in the device in this study (Cambell *et al.*, 1997; Cambell *et al.*, 1998). Nevertheless, data elucidate that the ssDNA/graphene/SiO_2 device in the series configuration can specifically and selectively discriminate between the complementary target and non-complementary mismatch.

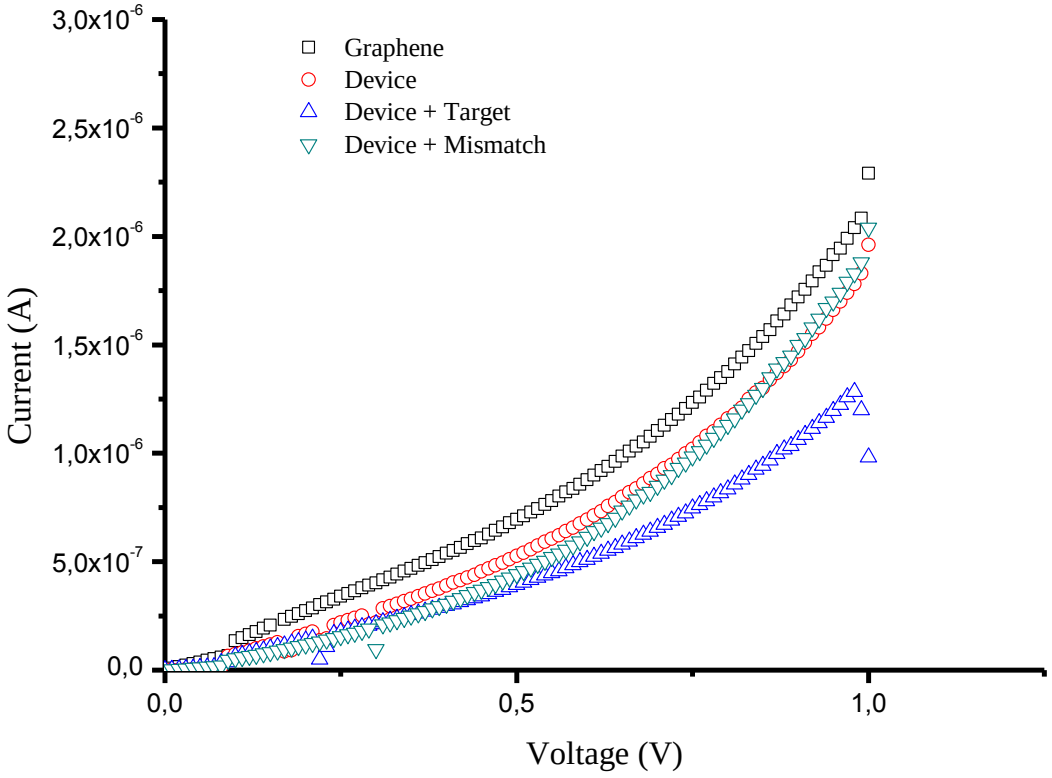

Figure 6.5 The Current-Voltage plot in the positive voltage (0 to 1 V) region of the ssDNA/graphene/SiO_2/Si sensor in the series configuration

Given that the device exhibited non-linear current voltage behaviour, the analysis was extended to the graphene-silicon interface in an attempt to understand the electronic transport properties of the device. This non-linear current-voltage characteristic behaviour can be described by the Schottky diode law presented in Equation 1.

$$I = I_{S\left[\exp\left(\frac{qV}{\eta kT}\right)-1\right]} \quad (1)$$

where I is the diode current, I_S is the reverse bias saturation current measured in ampere, q is the magnitude of electron charge in coulombs, V is the voltage across the diode measured in volts, η is the ideality factor, *k* is the Boltzmann constant presented in joules per kelvin, and T is the temperature measured in kelvin scale. I_s in the Schottky diode which is given by

$$I_S = AA^*T^2e^{-\frac{q\Phi_B}{kT}} \quad (2)$$

Where A = active area of the device. A^* = Richardson constant for the material in question. Φ_B = Schottky barrier height.

The Current-Voltage curves of only the device configured in series were fitted with the Schottky ideal diode equation to determine the ideality factor, η. Ideality factors greater than 2 were observed (Figure 6.6), which does not necessarily mean that the device is not ideal but that it is relatively imperfect as one would expect to find in graphene based devices. Furthermore, it must be noted that although ideal diodes should have an ideality factor, η = 1, there are not practical ideal devices. η values >2 indicate high series resistance in addition to recombination and generation. The η values in the range of ~1.3 to 30 have been reported for graphene diodes (Chen *et al.*, 2011; Miao *et al.*, 2012; Yim *et al.*, 2013). Graphene grown on copper foil such as the one used in this study, tends to contain impurities in a form of metal

residues from the copper substrate used during the production of the graphene (Kim *et al*., 2013). To realise an ideal behaviour, a defect free interface between graphene and the semiconductor (silicon) is necessary (Rajput *et al*., 2013; Shivaraman *et al*., 2012). A previous study identified inhomogeneity and impurities at the graphene and semiconductor interface as cause for the poor η values and non-ideality (Tongay *et al*., 2012). Therefore, the large ideality factors in this study could be attributed to the non-homogenous flow of recombination currents along the DNA-graphene interface ((Mamor, 2009; Rodrigues, 2007). It is also possible that the defect concentration induced in graphene are not only shallow levels but also high thus leading to trap assisted tunnelling (Choi *et al*., 2013; Roy *et al*., 2013). As can be observed in Figure 6.6, the current-voltage behaviour of the device in this study is non-linear and exhibit two distinct regions, a depletion region (circled regions in Figure 6.6) and an injection charge limited region (un-circled regions in Figure 6.6)(Moiz *et al*., 2016). These regions are visible in Figure 6.6 as logarithmic values of current are used. It can be observed that the transition from the depletion region recombination to the injection charge limited region is not direct. An indirect transition has been reported in public literature to be characteristic of traps distribution existence (Moiz et al., 2016). Therefore, this indirect transition from the two regions observed in this study further corroborates the possible occurrence of trap assisted tunnelling. It should be stressed that this aspect was not the focus of this study but it was carried out to provide insight to into the electronic transport at the DNA-graphene (i.e. biomolecule/nanomaterial) interface and the graphene-silicon (i.e. nanomaterial/substrate) interface during DNA hybridisation.

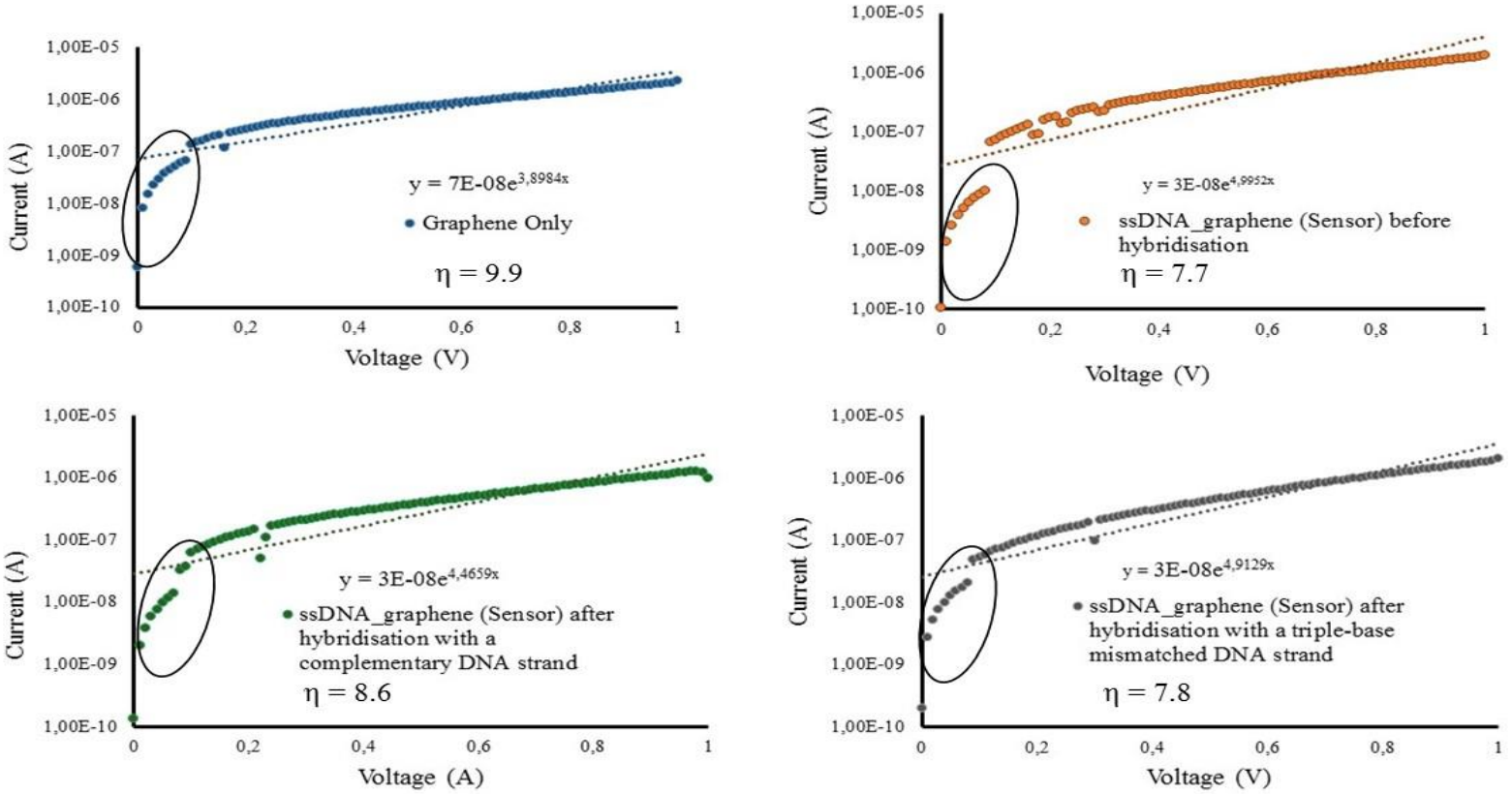

Figure 6.6 Current-Voltage Measurements Fitted with Diode Equation $I = I_S\left[exp\left(\frac{qV}{\eta kT}\right)-1\right]$ in the forward bias. Circled regions show the depletion region.

6.3.2 Electronic transport at the DNA-graphene interface

Electronic measurements expressed in terms of resistivity of two different electronic circuit configurations were examined. Significant differences in electronic response between the two electronic configurations were observed. One configuration showed a greater responsivity. Overall, it was noted that the parallel configuration (Figure 6.7 (a)) did not produce a good resolution between hybridisation reactions as the series configuration (Figure 6.7 (b)). Figure 6.7 shows the gate voltage dependent resistivity of pristine CVD-grown graphene, ssDNA coated graphene, and ssDNA coated graphene that is hybridised with complementary and mismatched ssDNA. The resistivity derived from current-voltage responses measured in 2-probe geometry using standard lock-in detection techniques. The Dirac point's back gate voltage (V_g) is identified by the maximum in the resistivity (Tan et al., 2007; Chen et al., 2008; Morozov *et al*, 2008).

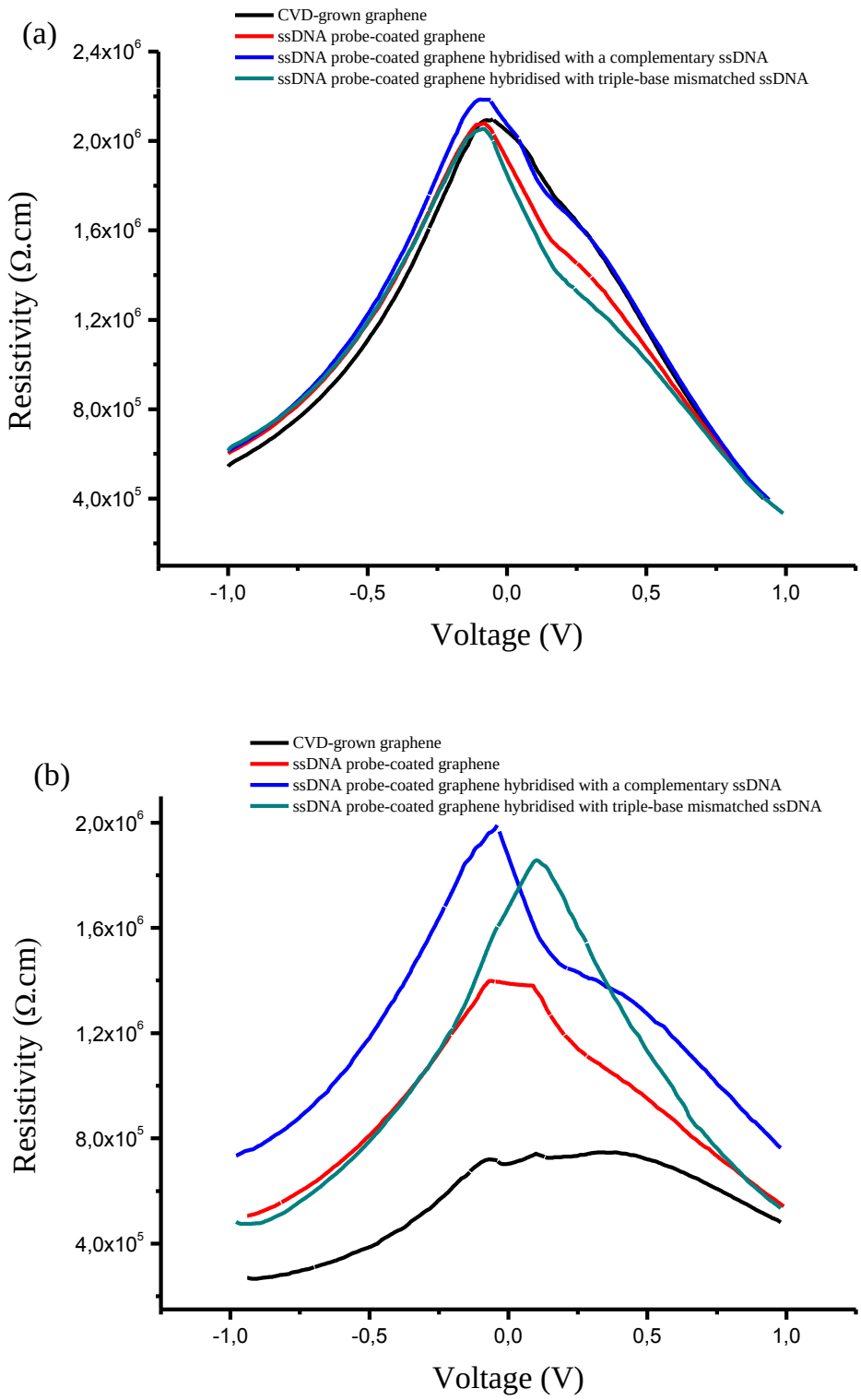

Figure 6.7 Gate voltage dependent resistivity of CVD-grown pristine graphene, ssDNA probe-coated graphene, ssDNA probe-coated graphene when hybridised with a complementary ssDNA and ssDNA probe-coated graphene is hybridised with triple-base mismatched ssDNA for (a) Parallel and (b) Series configurations

Gate voltage dependent resistivity values observed for adsorption and desorption reaction in both circuit configurations are summarised in Table 6.1. The Dirac point of pristine CVD-grown sample measured in the series and parallel circuit configurations was found to be V_g = −0.07 V and V_g = −0.05 V, respectively. These V_g values demonstrate an undoped nature of the graphene samples. In the series configuration, self-immobilisation of ssDNA probe on the CVD-grown graphene resulted in a small shift toward the less negative gate voltages, suggesting an increase in hole density as previously found by Lin *et al*. (2010). In addition, the observation is analogous to silicon complementary metal oxide semiconductor (CMOS) architectures when a negative gate potential is applied (Lin *et al*., 2010). The shift toward less negative V_g values observed in this study is also consistent with those observed by Kybert *et al*. (2014), which was described as a counteractive measure of the V_g to overcome the negative field induced by phosphate groups in single-stranded DNA. In the parallel configuration, self-immobilisation of ssDNA probe on the CVD-grown graphene resulted in a small shift towards more negative gate voltages. The shift towards more negative values has been reported in literature concerning the adsorption of DNA on graphene and Dong *et al*. (2011) attributed the shift to n-doping of graphene through its pi-pi interaction with electron rich aromatic rings of DNA nucleobases. In addition, this observation was also corroborated by Yin *et al*. (2012). However, it should be noted that similar more negative shifts have been attributed to p-doping (Mohanty and Berry, 2008; Lin *et al*., 2013), electrostatic gating (Artyukhin *et al*., 2006), and chemical gating (Lu *et al*., 2010).

Table 6.1 The gate voltage measured in Volts (V) at the Dirac point for CVD-grown pristine graphene, ssDNA probe-coated graphene, ssDNA probe-coated graphene when hybridised with a complementary ssDNA and ssDNA probe-coated graphene is hybridised with triple-base mismatched ssDNA

Material	Gate Voltage (V)	
	Series Circuit Configuration	Parallel Circuit Configuration
CVD-grown graphene	-0.07	-0.05
ssDNA probe-coated graphene	-0.04	-0.08
ssDNA probe-coated graphene hybridised with complementary strand	-0.04	-0.1
ssDNA probe-coated graphene hybridised with triple-base mismatched strand	0.09	-0.09

As depicted in Table 6.1, Hybridisation of the ssDNA coated graphene with a complementary DNA target shifted the Dirac point towards more negative gate voltage in the parallel configuration and remained in the same negative voltage in series configuration. Dirac points in the negative gate voltage indicate n-type doping during hybridisation with complementary targets (Yin *et al*., 2012). A p-type doping effect was observed for both configuration upon hybridisation of ssDNA coated graphene with a triple-base mismatched DNA target (Mohanty and Berry, 2008; Lin *et al*., 2013). This was indicated by the shift in the Dirac points towards less negative gate voltages. These electrical measurements are corroborated by Raman measurements as discussed in chapter 4. Hybridisation of the ssDNA coated graphene with a triple-base mismatched strands shifted the Dirac point towards more negative gate voltage in the parallel configuration and towards less negative potentials in series configuration.

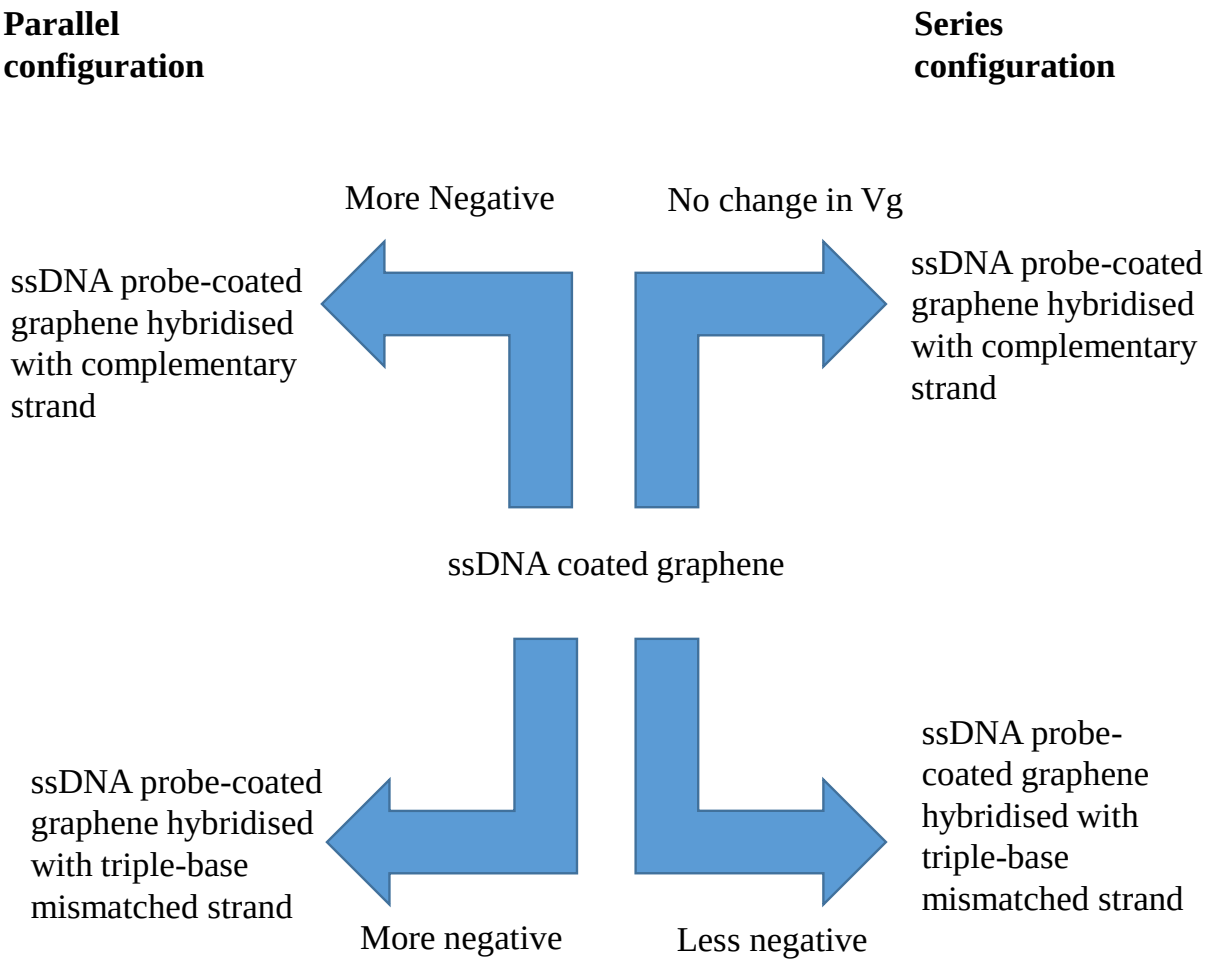

Figure 6.8 General trend observed in Gate voltage shifts of ssDNA probe-coated graphene when hybridised with a complementary ssDNA and ssDNA probe-coated graphene is hybridised with triple-base mismatched ssDNA in both parallel and series configurations

The hypothesis was that specific electronic configuration of the device affects the observed results. When electronic measurements expressed in terms of resistivity of two different electronic circuit configurations were examined, a significant differences in electronic response between the two electronic configurations were observed. Moreover, the trend as summarized in Figure 6.8 is not consistent between the two electronic configurations.

6.3.3 Geometric interpretation of current-voltage measurements

In order to represent the process of DNA adsorption, nature of DNA and DNA morphological changes during DNA hybridisation from current-voltage measurements, a new approach is proposed in this study. This method takes advantage of the computation of area in lieu of the maximum point (V_g), a technique that reduced noise-to-signal ratio, thereby smoothing experimental data error (Arujo and Sanchez, 1982). Dispersion effect has been known to influence current-voltage measurements in certain high mobility electronic devices, thereby resulting in inconsistent output conductance of the device (Golio *et al*., 1990; Meneghesso *et al*., 2004; Yan *et al*., 2011; Kayyalha and Chen 2015). However, dispersion effects have little effect on the area under the curve. If the extent of dispersion effect in the device changes between hybridisation reactions, then it is proposed that the area under the curve should be more accurate and reliable method of measurement (Hanley and McNeil, 1982; DeLong *et al*., 1988). In Table 6.2, the values of power obtained by using the method of area computation using Riemann method of integration and summation are summarised for adsorption and desorption reaction in both circuit configurations.

+

Table 6.2 The Power measured in Watts (W) at the Dirac point for CVD-grown pristine graphene, ssDNA probe-coated graphene, ssDNA probe-coated graphene when hybridised with a complementary ssDNA and ssDNA probe-coated graphene is hybridised with triple-base mismatched ssDNA

Material	Power (W)	
	Series Circuit Configuration	Parallel Circuit Configuration
CVD-grown graphene	6.09E-07	1.11E-07
ssDNA probe-coated graphene	6.86E-08	1.59E-07
ssDNA probe-coated graphene hybridised with complementary strand	3.90E-08	1.48E-07
ssDNA probe-coated graphene hybridised with triple-base mismatched strand	1.94E-07	1.99E-07

Using this simple integrative approach of geometric interpretation of current-voltage measurements, we found a consistent general trend in DNA hybridisation on graphene, a trend was not established using V_g values in this work and previous results reported in literature (Dong *et al*., 2010; Lu *et al*., 2010; Lin *et al*., 2013; Kybert *et al*., 2014). It was observed that in both parallel and series configuration; hybridisation of the ssDNA coated graphene with a complementary DNA target results in a decrease in power. When the ssDNA coated graphene was hybridised with triple-base mismatched strands, an increase in power was observed for both parallel and series configurations. This offers a consistent output electronic signal that deciphers selective and specific DNA hybridisation characteristics on graphene (Figure 6.9).

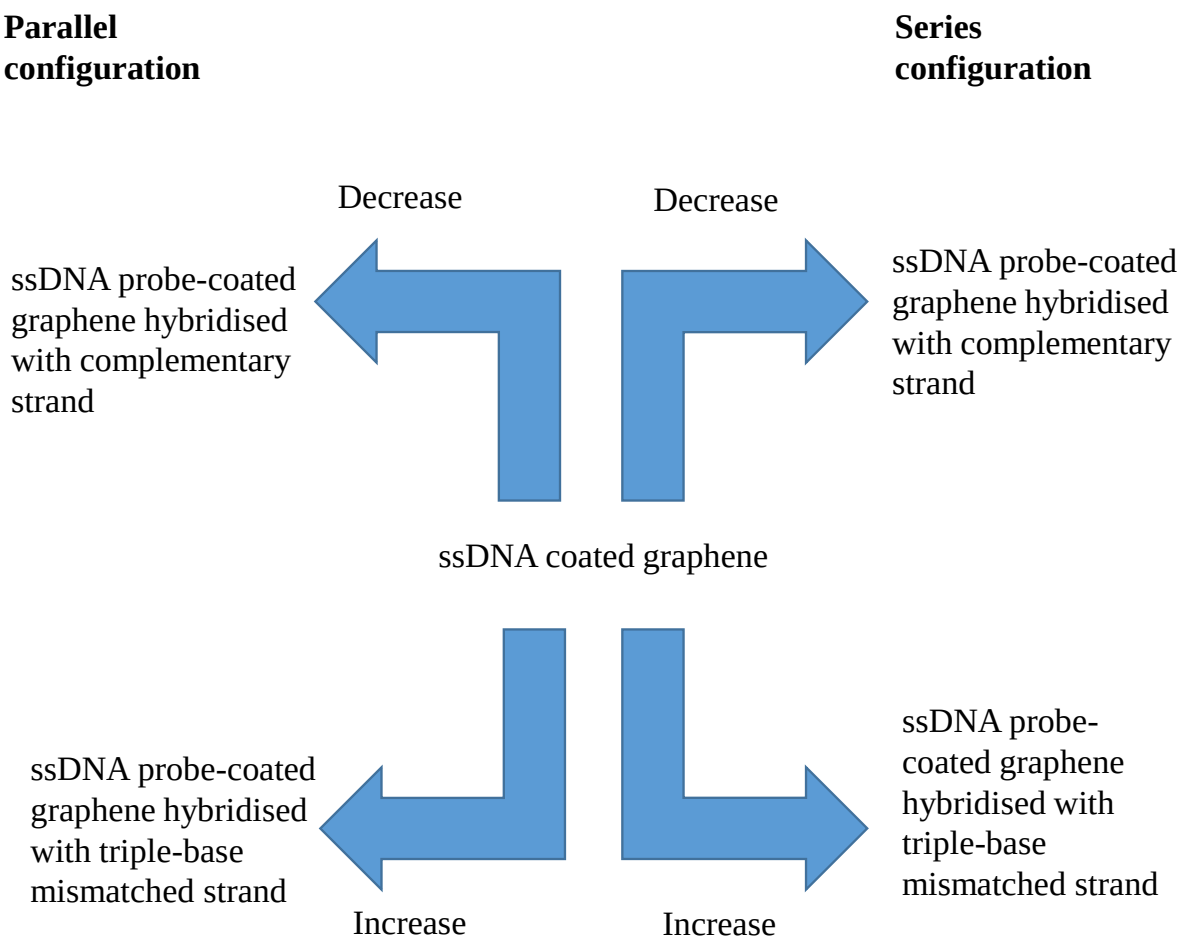

Figure 6.9 General trend observed in Power of the device, sDNA probe-coated graphene, when hybridised with a complementary ssDNA and ssDNA probe-coated graphene is hybridised with triple-base mismatched ssDNA in both parallel and series configurations

6.4 Summary

A simple integrative approach of geometric interpretation of current-voltage measurements was presented. Using this method of evaluating current-voltage measurements, we found a general trend in DNA hybridisation on graphene, a trend that could not be established using V_g values in this work and previous work reported in literature. When Dirac point's gate voltage (V_g) from current-voltage measured characteristics was used as output electronic signal of electronic events and DNA conformational changes during DNA detection on

graphene; inconsistencies in V_g values between the two devices of different electronic configurations (parallel and series) were observed. The Dirac point shifted towards more negative gate voltage in the parallel configuration and remained in the same negative voltage in series configuration upon hybridisation of the ssDNA coated graphene with a complementary DNA target. When ssDNA coated graphene was hybridised with a triple-base mismatched strands, the Dirac point shifted towards more negative gate voltages in the parallel configuration and toward less negative potentials in series configuration. However, consistent output electronic signal are observed when a parameter, Power obtained from current-voltage measurements is used to representing electronic events and DNA conformational changes during DNA detection on graphene. It was observed that in both parallel and series configuration; hybridisation of the ssDNA coated graphene with a complementary DNA target results in a decrease in power.

When the ssDNA coated graphene was hybridised with triple-base mismatched strands, an increase in power was observed for both parallel and series configurations. This offers a consistent output electronic signal that deciphers selective and specific DNA hybridisation characteristics on graphene. The power represents the electronic charge transfer events and conformational changes in DNA structure effects holistically offering consistent trend in signal output regardless of the design of the device. However, it is noted that this method was performed on only two device configuration in this study. Therefore, further exploration of variability in this output signal is required. Benchmark studies using this new method of evaluating current-voltage measurements in graphene based DNA sensors need to be explored for multiple biosensor systems by multiple laboratories and compared to biosensors that are commercially available in the market.

Chapter 7 Conclusions and recommendations

7.1 Conclusions

The findings from these studies have brought about the following novel contributions to research related to the development of label-free DNA-graphene based electrochemical/electrical biosensors through the illumination and expansion of the knowledge of interactions between DNA and graphene:

- The electronic structure of graphene as it uniquely evolved (during hetero-DNA hybridisation) and is altered as a result of DNA interaction with graphene is reported for the first time in this work. **N**ovel graphene parameters that evolve during DNA self-immobilisation and hybridisation on graphene were identified and defined. Self-immobilisation of ssDNA on graphene resulted in the disappearance of the small D peak, red shift of the G peak frequency and reduction of 2D peak intensity. Further shifts in the G and 2D peak positions demonstrated selectivity of graphene in DNA detection and display distinct doping of graphene by DNA clusters formed during DNA hybridisation. During formation of a perfectly matched dsDNA, CVD-grown graphene appeared to be n-type doped, and p-type doped formation of triple-base mismatched dsDNA. These Raman fingerprints offer a non-destructive reliable method for spatial and temporal monitoring of DNA hybridisation on graphene locally and is a step towards better understanding of the interactions between graphene and DNA.
- A number of practical analytical applications of various forms that use DNA-graphene interfaces for detection of DNA hybridisation have been demonstrated in open literature. But commercialisation of such devices is limited since detection relies on transducer converting the bio-recognition event (i.e. DNA hybridisation) into a

readable signal, but this change in DNA conformation is assumed, and really the nature of the change is unknown. From the study of DNA conformational changes on graphene, provided evidence that DNA adsorption and desorption on graphene not only occurs but that it is accompanied distinct DNA structural and conformational changes as was assumed in open literature. However, the findings of the study suggest that more complex interactions exist between the desorbed double stranded DNA molecules formed during hybridisation. The results suggested that the denatured region of the dsDNA chain further fold over and interact with the graphene surface after desorption. Complexities in the XRD pattern of ssDNA-coated graphene when hybridised with a triple-base mismatch between $2\theta = 11°$ to around $2\theta = 40°$ further corroborated these findings. Moreover, it was found that DNA hybridisation graphene (solid-phase hybridisation) may not be as effective as that performed in solution. This was evidenced by the coverage of the signature DNA absorbance wavelength peak at known to be at 260 nm. A peak at 260 nm was easily seen when DNA hybridisation of ssDNA and its complementary target strand was performed in solution in the absence of graphene. A research line concerned with optimisation of DNA adsorption and desorption mechanisms on graphene to avoid false positive results in graphene-based DNA sensing systems is opened by the research findings of this study.

- For a bio-sensing technology to have wide range applicability and operated by individuals with little to no laboratory training or experience, it is critical that the output signal of the device is not only easy-to-read and understand, but that it is consistent. In this study, a simple integrative approach of geometric interpretation of current-voltage measurements as means to decipher graphene electronic properties and conformational changes in DNA structure that occur in DNA-graphene interfaces be deciphered into an easy to read consistent electronic signal was proposed and

presented. Using this method of evaluating current-voltage measurements, a general trend in DNA hybridisation on graphene was found, a trend that is not established using V_g values in this work and previous work reported in literature. When current-voltage measurements are presented as the parameter Power, trends in electronic events and DNA conformational changes during DNA detection on graphene are consistent irrespective of the design of the device. It was observed that in both parallel and series configuration; hybridisation of the ssDNA coated graphene with a complementary DNA target results in a decreased in Power but increased upon hybridisation of the ssDNA coated graphene with a DNA target that contained mismatches. These findings provide the field a different approach in which current-voltage measurements can be viewed and interpreted.

These novel insightful contributions to the knowledge and advancement of the field, have been presented in a form of posters and oral presentations at local and international conferences, seminars and workshops. A list of such presentations on this work is presented in Appendix B. Further communication in the field of biosensors, bioelectronics and nanotechnology as articles in international peer reviewed scientific journals can be found in Appendix C.

7.2 Recommendations

Although this study provided a much needed fundamental conceptualisation of interactions between DNA and graphene, and presents distinct fingerprints of both the effects that DNA and Graphene have on one another, there is room for further development. Further work should explore both graphene characteristics and DNA

structural transitions as they uniquely evolve during DNA adsorption and desorption on graphene for detection of hetero-DNA hybridisation using DNA strands of various lengths of nucleobases and percentages of nucleobase compositions.

Regarding the geometric interpretation of current-voltage measurements as a means to decipher interactions between graphene and DNA into a consistent readable output signal, further research efforts on the variability in the output signal when presented as power is required to provide a more solid standard method of evaluation. Benchmark studies using this new method of evaluating current-voltage measurements in graphene based DNA sensors should be investigated for multiple biosensor systems by researchers and the results compared to biosensors that are commercially available in the market.

References

Abd-Elsalam, K.A., 2003. Bioinformatic tools and guideline for PCR primer design. *African Journal of Biotechnology*, *2*(5), pp.91-95.

Abramowitz, M. and Stegun, I.A., 1966. Handbook of mathematical functions. *Applied Mathematics Series*, *55*(62), p.39.

Ahmed, F. and Rodrigues, D.F., 2013. Investigation of acute effects of graphene oxide on wastewater microbial community: a case study. *Journal of Hazardous Materials*, *256*, pp.33-39.

Ahmed, F.E., 2002. Detection of genetically modified organisms in foods. *Trends in Biotechnology*, *20*(5), pp.215-223.

Ahmed, T., Kilina, S., Das, T., Haraldsen, J.T., Rehr, J.J. and Balatsky, A.V., 2012. Electronic fingerprints of DNA bases on graphene. *Nano Letters*, *12*(2), pp.927-931.

Akca, S., Foroughi, A., Frochtzwajg, D. and Postma, H.W.C., 2011. Competing interactions in DNA assembly on graphene. *PLoS One*, *6*(4), p.e18442.

Aliofkhazraei, M., Ali, N., Milne, W.I., Ozkan, C.S., Mitura, S. and Gervasoni, J.L. eds., 2016. *Graphene Science Handbook: Applications and Industrialization*. Crc Press. pp 1-30.

Allen, M.J., Tung, V.C. and Kaner, R.B., 2009. Honeycomb carbon: a review of graphene. *Chemical Reviews*, *110*(1), pp.132-145.

Alshehri, M.H., Cox, B.J. and Hill, J.M., 2013. DNA adsorption on graphene. *The European Physical Journal D*, *67*(11), pp.1-9.

Angulo, A.M. and Gil, J.M., 2007. Risk perception and consumer willingness to pay for certified beef in Spain. *Food Quality and Preference*, *18*(8), pp.1106-1117.

Anklam, E., 1999. The validation of methods based on polymerase chain reaction for the detection of genetically modified organisms in food. *Analytica Chimica Acta*, *393*(1), pp.177-179.

Artyukhin, A.B., Stadermann, M., Friddle, R.W., Stroeve, P., Bakajin, O. and Noy, A., 2006. Controlled electrostatic gating of carbon nanotube FET devices. *Nano letters*, *6*(9), pp.2080-2085.

Araujo, G.L. and Sanchez, E., 1982. A new method for experimental determination of the series resistance of a solar cell. *IEEE Transactions on Electron Devices*, *29*(10), pp.1511-1513.

Artyukhin, A.B., Stadermann, M., Friddle, R.W., Stroeve, P., Bakajin, O. and Noy, A., 2006. Controlled electrostatic gating of carbon nanotube FET devices. *Nano letters*, *6*(9), pp.2080-2085.

Avouris, P., Hertel, T., Martel, R., Schmidt, T.H.R.H.S., Shea, H.R. and Walkup, R.E., 1999. Carbon nanotubes: nanomechanics, manipulation, and electronic devices. *Applied Surface Science*, *141*(3), pp.201-209.

Badertscher, M., Bühlmann, P. and Pretsch, E., 2009. *Structure determination of organic compounds*. Springer Berlin Heidelberg.

Bae, S., Kim, H., Lee, Y., Xu, X., Park, J.S., Zheng, Y., Balakrishnan, J., Lei, T., Kim, H.R., Song, Y.I. and Kim, Y.J., 2010. Roll-to-roll production of 30-inch graphene films for transparent electrodes. *Nature Nanotechnology*, *5*(8), pp.574-578.

Balandin, A.A., 2011. Thermal properties of graphene and nanostructured carbon materials. *Nature Materials*, *10*(8), pp.569-581.

Balandin, A.A., Ghosh, S., Bao, W., Calizo, I., Teweldebrhan, D., Miao, F. and Lau, C.N., 2008. Superior thermal conductivity of single-layer graphene. *Nano Letters*, *8*(3), pp.902-907.

Bardaki, C., Kourouthanassis, P. and Pramatari, K., 2011. Modeling the information completeness of object tracking systems. *The Journal of Strategic Information Systems*, *20*(3), pp.268-282.

Batchelor-McAuley, C., Wildgoose, G.G. and Compton, R.G., 2009. The physicochemical aspects of DNA sensing using electrochemical methods. *Biosensors and Bioelectronics*, *24*(11), pp.3183-3190.

Benesi, H.A. and Hildebrand, J.H., 1949. A spectrophotometric investigation of the interaction of iodine with aromatic hydrocarbons. *Journal of the American Chemical Society*, *71*(8), pp.2703-2707.

Benjaphokee, S., Koedrith, P., Auesukaree, C., Asvarak, T., Sugiyama, M., Kaneko, Y., Boonchird, C. and Harashima, S., 2012. CDC19 encoding pyruvate kinase is important for high-temperature tolerance in Saccharomyces cerevisiae. *New Biotechnology*, *29*(2), pp.166-176.

Benvidi, A., Rajabzadeh, N., Zahedi, H.M., Mazloum-Ardakani, M., Heidari, M.M. and Hosseinzadeh, L., 2015. Simple and label-free detection of DNA hybridization on a modified graphene nanosheets electrode. *Talanta*, *137*, pp.80-86.

Berg, L., 2004. Trust in food in the age of mad cow disease: a comparative study of consumers' evaluation of food safety in Belgium, Britain and Norway. *Appetite*, *42*(1), pp.21-32.

Berger, C., Song, Z., Li, X., Wu, X., Brown, N., Naud, C., Mayou, D., Li, T., Hass, J., Marchenkov, A.N. and Conrad, E.H., 2006. Electronic confinement and coherence in patterned epitaxial graphene. *Science*, *312*(5777), pp.1191-1196.

Bertheau, Y., Davison, J. and Kobilinsky, A., 2005. Key issues and open questions in GMO controls. *Co-existence between GM and non-GM based agricultural supply chains*, p.111.

Bhattacharya, S. and Mandal, S.S., 1997. Interaction of surfactants with DNA. Role of hydrophobicity and surface charge on intercalation and DNA melting. *Biochimica et Biophysica Acta (BBA)-Biomembranes*, *1323*(1), pp.29-44.

Bo, Y., Wang, W., Qi, J. and Huang, S., 2011. A DNA biosensor based on graphene paste electrode modified with Prussian blue and chitosan. *Analyst*, *136*(9), pp.1946-1951.

Bonanni, A. and Del Valle, M., 2010. Use of nanomaterials for impedimetric DNA sensors: a review. *Analytica Chimica Acta*, *678*(1), pp.7-17.

Bora, U., Sett, A. and Singh, D., 2013. Nucleic acid based biosensors for clinical applications. *Biosensors Journal*, *2013, 2(1)*, pp.1-8.

Branton, D., Deamer, D.W., Marziali, A., Bayley, H., Benner, S.A., Butler, T., Di Ventra, M., Garaj, S., Hibbs, A., Huang, X. and Jovanovich, S.B., 2008. The potential and challenges of nanopore sequencing. *Nature Biotechnology*, *26*(10), pp.1146-1153.

Braun, E., Eichen, Y., Sivan, U. and Ben-Yoseph, G., 1998. DNA-templated assembly and electrode attachment of a conducting silver wire. *Nature*, *391*(6669), pp.775-778.

Breslauer, K.J., Frank, R., Blöcker, H. and Marky, L.A., 1986. Predicting DNA duplex stability from the base sequence. *Proceedings of the National Academy of Sciences*, *83*(11), pp.3746-3750.

Cai, L., Tabata, H. and Kawai, T., 2000. Self-assembled DNA networks and their electrical conductivity. *Applied Physics Letters*, *77*(19), pp.3105-3106.

Calizo, I., Balandin, A.A., Bao, W., Miao, F. and Lau, C.N., 2007b. Temperature dependence of the Raman spectra of graphene and graphene multilayers. *Nano Letters*, *7*(9), pp.2645-2649.

Calizo, I., Miao, F., Bao, W., Lau, C.N. and Balandin, A.A., 2007a. Variable temperature Raman microscopy as a nanometrology tool for graphene layers and graphene-based devices. *Applied Physics Letters*, *91*(7), pp.71913-71913.

Campbell, I.H., Davids, P.S., Smith, D.L., Barashkov, N.N. and Ferraris, J.P., 1998. The Schottky energy barrier dependence of charge injection in organic light-emitting diodes. *Applied Physics Letters*, *72*(15), pp.1863-1865.

Campbell, I.H., Kress, J.D., Martin, R.L., Smith, D.L., Barashkov, N.N. and Ferraris, J.P., 1997. Controlling charge injection in organic electronic devices using self-assembled monolayers. *Applied Physics Letters*, *71*(24), pp.3528-3530.

Carloni, A. and Turner, A.P., 2011. Bioprocess monitoring. *Encyclopedia of Industrial Biotechnology*.

Casiraghi, C., 2009. Doping dependence of the Raman peaks intensity of graphene close to the Dirac point. *Physical Review B*, *80*(23), p.233407.

Casiraghi, C., Hartschuh, A., Lidorikis, E., Qian, H., Harutyunyan, H., Gokus, T., Novoselov, K.S. and Ferrari, A.C., 2007. Rayleigh imaging of graphene and graphene layers. *Nano Letters*, *7*(9), pp.2711-2717.

Casiraghi, C., Pisana, S., Novoselov, K.S., Geim, A.K. and Ferrari, A.C., 2007. Raman fingerprint of charged impurities in graphene. *Applied Physics Letters*, *91*(23), p.233108.

Cederquist, K.B. and Keating, C.D., 2009. Curvature effects in DNA: Au nanoparticle conjugates. *Acs Nano*, *3*(2), pp.256-260.

Chen, C., Wang, W., Ge, J. and Zhao, X.S., 2009. Kinetics and thermodynamics of DNA hybridization on gold nanoparticles. *Nucleic Acids Research*, *37*(11), pp.3756-3765.

Chen, C.C., Aykol, M., Chang, C.C., Levi, A.F.J. and Cronin, S.B., 2011. Graphene-silicon Schottky diodes. *Nano Letters*, *11*(5), pp.1863-1867.

Chen, D., Tang, L. and Li, J., 2010. Graphene-based materials in electrochemistry. *Chemical Society Reviews*, *39*(8), pp.3157-3180.

Chen, F., Qing, Q., Xia, J., Li, J. and Tao, N., 2009. Electrochemical gate-controlled charge transport in graphene in ionic liquid and aqueous solution. *Journal of the American Chemical Society*, *131*(29), pp.9908-9909.

Chen, F., Xia, J. and Tao, N., 2009. Ionic screening of charged-impurity scattering in graphene. *Nano Letters*, *9*(4), pp.1621-1625.

Chen, J., Chen, L., Wang, Y. and Chen, S., 2014. Molecular dynamics simulations of the adsorption of DNA segments onto graphene oxide. *Journal of Physics D: Applied Physics*, *47*(50), p.505401.

Chen, J.H., Jang, C., Adam, S., Fuhrer, M.S., Williams, E.D. and Ishigami, M., 2008. Charged-impurity scattering in graphene. *Nature Physics*, *4*(5), pp.377-381.

Chen, S., Li, Q., Zhang, Q., Qu, Y., Ji, H., Ruoff, R.S. and Cai, W., 2012. Thermal conductivity measurements of suspended graphene with and without wrinkles by micro-Raman mapping. Nanotechnology, 23(36), p.365701.

Choi, M.S., Lee, G.H., Yu, Y.J., Lee, D.Y., Lee, S.H., Kim, P., Hone, J. and Yoo, W.J., 2013. Controlled charge trapping by molybdenum disulphide and graphene in ultrathin heterostructured memory devices. *Nature Communications*, *4*, p.1624.

Clark, L.C. and Lyons, C., 1962. Electrode systems for continuous monitoring in cardiovascular surgery. *Annals of the New York Academy of Sciences*, *102*(1), pp.29-45.

Cohen, J., 1988. Statistical power analysis for the behavioral sciences Lawrence Earlbaum Associates. *Hillsdale, NJ*, pp.20-26.

Cohen-Karni, T., Qing, Q., Li, Q., Fang, Y. and Lieber, C.M., 2010. Graphene and nanowire transistors for cellular interfaces and electrical recording. *Nano Letters*, *10*(3), pp.1098-1102.

Compton, O.C. and Nguyen, S.T., 2010. Graphene Oxide, Highly Reduced Graphene Oxide, and Graphene: Versatile Building Blocks for Carbon-Based Materials. *Small*, *6*(6), pp.711-723.

Cortijo, A. and Vozmediano, M.A., 2007. Effects of topological defects and local curvature on the electronic properties of planar graphene. *Nuclear Physics B*, *763*(3), pp.293-308.

Costa, J., Mafra, I. and Oliveira, M.B.P., 2012. Advances in vegetable oil authentication by DNA-based markers. *Trends in food science & technology*, *26*(1), pp.43-55.Dandy, D.S., Wu, P., and Grainger, D.W., 2007. Array feature size influences nucleic acid surface capture in DNA microarrays. Proceedings of the National Academy of Sciences of the United States of America, 104: 8223-8228.

Cullity, B.D. and Stock, S.R., 1978. Diffraction. II. Intensities of diffracted beams. *Elements of X-ray Diffraction, 2nd ed.(Addison-Wesley, Reading, MA, 1978)*, pp.102-111.

Cullity, B.D. and Weymouth, J.W., 1957. Elements of X-ray Diffraction. *American Journal of Physics*, *25*(6), pp.394-395.

Das, A., Pisana, S., Chakraborty, B., Piscanec, S., Saha, S.K., Waghmare, U.V., Novoselov, K.S., Krishnamurthy, H.R., Geim, A.K., Ferrari, A.C. and Sood, A.K., 2008. Monitoring dopants by Raman scattering in an electrochemically top-gated graphene transistor. *Nature Nanotechnology*, *3*(4), pp.210-215.

Das, A., Pisana, S., Piscanec, S., Chakraborty, B., Saha, S.K., Waghmare, U.V., Yiang, R., Krishnamurhthy, H.R., Geim, A.K., Ferrari, A.C. and Sood, A.K., 2007. Electrochemically top gated graphene: Monitoring dopants by Raman scattering. *arXiv preprint arXiv:0709.1174*.

Das, A., Sood, A.K., Maiti, P.K., Das, M., Varadarajan, R. and Rao, C.N.R., 2008. Binding of nucleobases with single-walled carbon nanotubes: Theory and experiment. *Chemical Physics Letters*, *453*(4), pp.266-273.

Deamer, D., Akeson, M. and Branton, D., 2016. Three decades of nanopore sequencing. *Nature Biotechnology*, *34*(5), pp.518-524.

Dean, N., Murphy, T.B. and Downey, G., 2006. Using unlabelled data to update classification rules with applications in food authenticity studies. *Journal of the Royal Statistical Society: Series C (Applied Statistics)*, *55*(1), pp.1-14.

Dekker, C. and Ratner, M., 2001. Electronic properties of DNA. *Physics World*, *14*(8), p.29.

DeLong, E.R., DeLong, D.M. and Clarke-Pearson, D.L., 1988. Comparing the areas under two or more correlated receiver operating characteristic curves: a nonparametric approach. *Biometrics*, pp.837-845.

DeVoe, H., 1969. The theory of hypochromism of biopolymers: calculated spectra for DNA. *Annals of the New York Academy of Sciences*, *158*(1), pp.298-307.

Dikin D.A., Stankovich, S., Zimney E.J., Piner, R.D., Dommett, G.H.B,, Evmenenko, G., Nguyen S.T., and Ruoff, R.S., 2007. Preparation and Characterisation of Graphene Oxide. *Nature*, *448(7152)*, pp. 457460.

Domínguez-Renedo, O., Alonso-Lomillo, M.A. and Arcos-Martínez, M.J., 2007. Disposable electrochemical biosensors in microbiology. *Talanta*, *73*, pp.202-219.

Dong, X., Shi, Y., Huang, W., Chen, P. and Li, L.J., 2010. Electrical detection of DNA hybridization with single-base specificity using transistors based on CVD-grown graphene sheets. *Advanced Materials*, *22*(14), pp.1649-1653.

Dooley, J.S.G., 1994. Nucleic acid probes for the food industry. *Biotechnology Advances*, *12*(4), pp.669-677.

Drummond, T.G., Hill, M.G. and Barton, J.K., 2003. Electrochemical DNA sensors. *Nature Biotechnology*, *21*(10), pp.1192-1199.

Du, M., Yang, T., Li, X. and Jiao, K., 2012. Fabrication of DNA/graphene/polyaniline nanocomplex for label-free voltammetric detection of DNA hybridization. *Talanta*, *88*, pp.439-444.

Duch, M.C., Budinger, G.S., Liang, Y.T., Soberanes, S., Urich, D., Chiarella, S.E., Campochiaro, L.A., Gonzalez, A., Chandel, N.S., Hersam, M.C. and Mutlu, G.M., 2011. Minimizing oxidation and stable nanoscale dispersion improves the biocompatibility of graphene in the lung. *Nano Letters*, *11*(12), pp.5201-5207.

Eda, G., Fanchini, G. and Chhowalla, M., 2008. Large-area ultrathin films of reduced graphene oxide as a transparent and flexible electronic material. *Nature Nanotechnology*, *3*(5), pp.270-274.

Elbing, M., Ochs, R., Koentopp, M., Fischer, M., von Hänisch, C., Weigend, F., Evers, F., Weber, H.B. and Mayor, M., 2005. A single-molecule diode. *Proceedings of the National Academy of Sciences of the United States of America*, *102*(25), pp.8815-8820.

Elias, D.C., Nair, R.R., Mohiuddin, T.M.G., Morozov, S.V., Blake, P., Halsall, M.P., Ferrari, A.C., Boukhvalov, D.W., Katsnelson, M.I., Geim, A.K. and Novoselov, K.S., 2009. Control of graphene's properties by reversible hydrogenation: evidence for graphane. *Science*, *323*(5914), pp.610-613.

Elsanhoty, R.M., Ramadan, M.F. and Jany, K.D., 2011. DNA extraction methods for detecting genetically modified foods: A comparative study. *Food Chemistry*, *126*(4), pp.1883-1889.

Elstner, M., Hobza, P., Frauenheim, T., Suhai, S. and Kaxiras, E., 2001. Hydrogen bonding and stacking interactions of nucleic acid base pairs: a density-functional-theory based treatment. *The Journal of Chemical Physics*, *114*(12), pp.5149-5155.

Emtsev, K.V., Bostwick, A., Horn, K., Jobst, J., Kellogg, G.L., Ley, L., McChesney, J.L., Ohta, T., Reshanov, S.A., Röhrl, J. and Rotenberg, E., 2009. Towards wafer-size graphene layers by atmospheric pressure graphitization of silicon carbide. *Nature materials*, *8*(3), pp.203-207.

Feng, L., Zhang, S., and Liu, Z. Graphene based gene transfection. *Nanoscale*, 2011, 3, 1252-1257.

Endres, R.G., Cox, D.L. and Singh, R.R., 2004. Colloquium: The quest for high-conductance DNA. *Reviews of Modern Physics*, *76*(1), p.195.

Feng, L. and Liu, Z., 2011. Graphene in biomedicine: opportunities and challenges. *Nanomedicine*, *6*(2), pp.317-324.

Ferrari, A.C. and Basko, D.M., 2013. Raman spectroscopy as a versatile tool for studying the properties of graphene. *Nature Nanotechnology*, *8*(4), pp.235-246.

Ferrari, A.C. and Robertson, J., 2004. Raman spectroscopy of amorphous, nanostructured, diamond–like carbon, and nanodiamond. *Philosophical Transactions of the Royal Society of London A: Mathematical, Physical and Engineering Sciences*, *362*(1824), pp.2477-2512.

Ferrari, A.C., 2007. Raman spectroscopy of graphene and graphite: disorder, electron–phonon coupling, doping and nonadiabatic effects. *Solid State Communications*, *143*(1), pp.47-57.

Ferrari, A.C., Meyer, J.C., Scardaci, V., Casiraghi, C., Lazzeri, M., Mauri, F., Piscanec, S., Jiang, D., Novoselov, K.S., Roth, S. and Geim, A.K., 2006. Raman spectrum of graphene and graphene layers. *Physical Review Letters*, *97*(18), p.187401.

Fiche, J.B., Buhot, A., Calemczuk, R. and Livache, T., 2007. Temperature effects on DNA chip experiments from surface plasmon resonance imaging: isotherms and melting curves. *Biophysical Journal*, *92*(3), pp.935-946.

Friedel, R.A. and Orchin, M., 1951. *Ultraviolet spectra of aromatic compounds* (Vol. 40). New York: Wiley.

Fu, D. and Li, L.J., 2010. Label-free electrical detection of DNA hybridization using carbon nanotubes and graphene. *Nano Reviews & Experiments, 1*, pp. 5354-5363.

Gao, Y., Wolf, L.K. and Georgiadis, R.M., 2006. Secondary structure effects on DNA hybridization kinetics: a solution versus surface comparison. *Nucleic Acids Research*, *34*(11), pp.3370-3377.

Gardiner, D.J., 1989. Introduction to Raman scattering. In *Practical Raman Spectroscopy* (pp. 1-12). Springer Berlin Heidelberg.

Ge, C., Liao, J., Yu, W. and Gu, N., 2003. Electric potential control of DNA immobilization on gold electrode. *Biosensors and Bioelectronics*, *18*(1), pp.53-58.

Geim, A.K., and Novoselov, K.S., 2007. The rise of graphene. *Nature Materials*, *6*(3), pp.183-191.

Geim, A.K., 2009. Graphene: status and prospects. S*cience*, *324*(5934), pp.1530-1534.

Gholami, S., ShokuhiRad, A., Heydarinasab, A. and Ardjmand, M., 2016. Adsorption of adenine on the surface of nickel-decorated graphene; a DFT study. *Journal of Alloys and Compounds*, 686, pp. 662-668.

Gifford, L.K., Sendroiu, I.E., Corn, R.M. and Lupták, A., 2010. Attomole detection of mesophilic DNA polymerase products by nanoparticle-enhanced surface plasmon resonance imaging on glassified gold surfaces. *Journal of the American Chemical Society*, *132*(27), pp.9265-9267.

Goda, T., Singi, A.B., Maeda, Y., Matsumoto, A., Torimura, M., Aoki, H. and Miyahara, Y., 2013. Label-free potentiometry for detecting DNA hybridization using peptide nucleic acid and DNA probes. *Sensors*, *13*(2), pp.2267-2278.

Golio, J.M., Miller, M.G., Maracas, G.N. and Johnson, D.A., 1990. Frequency-dependent electrical characteristics of GaAs MESFETs. *IEEE Transactions on Electron Devices*, *37*(5), pp.1217-1227.

Gooding, J.J., 2002. Electrochemical DNA hybridization biosensors. *Electroanalysis*, *14*(17), pp.1149-1156.

Gowtham, S., Scheicher, R.H., Ahuja, R., Pandey, R. and Karna, S.P., 2007. Physisorption of nucleobases on graphene: Density-functional calculations. *Physical Review B*, *76*(3), p.033401.

Gowtham, S., Scheicher, R.H., Ahuja, R., Pandey, R. and Karna, S.P., 2007. Physisorption of nucleobases on graphene: Density-functional calculations. *Physical Review B*, *76*(3), p.033401.

Green, N.S. and Norton, M.L., 2015. Interactions of DNA with graphene and sensing applications of graphene field-effect transistor devices: A review. *Analytica Chimica Acta*, *853*, pp.127-142.

Green, N.S. and Norton, M.L., 2015. Interactions of DNA with graphene and sensing applications of graphene field-effect transistor devices: A review. *Analytica Chimica Acta*, *853*, pp.127-142.

Grover, S. and Moddel, G., 2012. Engineering the current–voltage characteristics of metal–insulator–metal diodes using double-insulator tunnel barriers. *Solid-State Electronics*, *67*(1), pp.94-99.

Gupta, A., Chen, G., Joshi, P., Tadigadapa, S. and Eklund, P.C., 2006. Raman scattering from high-frequency phonons in supported n-graphene layer films. *Nano Letters*, *6*(12), pp.2667-2673.

Hahn, S., Mergenthaler, S., Zimmermann, B. and Holzgreve, W., 2005. Nucleic acid based biosensors: the desires of the user. *Bioelectrochemistry*, *67*(2), pp.151-154.

Halperin, A., Buhot, A. and Zhulina, E.B., 2006. On the hybridization isotherms of DNA microarrays: the Langmuir model and its extensions. *Journal of Physics: Condensed Matter*, *18*(18), p.S463.

Hanley, J.A. and McNeil, B.J., 1982. The meaning and use of the area under a receiver operating characteristic (ROC) curve. *Radiology*, *143*(1), pp.29-36.

He, P., Sun, J., Tian, S., Yang, S., Ding, S., Ding, G., Xie, X. and Jiang, M., 2014. Processable aqueous dispersions of graphene stabilized by graphene quantum dots. *Chemistry of Materials*, *27*(1), pp.218-226.

He, S., Song, B., Li, D., Zhu, C., Qi, W., Wen, Y., Wang, L., Song, S., Fang, H. and Fan, C., 2010. A graphene nanoprobe for rapid, sensitive, and multicolor fluorescent DNA analysis. *Advanced Functional Materials*, *20*(3), pp.453-459.

Heerema, S.J. and Dekker, C., 2016. Graphene nanodevices for DNA sequencing. *Nature Nanotechnology*, *11*(2), pp.127-136.

Heilig, G.K., 2003. Do we really care about food safety? Facts and myths about consumers' preferences. In *Proceedings of the International Symposium Food Safety: Consumer, Trade, and Regulation.*

Heller, D.A., Jeng, E.S., Yeung, T.K., Martinez, B.M., Moll, A.E., Gastala, J.B. and Strano, M.S., 2006. Optical detection of DNA conformational polymorphism on single-walled carbon nanotubes. *Science*, *311*(5760), pp.508-511.

Hess, L.H., Jansen, M., Maybeck, V., Hauf, M.V., Seifert, M., Stutzmann, M., Sharp, I.D., Offenhäusser, A. and Garrido, J.A., 2011. Graphene transistor arrays for recording action potentials from electrogenic cells. *Advanced Materials*, *23*(43), pp.5045-5049.

Hong, I.H., Dang, J.F., Tsai, Y.H., Liu, C.S., Lee, W.T., Wang, M.L. and Chen, P.C., 2011. An RFID application in the food supply chain: A case study of convenience stores in Taiwan. *Journal of Food Engineering*, *106*(2), pp.119-126.

Hoyle, C.E. and Bowman, C.N., 2010. Thiol–ene click chemistry. *Angewandte Chemie International Edition*, *49*(9), pp.1540-1573.

Huang, Y., Dong, X., Liu, Y., Li, L.J. and Chen, P., 2011. Graphene-based biosensors for detection of bacteria and their metabolic activities. *Journal of Materials Chemistry*, *21*(33), pp.12358-12362.

Husale, B.S., Sahoo, S., Radenovic, A., Traversi, F., Annibale, P. and Kis, A., 2010. ssDNA binding reveals the atomic structure of graphene. *Langmuir*, *26*(23), pp.18078-18082.

Hvastkovs, E.G. and Buttry, D.A., 2010. Recent advances in electrochemical DNA hybridization sensors. *Analyst*, *135*(8), pp.1817-1829.

Jaakola, L., Suokas, M. and Häggman, H., 2010. Novel approaches based on DNA barcoding and high-resolution melting of amplicons for authenticity analyses of berry species. *Food Chemistry*, *123*(2), pp.494-500.

Jang, H., Kim, Y.K., Kwon, H.M., Yeo, W.S., Kim, D.E. and Min, D.H., 2010. A Graphene-Based Platform for the Assay of Duplex-DNA Unwinding by Helicase. *Angewandte Chemie*, *122*(33), pp.5839-5843.

Jauregui, L.A., Yue, Y., Sidorov, A.N., Hu, J., Yu, Q., Lopez, G., Jalilian, R., Benjamin, D.K., Delkd, D.A., Wu, W. and Liu, Z., 2010. Thermal transport in graphene nanostructures: Experiments and simulations. *Ecs Transactions*, *28*(5), pp.73-83.

Jobling, M.A. and Gill, P., 2004. Encoded evidence: DNA in forensic analysis. *Nature Reviews Genetics*, *5*(10), pp.739-751.

Jobling, M.A. and Gill, P., 2004. Encoded evidence: DNA in forensic analysis. *Nature Reviews Genetics*, *5*(10), pp.739-751.

Jung, N., Crowther, A.C., Kim, N., Kim, P. and Brus, L., 2010. Raman enhancement on graphene: adsorbed and intercalated molecular species. *ACS Nano*, *4*(11), pp.7005-7013.

Jung, N., Kim, N., Jockusch, S., Turro, N.J., Kim, P. and Brus, L., 2009. Charge transfer chemical doping of few layer graphenes: charge distribution and peak gap formation. *Nano Letters*, *9*(12), pp.4133-4137.

Jung, Y.K., Lee, T., Shin, E. and Kim, B.S., 2013. Highly tunable aptasensing microarrays with graphene oxide multilayers. *Scientific Reports*, *3*.

Junker, B.H. and Wang, H.Y., 2006. Bioprocess monitoring and computer control: key roots of the current PAT initiative. *Biotechnology and Bioengineering*, *95*(2), pp.226-261.

Kagan, M.R. and McCreery, R.L., 1994. Reduction of fluorescence interference in Raman spectroscopy via analyte adsorption on graphitic carbon. *Analytical Chemistry*, *66*(23), pp.4159-4165.

Kalita, G., Qi, L., Namba, Y., Wakita, K. and Umeno, M., 2011. Femtosecond laser induced micropatterning of graphene film. *Materials Letters*, *65*(11), pp.1569-1572.

Karamollaoğlu, İ., Öktem, H.A. and Mutlu, M., 2009. QCM-based DNA biosensor for detection of genetically modified organisms (GMOs). *Biochemical Engineering Journal*, *44*(2), pp.142-150.

Kayyalha, M. and Chen, Y.P., 2015. Observation of reduced 1/f noise in graphene field effect transistors on boron nitride substrates. *Applied Physics Letters*, *107*(11), p.113101.

Kemp, W., 1991. Organic spectroscopy. *Molecules*, *7*(1), p.11.

Kergoat, L., Herlogsson, L., Braga, D., Piro, B., Pham, M.C., Crispin, X., Berggren, M. and Horowitz, G., 2010. A Water-Gate Organic Field-Effect Transistor. *Advanced Materials*, *22*(23), pp.2565-2569.

Kerman, K., Kobayashi, M. and Tamiya, E., 2003. Recent trends in electrochemical DNA biosensor technology. *Measurement Science and Technology*, *15*(2), p.R1.

Khatayevich, D., Page, T., Gresswell, C., Hayamizu, Y., Grady, W. and Sarikaya, M., 2014. Selective Detection of Target Proteins by Peptide-Enabled Graphene Biosensor. *Small*, *10*(8), pp.1505-1513.

Kim, S.M., Hsu, A., Lee, Y.H., Dresselhaus, M., Palacios, T., Kim, K.K. and Kong, J., 2013. The effect of copper pre-cleaning on graphene synthesis. *Nanotechnology*, *24*(36), p.365602.

Kingsbury, D.T., 1987. DNA probes in the diagnosis of genetic and infectious diseases. *Trends in Biotechnology*, *5*(4), pp.107-111.

Kruse, H., 1999. Globalization of the food supply–food safety implications: Special regional requirements: future concerns. *Food Control*, *10*(4), pp.315-320.

Kumar, C.V. and Asuncion, E.H., 1993. DNA binding studies and site selective fluorescence sensitization of an anthryl probe. *Journal-American Chemical Society*, *115*, pp.8547-8547.

Kumar, S., 2006. Spectroscopy of organic compounds. *Cosmic Rays*, *10*, p.4.

Kundu, S. and Karmakar, S.N., 2016. Detection of base-pair mismatches in DNA using graphene-based nanopore device. *Nanotechnology*, *27*(13), p.135101.

Kybert, N.J., Han, G.H., Lerner, M.B., Dattoli, E.N., Esfandiar, A. and Johnson, A.C., 2014. Scalable arrays of chemical vapor sensors based on DNA-decorated graphene. *Nano Research*, *7*(1), pp.95-103.

Labarca, C. and Paigen, K., 1980. A simple, rapid, and sensitive DNA assay procedure. *Analytical Biochemistry*, *102*(2), pp.344-352.

Labuda, J., Brett, A.M.O., Evtugyn, G., Fojta, M., Mascini, M., Ozsoz, M., Palchetti, I., Paleček, E. and Wang, J., 2010. Electrochemical nucleic acid-based biosensors: concepts, terms, and methodology (IUPAC Technical Report). *Pure and Applied Chemistry*, *82*(5), pp.1161-1187.

Lanphere, J.D., Rogers, B., Luth, C., Bolster, C.H. and Walker, S.L., 2014. Stability and transport of graphene oxide nanoparticles in groundwater and surface water. *Environmental Engineering Science*, *31*(7), pp.350-359.

Lazzeri, M. and Mauri, F., 2006. Nonadiabatic Kohn anomaly in a doped graphene monolayer. *Physical Review Letters*, *97*(26), p.266407.

Lee, C., Wei, X., Kysar, J.W. and Hone, J., 2008. Measurement of the elastic properties and intrinsic strength of monolayer graphene. *Science*, *321*(5887), pp.385-388.

Lee, C.Y., Gong, P., Harbers, G.M., Grainger, D.W., Castner, D.G. and Gamble, L.J., 2006. Surface coverage and structure of mixed DNA/alkylthiol monolayers on gold: characterization by XPS, NEXAFS, and fluorescence intensity measurements. *Analytical Chemistry*, *78*(10), pp.3316-3325.

Lee, J.H., Choi, Y.K., Kim, H.J., Scheicher, R.H. and Cho, J.H., 2013. Physisorption of DNA nucleobases on h-BN and graphene: vdW-corrected DFT calculations. *The Journal of Physical Chemistry C*, *117*(26), pp.13435-13441.

Lee, T.M.H., 2008. Over-the-counter biosensors: Past, present, and future. *Sensors*, *8*(9), pp.5535-5559.

Lerner, M.B., Resczenski, J.M., Amin, A., Johnson, R.R., Goldsmith, J.I. and Johnson, A.C., 2012. Toward quantifying the electrostatic transduction mechanism in carbon nanotube molecular sensors. *Journal of the American Chemical Society*, *134*(35), pp.14318-14321.

Levicky, R. and Horgan, A., 2005. Physicochemical perspectives on DNA microarray and biosensor technologies. *Trends in Biotechnology*, *23*(3), pp.143-149.

Li, X., Cai, W., An, J., Kim, S., Nah, J., Yang, D., Piner, R., Velamakanni, A., Jung, I., Tutuc, E. and Banerjee, S.K., 2009a. Large-area synthesis of high-quality and uniform graphene films on copper foils. *Science*, *324*(5932), pp.1312-1314.

Li, X., Zhu, Y., Cai, W., Borysiak, M., Han, B., Chen, D., Piner, R.D., Colombo, L. and Ruoff, R.S., 2009b. Transfer of large-area graphene films for high-performance transparent conductive electrodes. *Nano Letters*, *9*(12), pp.4359-4363.

Li, Y., Tang, L. and Li, J., 2009. Preparation and electrochemical performance for methanol oxidation of Pt/graphene nanocomposites. *Electrochemistry Communications*, *11*(4), pp.846-849.

Liang, X., Sperling, B.A., Calizo, I., Cheng, G., Hacker, C.A., Zhang, Q., Obeng, Y., Yan, K., Peng, H., Li, Q. and Zhu, X., 2011. Toward clean and crackless transfer of graphene. *ACS Nano*, *5*(11), pp.9144-9153.

Liao, J.C., Mastali, M., Gau, V., Suchard, M.A., Møller, A.K., Bruckner, D.A., Babbitt, J.T., Li, Y., Gornbein, J., Landaw, E.M. and McCabe, E.R., 2006. Use of electrochemical DNA biosensors for rapid molecular identification of uropathogens in clinical urine specimens. *Journal of Clinical Microbiology*, *44*(2), pp.561-570.

Lin, C.T., Loan, P.T.K., Chen, T.Y., Liu, K.K., Chen, C.H., Wei, K.H. and Li, L.J., 2013. Label-Free Electrical Detection of DNA Hybridization on Graphene using Hall Effect Measurements: Revisiting the Sensing Mechanism. *Advanced Functional Materials*, *23*(18), pp.2301-2307.

Lin, J., Teweldebrhan, D., Ashraf, K., Liu, G., Jing, X., Yan, Z., Li, R., Ozkan, M., Lake, R.K., Balandin, A.A. and Ozkan, C.S., 2010. Gating of Single-Layer Graphene with Single-Stranded Deoxyribonucleic Acids. *Small*, *6*(10), pp.1150-1155.

Lin, P., Luo, X., Hsing, I. and Yan, F., 2011. Organic electrochemical transistors integrated in flexible microfluidic systems and used for label-free DNA sensing. *Advanced Materials*, *23*(35), pp.4035-4040.

Liu, B., Salgado, S., Maheshwari, V. and Liu, J., 2016. DNA adsorbed on graphene and graphene oxide: Fundamental interactions, desorption and applications. *Current Opinion in Colloid & Interface Science*, *26*, pp.41-49.

Liu, F., Choi, J.Y. and Seo, T.S., 2010. Graphene oxide arrays for detecting specific DNA hybridization by fluorescence resonance energy transfer. *Biosensors and Bioelectronics*, *25*(10), pp.2361-2365.

Liu, J., Li, Y., Li, Y., Li, J. and Deng, Z., 2010. Noncovalent DNA decorations of graphene oxide and reduced graphene oxide toward water-soluble metal–carbon hybrid nanostructures via self-assembly. *Journal of Materials Chemistry*, *20*(5), pp.900-906.

Liu, L., Ryu, S., Tomasik, M.R., Stolyarova, E., Jung, N., Hybertsen, M.S., Steigerwald, M.L., Brus, L.E. and Flynn, G.W., 2008. Graphene oxidation: thickness-dependent etching and strong chemical doping. *Nano Letters*, *8*(7), pp.1965-1970.

Liu, W., Zhong, H., Wang, R. and Seeman, N.C., 2011. Crystalline two-dimensional DNA-origami arrays. *Angewandte Chemie*, *123*(1), pp.278-281.

Liu, Y., Dong, X. and Chen, P., 2012. Biological and chemical sensors based on graphene materials. *Chemical Society Reviews*, *41*(6), pp.2283-2307.

Lo, S.T., Chuang, C., Puddy, R.K., Chen, T.M., Smith, C.G. and Liang, C.T., 2013. Non-ohmic behavior of carrier transport in highly disordered graphene. *Nanotechnology*, *24*(16), p.165201.

Lockett, M.R., Phillips, M.F., Jarecki, J.L., Peelen, D. and Smith, L.M., 2008. A tetrafluorophenyl activated ester self-assembled monolayer for the immobilization of amine-modified oligonucleotides. *Langmuir*, *24(1)*, pp.69-75.

Loureiro, M.L. and Umberger, W.J., 2007. A choice experiment model for beef: What US consumer responses tell us about relative preferences for food safety, country-of-origin labeling and traceability. *Food Policy*, *32*(4), pp.496-514.

Lu, C.H., Li, J., Liu, J.J., Yang, H.H., Chen, X. and Chen, G.N., 2010b. Increasing the sensitivity and single-base mismatch selectivity of the molecular beacon using graphene oxide as the "nanoquencher". *Chemistry–A European Journal*, *16*(16), pp.4889-4894.

Lu, C.H., Yang, H.H., Zhu, C.L., Chen, X. and Chen, G.N., 2009. A graphene platform for sensing biomolecules. *Angewandte Chemie*, *121*(26), pp.4879-4881.

Lu, C.H., Zhu, C.L., Li, J., Liu, J.J., Chen, X. and Yang, H.H., 2010a. Using graphene to protect DNA from cleavage during cellular delivery. *Chemical Communications*, *46*(18), pp.3116-3118.

Lu, Y., Goldsmith, B.R., Kybert, N.J. and Johnson, A.C., 2010. DNA-decorated graphene chemical sensors. *Applied Physics Letters*, *97*(8), p.083107.

Lucarelli, F., Tombelli, S., Minunni, M., Marrazza, G. and Mascini, M., 2008. Electrochemical and piezoelectric DNA biosensors for hybridisation detection. *Analytica Chimica Acta*, *609*(2), pp.139-159.

Ludwig, W., Brockmann, E., Beimfohr, C., Hertel, C., Jacobsen, B. and Schleifer, K.H., 1995. Nucleic acid based detection systems for genetically modified bacteria. *Systematic and Applied Microbiology*, *18*(4), pp.477-485.

Luong, J.H., Male, K.B. and Glennon, J.D., 2008. Biosensor technology: technology push versus market pull. *Biotechnology Advances*, *26*(5), pp.492-500.

Lüthy, J., 1999. Detection strategies for food authenticity and genetically modified foods. *Food Control*, *10*(6), pp.359-361.

Mak, K.F., Sfeir, M.Y., Wu, Y., Lui, C.H., Misewich, J.A. and Heinz, T.F., 2008. Measurement of the optical conductivity of graphene. *Physical Review Letters*, *101*(19), p.196405.

Malesevic, A., Vitchev, R., Schouteden, K., Volodin, A., Zhang, L., Van Tendeloo, G., Vanhulsel, A. and Van Haesendonck, C., 2008. Synthesis of few-layer graphene via microwave plasma-enhanced chemical vapour deposition. *Nanotechnology*, *19*(30), p.305604.

Malmqvist, M., 1993. Biospecific interaction analysis using biosensor technology. *Nature*, *361*(6408), pp.186-187.

Mamor, M., 2009. Interface gap states and Schottky barrier inhomogeneity at metal/n-type GaN Schottky contacts. *Journal of Physics: Condensed Matter*, *21*(33), p.335802.

Mascini, M., 2006. A Brief Story of Biosensor Technology. In *Biotechnological Applications of Photosynthetic Proteins: Biochips, Biosensors and Biodevices* (pp. 4-10). Springer US.

Mascini, M., Palchetti, I. and Marrazza, G., 2001. DNA electrochemical biosensors. *Fresenius' Journal of Analytical Chemistry*, *369*(1), pp.15-22.

May, P., Lazzeri, M., Venezuela, P., Herziger, F., Callsen, G., Reparaz, J.S., Hoffmann, A., Mauri, F. and Maultzsch, J., 2013. Signature of the two-dimensional phonon dispersion in graphene probed by double-resonant Raman scattering. *Physical Review B*, *87*(7), p.075402.

Mayorov, A.S., Gorbachev, R.V., Morozov, S.V., Britnell, L., Jalil, R., Ponomarenko, L.A., Blake, P., Novoselov, K.S., Watanabe, K., Taniguchi, T. and Geim, A.K., 2011. Micrometer-scale ballistic transport in encapsulated graphene at room temperature. *Nano Letters*, *11*(6), pp.2396-2399.

Melios, C., Panchal, V., Giusca, C.E., Strupiński, W., Silva, S.R.P. and Kazakova, O., 2015. Carrier type inversion in quasi-free standing graphene: studies of local electronic and structural properties. *Scientific Reports*, *5*.

Meneghesso, G., Verzellesi, G., Pierobon, R., Rampazzo, F., Chini, A., Mishra, U.K., Canali, C. and Zanoni, E., 2004. Surface-related drain current dispersion effects in AlGaN-GaN HEMTs. *IEEE Transactions on Electron Devices*, *51*(10), pp.1554-1561.

Merchant, C.A., Healy, K., Wanunu, M., Ray, V., Peterman, N., Bartel, J., Fischbein, M.D., Venta, K., Luo, Z., Johnson, A.C. and Drndic, M., 2010. DNA translocation through graphene nanopores. *Nano Letters*, *10*(8), pp.2915-2921.

Miao, X., Tongay, S., Petterson, M.K., Berke, K., Rinzler, A.G., Appleton, B.R. and Hebard, A.F., 2012. High efficiency graphene solar cells by chemical doping. *Nano Letters*, *12*(6), pp.2745-2750.

Millan, K.M. and Mikkelsen, S.R., 1993. Sequence-selective biosensor for DNA based on electroactive hybridization indicators. *Analytical Chemistry, 65(17)*, pp.2317-2323.

Miyamoto, Y., Zhang, H. and Tománek, D., 2010. Photoexfoliation of graphene from graphite: an Ab initio study. *Physical Review Letters*, *104*(20), p.208302.

Mohanty, N. and Berry, V., 2008. Graphene-based single-bacterium resolution biodevice and DNA transistor: interfacing graphene derivatives with nanoscale and microscale biocomponents. *Nano Letters*, *8*(12), pp.4469-4476.

Mohiuddin, T.M.G., Lombardo, A., Nair, R.R., Bonetti, A., Savini, G., Jalil, R., Bonini, N., Basko, D.M., Galiotis, C., Marzari, N. and Novoselov, K.S., 2009. Uniaxial strain in graphene by Raman spectroscopy: G peak splitting, Grüneisen parameters, and sample orientation. *Physical Review B*, *79*(20), p.205433.

Mohiuddin, T.M.G., Lombardo, A., Nair, R.R., Bonetti, A., Savini, G., Jalil, R., Bonini, N., Basko, D.M., Galiotis, C., Marzari, N. and Novoselov, K.S., 2009. Uniaxial strain in graphene by Raman spectroscopy: G peak splitting, Grüneisen parameters, and sample orientation. *Physical Review B*, *79*(20), p.205433.

Moiz, S.A., Khan, I.A., Younis, W.A. and Karimov, K.S., 2016. Space Charge–Limited Current Model for Polymers.

Monk, M.A.R.I.L.Y.N., Boubelik, M.I.C.H.A.E.L. and Lehnert, S.I.G.R.I.D., 1987. Temporal and regional changes in DNA methylation in the embryonic, extraembryonic and germ cell lineages during mouse embryo development. *Development*, *99*(3), pp.371-382.

Morozov, S.V., Novoselov, K.S., Katsnelson, M.I., Schedin, F., Elias, D.C., Jaszczak, J.A. and Geim, A.K., 2008. Giant intrinsic carrier mobilities in graphene and its bilayer. *Physical Review Letters*, *100*(1), p.016602.

Mukhopadhyay, S., Gowtham, S., Scheicher, R.H., Pandey, R. and Karna, S.P., 2010. Theoretical study of physisorption of nucleobases on boron nitride nanotubes: a new class of hybrid nano-biomaterials. *Nanotechnology*, *21*(16), pp.165703.

Murphy, T.B., Dean, N. and Raftery, A.E., 2010. Variable selection and updating in model-based discriminant analysis for high dimensional data with food authenticity applications. *The Annals of Applied Statistics*, *4*(1), p.396.

Nair, R.R., Blake, P., Grigorenko, A.N., Novoselov, K.S., Booth, T.J., Stauber, T., Peres, N.M. and Geim, A.K., 2008. Fine structure constant defines visual transparency of graphene. *Science*, *320*(5881), pp.1308-1308.

Nandy, B., Santosh, M. and Maiti, P.K., 2012. Interaction of nucleic acids with carbon nanotubes and dendrimers. *Journal of Biosciences*, *37*(3), pp.457-474.

Neto, A.C., Guinea, F., Peres, N.M., Novoselov, K.S. and Geim, A.K., 2009. The electronic properties of graphene. *Reviews of Modern Physics*, *81*(1), p.109.

Ngo, H.T., Wang, H.N., Fales, A.M. and Vo-Dinh, T., 2013. Label-free DNA biosensor based on SERS molecular sentinel on nanowave chip. *Analytical Chemistry*, *85*(13), pp.6378-6383.

Nguyen, P. and Berry, V., 2012. Graphene interfaced with biological cells: opportunities and challenges. *The Journal of Physical Chemistry Letters*, *3*(8), pp.1024-1029.

Ni, Z., Wang, Y., Yu, T., You, Y. and Shen, Z., 2008. Reduction of Fermi velocity in folded graphene observed by resonance Raman spectroscopy. *Physical Review B*, *77*(23), p.235403.

Niyogi, S., Bekyarova, E., Itkis, M.E., Zhang, H., Shepperd, K., Hicks, J., Sprinkle, M., Berger, C., Lau, C.N., Deheer, W.A. and Conrad, E.H., 2010. Spectroscopy of covalently functionalized graphene. *Nano Letters*, *10*(10), pp.4061-4066.

Novoselov, K.S., Fal, V.I., Colombo, L., Gellert, P.R., Schwab, M.G. and Kim, K., 2012. A roadmap for graphene. *Nature*, *490*(7419), pp.192-200.

Novoselov, K.S., Geim, A.K., Morozov, S.V., Jiang, D., Zhang, Y., Dubonos, S.V., Grigorieva, I.V. and Firsov, A.A., 2004. Electric field effect in atomically thin carbon films. *science*, *306*(5696), pp.666-669.

Novoselov, K.S., Jiang, D., Schedin, F., Booth, T.J., Khotkevich, V.V., Morozov, S.V. and Geim, A.K., 2005. Two-dimensional atomic crystals. *Proceedings of the National Academy of Sciences of the United States of America*, *102*(30), pp.10451-10453.

Novoselov, K.S.A., Geim, A.K., Morozov, S., Jiang, D., Katsnelson, M., Grigorieva, I., Dubonos, S. and Firsov, A., 2005. Two-dimensional gas of massless Dirac fermions in graphene. *Nature*, *438*(7065), pp.197-200.

Nugen, S.R. and Baeumner, A.J., 2008. Trends and opportunities in food pathogen detection. *Analytical and Bioanalytical Chemistry*, *391*(2), pp.451-454.

Ohno, Y., Maehashi, K. and Matsumoto, K., 2010. Label-free biosensors based on aptamer-modified graphene field-effect transistors. *Journal of the American Chemical Society*, *132*(51), pp.18012-18013.

Okahata, Y., Kobayashi, T., Tanaka, K. and Shimomura, M., 1998. Anisotropic electric conductivity in an aligned DNA cast film. *Journal of the American Chemical Society*, *120*(24), pp.6165-6166.

Oliveira Brett, A.M. and Chiorcea, A.M., 2003. Atomic force microscopy of DNA immobilized onto a highly oriented pyrolytic graphite electrode surface. *Langmuir*, *19*(9), pp.3830-3839.

Oliveira Brett, A.M. and Chiorcea, A.M., 2003. Atomic force microscopy of DNA immobilized onto a highly oriented pyrolytic graphite electrode surface. *Langmuir*, *19*(9), pp.3830-3839.

Özkumur, E., Ahn, S., Yalçın, A., Lopez, C.A., Çevik, E., Irani, R.J., DeLisi, C., Chiari, M. and Ünlü, M.S., 2010. Label-free microarray imaging for direct detection of DNA hybridization and single-nucleotide mismatches. *Biosensors and Bioelectronics, 25(7)*, pp.1789-1795.

Pallant, J., 2010. SPSS survival manual: A step by step guide to data analysis using SPSS . Maidenhead.

Pallant, J., 2013. SPSS survival manual. McGraw-Hill Education (UK).

Park, J.S., Goo, N.I. and Kim, D.E., 2014. Mechanism of DNA adsorption and desorption on graphene oxide. *Langmuir*, *30*(42), pp.12587-12595.

Passamano, M. and Pighini, M., 2006. QCM DNA-sensor for GMOs detection. *Sensors and Actuators B: Chemical*, *118*(1), pp.177-181.

Paulus, G.L., Wang, Q.H., Ulissi, Z.W., McNicholas, T.P., Vijayaraghavan, A., Shih, C.J., Jin, Z. and Strano, M.S., 2013. Charge transfer at junctions of a single layer of graphene and a metallic single walled carbon nanotube. *Small*, *9*(11), pp.1954-1963.

Pechenaya, V.I., 1975. Hypochromism of polynucleotides in the nearest neighbour approximation. *Chemical Physics Letters*, *34*(3), pp.585-587.

Pei, X., Tandon, A., Alldrick, A., Giorgi, L., Huang, W. and Yang, R., 2011. The China melamine milk scandal and its implications for food safety regulation. *Food Policy*, *36*(3), pp.412-420.

Pisana, S., Lazzeri, M., Casiraghi, C., Novoselov, K.S., Geim, A.K., Ferrari, A.C. and Mauri, F., 2007. Breakdown of the adiabatic Born–Oppenheimer approximation in graphene. *Nature Materials*, *6*(3), pp.198-201.

Popping, B., 2002. The application of biotechnological methods in authenticity testing. *Journal of Biotechnology*, *98*(1), pp.107-112.

Postma, H.W.C., 2010. Rapid sequencing of individual DNA molecules in graphene nanogaps. *Nano Letters*, *10*(2), pp.420-425.

Power, A.C. and Morrin, A., 2013. *Electroanalytical sensor technology*. INTECH Open Access Publisher.

Premkumar, T. and Geckeler, K.E., 2012. Graphene–DNA hybrid materials: Assembly, applications, and prospects. *Progress in Polymer Science*, *37*(4), pp.515-529.

Pretsch, E., Bühlmann, P., Affolter, C., Pretsch, E., Bhuhlmann, P. and Affolter, C., 2009. *Structure Determination of Organic Compounds* (Vol. 13). Berlin: Springer.

Primrose, S., Woolfe, M. and Rollinson, S., 2010. Food forensics: methods for determining the authenticity of foodstuffs. *Trends in Food Science & Technology*, *21*(12), pp.582-590.

Pumera, M., 2011. Graphene in biosensing. *Materials Today*, *14*(7), pp.308-315.

Rad, A.S., Zareyee, D., Peyravi, M. and Jahanshahi, M., 2016. Surface study of gallium-and aluminum-doped graphenes upon adsorption of cytosine: DFT calculations. *Applied Surface Science*, *390*, pp.444-451.

Rahman, M.M., Li, X.B., Lopa, N.S., Ahn, S.J. and Lee, J.J., 2015. Electrochemical DNA hybridization sensors based on conducting polymers. *Sensors*, *15*(2), pp.3801-3829.

Rajput, S., Chen, M.X., Liu, Y., Li, Y.Y., Weinert, M. and Li, L., 2013. Spatial fluctuations in barrier height at the graphene–silicon carbide Schottky junction. *Nature Communications*, *4*.

Rao, C.E.E., Sood, A.E., Subrahmanyam, K.E. and Govindaraj, A., 2009. Graphene: the new two-dimensional nanomaterial. *Angewandte Chemie International Edition*, *48*(42), pp.7752-7777.

Ratinac, K.R., Yang, W., Ringer, S.P. and Braet, F., 2010. Toward Ubiquitous Environmental Gas Sensors: Capitalizing on the Promise of Graphene. *Environmental Science & Technology*, *44*(4), pp.1167-1176.

Reid, L.M., O'donnell, C.P. and Downey, G., 2006. Recent technological advances for the determination of food authenticity. *Trends in Food Science & Technology*, *17*(7), pp.344-353.

Reina, A., Jia, X., Ho, J., Nezich, D., Son, H., Bulovic, V., Dresselhaus, M.S. and Kong, J., 2008. Large area, few-layer graphene films on arbitrary substrates by chemical vapor deposition. *Nano Letters*, *9*(1), pp.30-35.

Reuven, D.G., Shashikala, H.M., Mandal, S., Williams, M.N., Chaudhary, J. and Wang, X.Q., 2013. Supramolecular assembly of DNA on graphene nanoribbons. *Journal of Materials Chemistry B*, *1*(32), pp.3926-3931.

Rhodes, W., 1961. Hypochromism and other spectral properties of helical polynucleotides. *Journal of the American Chemical Society*, *83*(17), pp.3609-3617.

Richards, J.C., 1991. Gene probes. *Current Opinion in Biotechnology*, *2*(1), pp.76-85.

Robinson, R.N. and Clifford, C., 2012. Authenticity and festival foodservice experiences. *Annals of Tourism Research*, *39*(2), pp.571-600.

Rodrigues, A.M., 2007. Analysis of the current-transport mechanism across a CVD diamond/silicon interface. *Applied Surface Science*, *253*(14), pp.5992-5999.

Roy, T., Hesabi, Z.R., Joiner, C.A., Fujimoto, A. and Vogel, E.M., 2013. Barrier engineering for double layer CVD graphene tunnel FETs. *Microelectronic Engineering*, *109*, pp.117-119.

Ryu, S., Han, M.Y., Maultzsch, J., Heinz, T.F., Kim, P., Steigerwald, M.L. and Brus, L.E., 2008. Reversible basal plane hydrogenation of graphene. *Nano Letters*, *8*(12), pp.4597-4602.

Saccà, B. and Niemeyer, C.M., 2012. DNA origami: the art of folding DNA. *Angewandte Chemie International Edition*, *51*(1), pp.58-66.

Saito, R., Hofmann, M., Dresselhaus, G., Jorio, A. and Dresselhaus, M.S., 2011. Raman spectroscopy of graphene and carbon nanotubes. *Advances in Physics*, *60*(3), pp.413-550.

Saito, R., Jorio, A., Souza Filho, A.G., Dresselhaus, G., Dresselhaus, M.S. and Pimenta, M.A., 2001. Probing phonon dispersion relations of graphite by double resonance Raman scattering. *Physical Review Letters*, *88*(2), p.027401.

Saleem, M., 2013. Biosensors a promising future in measurements. In *IOP Conference Series: Materials Science and Engineering* (Vol. 51, No. 1, p. 012012). IOP Publishing.

SantaLucia Jr, J. and Hicks, D., 2004. The thermodynamics of DNA structural motifs. *Annual Review of Biophysics and Biomolecular Structure*, *33*, pp.415-440.

SantaLucia, J., 1998. A unified view of polymer, dumbbell, and oligonucleotide DNA nearest-neighbor thermodynamics. *Proceedings of the National Academy of Sciences*, *95*(4), pp.1460-1465.

Sarkar, D., Liu, W., Xie, X., Anselmo, A.C., Mitragotri, S. and Banerjee, K., 2014. MoS2 field-effect transistor for next-generation label-free biosensors. *ACS Nano*, *8*(4), pp.3992-4003.

Schedin, F., Geim, A.K., Morozov, S.V., Hill, E.W., Blake, P., Katsnelson, M.I. and Novoselov, K.S., 2007. Detection of individual gas molecules adsorbed on graphene. *Nature Materials*, *6*(9), pp.652-655.

Schilter, B. and Constable, A., 2002. Regulatory control of genetically modified (GM) foods: likely developments. *Toxicology Letters*, *127*(1), pp.341-349.

Schneider, G.F., Kowalczyk, S.W., Calado, V.E., Pandraud, G., Zandbergen, H.W., Vandersypen, L.M. and Dekker, C., 2010. DNA translocation through graphene nanopores. *Nano Letters*, *10*(8), pp.3163-3167.

Schügerl, K., 2001. Progress in monitoring, modeling and control of bioprocesses during the last 20 years. *Journal of Biotechnology*, *85*(2), pp.149-173.

Schweitzer, B.A. and Kool, E.T., 1995. Hydrophobic, non-hydrogen-bonding bases and base pairs in DNA. *Journal of the American Chemical Society*, *117*(7), p.1863.

Sharma, D., Kanchi, S., Sabela, M.I. and Bisetty, K., 2016. Insight into the biosensing of graphene oxide: present and future prospects. *Arabian Journal of Chemistry*, *9*(2), pp.238-261.

Shimron, S., Cecconello, A., Lu, C.H. and Willner, I., 2013. Metal nanoparticle-functionalized DNA tweezers: from mechanically programmed nanostructures to switchable fluorescence properties. *Nano Letters, 13(8)*, pp.3791-3795.

Shivaraman, S., Herman, L.H., Rana, F., Park, J. and Spencer, M.G., 2012. Schottky barrier inhomogeneities at the interface of few layer epitaxial graphene and silicon carbide. *Applied Physics Letters*, *100*(18), p.183112.

Shrestha, H.K., Hwu, K.K. and Chang, M.C., 2010. Advances in detection of genetically engineered crops by multiplex polymerase chain reaction methods. *Trends in Food Science and Technology*, *21*(9), pp.442-454.

Shushama, K.N., Rana, M.M., Inum, R. and Hossain, M.B., 2017. Graphene coated fiber optic surface plasmon resonance biosensor for the DNA hybridization detection: Simulation analysis. *Optics Communications*, *383*, pp.186-190.

Siddiquee, S., Yusof, N.A., Salleh, A.B., Bakar, F.A. and Heng, L.Y., 2010. Electrochemical DNA biosensor for the detection of specific gene related to Trichoderma harzianum species. *Bioelectrochemistry*, *79*(1), pp.31-36.

Sinanoğlu, O., 1963. On the theories of hypochromism in polynucleotides. *Radiation Research*, *20*(1), pp.149-153.

Song, H. and Chen, K., 2010. Trade effects and compliance costs of food safety regulations: the case of China. *Agriculture and Agricultural Science Procedia*, *1*, pp.429-438.

Spadavecchia, J., Manera, M.G., Quaranta, F., Siciliano, P. and Rella, R., 2005. Surface plamon resonance imaging of DNA based biosensors for potential applications in food analysis. *Biosensors and Bioelectronics*, *21*(6), pp.894-900.

Šponer, J., Leszczynski, J. and Hobza, P., 2001. Electronic properties, hydrogen bonding, stacking, and cation binding of DNA and RNA bases. *Biopolymers*, *61*(1), pp.3-31.

Steckl, A.J., Spaeth, H., You, H., Gomez, E. and Grote, J., 2011. DNA as an optical material. *Optics and Photonics News*, *22*(7), pp.34-39.

Strachan, T. and Read, A.P., 1999. Nucleic acid hybridization assays.

Strachan, T., Read, A.P., 1999. Human Molecular Genetics. 2nd edition. New York: Wiley-Liss; Chapter5.

Stulz, E., 2016. CD spectroscopy of DNA nano-materials. *Diamond*, *2015*, p.2014.

Sutter, P.W., Flege, J.I. and Sutter, E.A., 2008. Epitaxial graphene on ruthenium. *Nature Materials*, *7*(5), pp.406-411.

Sweeney, J.A. and Hennessey, J.P., 2002. Evaluation of accuracy and precision of adenovirus absorptivity at 260 nm under conditions of complete DNA disruption. *Virology*, *295*(2), pp.284-288.

Tan, X., Chen, T., Xiong, X., Mao, Y., Zhu, G., Yasun, E., Li, C., Zhu, Z. and Tan, W., 2012. Semiquantification of ATP in live cells using nonspecific desorption of DNA from graphene oxide as the internal reference. *Analytical Chemistry*, *84*(20), pp.8622-8627.

Tan, Y.W., Zhang, Y., Bolotin, K., Zhao, Y., Adam, S., Hwang, E.H., Sarma, S.D., Stormer, H.L. and Kim, P., 2007. Measurement of scattering rate and minimum conductivity in graphene. *Physical Review Letters*, *99*(24), p.246803.

Tang, L., Chang, H., Liu, Y. and Li, J., 2012. Duplex DNA/graphene oxide biointerface: from fundamental understanding to specific enzymatic effects. *Advanced Functional Materials*, *22*(14), pp.3083-3088.

Tang, L., Wang, Y., Liu, Y. and Li, J., 2011. DNA-directed self-assembly of graphene oxide with applications to ultrasensitive oligonucleotide assay. *Acs Nano*, *5*(5), pp.3817-3822.

Tang, Z., Wu, H., Cort, J.R., Buchko, G.W., Zhang, Y., Shao, Y., Aksay, I.A., Liu, J. and Lin, Y., 2010. Constraint of DNA on functionalized graphene improves its biostability and specificity. *Small*, *6*(11), pp.1205-1209.

Tataurov, A.V., You, Y. and Owczarzy, R., 2008. Predicting ultraviolet spectrum of single stranded and double stranded deoxyribonucleic acids. *Biophysical Chemistry*, *133*(1), pp.66-70.

Teles, F.R.R. and Fonseca, L.P., 2008. Applications of polymers for biomolecule immobilization in electrochemical biosensors. *Materials Science and Engineering: C*, *28*(8), pp.1530-1543.

Thévenot, D.R., Toth, K., Durst, R.A. and Wilson, G.S., 2001. Electrochemical biosensors: recommended definitions and classification. *Biosensors and Bioelectronics*, *16*(1), pp.121-131.

Thompson, P.W. and Silverman, J., 2008. The concept of accumulation in calculus. *Making the connection: Research and Teaching in Undergraduate Mathematics*, *73*, pp.43-52.

Thongrattanasiri, S., Koppens, F.H. and De Abajo, F.J.G., 2012. Complete optical absorption in periodically patterned graphene. *Physical Review Letters*, *108*(4), p.047401.

Tinoco Jr, I., 1960. Hypochromism in Polynucleotides1. *Journal of the American Chemical Society*, *82*(18), pp.4785-4790.

Tjong, V., Tang, L., Zauscher, S. and Chilkoti, A., 2014. "Smart" DNA interfaces. *Chemical Society Reviews*, *43*(5), pp.1612-1626.

Tongay, S., Lemaitre, M., Miao, X., Gila, B., Appleton, B.R. and Hebard, A.F., 2012. Rectification at graphene-semiconductor interfaces: zero-gap semiconductor-based diodes. *Physical Review X*, *2*(1), p.011002.

Torkel, W.J., Rca Corp, 1959. Field-effect transistor. U.S. Patent 2,900,531.

Trevors, J.T., 1985. DNA probes for the detection of specific genes in bacteria isolated from the environment. *Trends in Biotechnology*, *3*(11), pp.291-293.

Turner, A.P., 2013. Biosensors: sense and sensibility. *Chemical Society Reviews*, *42*(8), pp.3184-3196.

United States' Food and Drug Administration (FDA), http://www.fda.gov/cvm/guidance/published.html (2004).

Varghese, N., Mogera, U., Govindaraj, A., Das, A., Maiti, P.K., Sood, A.K. and Rao, C.N.R., 2009. Binding of DNA nucleobases and nucleosides with graphene. *ChemPhysChem*, *10*(1), pp.206-210.

Velasco-Garcia, M.N. and Mottram, T., 2003. Biosensor technology addressing agricultural problems. *Biosystems Engineering*, *84*(1), pp.1-12.

Velusamy, V., Arshak, K., Korostynska, O., Oliwa, K. and Adley, C., 2010. An overview of foodborne pathogen detection: In the perspective of biosensors. *Biotechnology Advances*, *28*(2), pp.232-254.

Verbeke, W. and Ward, R.W., 2006. Consumer interest in information cues denoting quality, traceability and origin: An application of ordered probit models to beef labels. *Food quality and Preference*, *17*(6), pp.453-467.

Vigneshvar, S., Sudhakumari, C.C., Senthilkumaran, B. and Prakash, H., 2016. Recent Advances in Biosensor Technology for Potential Applications–An Overview. *Frontiers in Bioengineering and Biotechnology*, *4(11)*, pp.1-9.

Vo-Dinh, T., 1989. *Chemical Analysis of Polycyclic Aromatic Compounds*. Wiley.

Vo-Dinh, T., 2004. Nanobiosensors. In *Encyclopedia of Nanoscience and Nanotechnology* (Vol. 5, No. 60, pp. 53-60). American Scientific Publishers.

Vovusha, H. and Sanyal, B., 2015. Adsorption of nucleobases on 2D transition-metal dichalcogenides and graphene sheet: a first principles density functional theory study. *RSC Advances*, *5*(83), pp.67427-67434.

Vovusha, H., Sanyal, S. and Sanyal, B., 2013. Interaction of nucleobases and aromatic amino acids with graphene oxide and graphene flakes. *The Journal of Physical Chemistry Letters*, *4*(21), pp.3710-3718.

Walls, I. and Buchanan, R.L., 2005. Use of food safety objectives as a tool for reducing foodborne listeriosis. *Food Control*, *16*(9), pp.795-799.

Wang, C., Jia, X.M., Jiang, C., Zhuang, G.N., Yan, Q. and Xiao, S.J., 2012. DNA microarray fabricated on poly (acrylic acid) brushes-coated porous silicon by in situ rolling circle amplification. *Analyst*, *137(19)*, pp.4539-4545.

Wang, H., Yang, R., Yang, L. and Tan, W., 2009. Nucleic acid conjugated nanomaterials for enhanced molecular recognition. *ACS Nano*, *3*(9), pp.2451-2460.

Wang, J., 1999. PNA biosensors for nucleic acid detection. *Current Issues in Molecular Biology*, *1*, pp.117-122.

Wang, J., 2000. Survey and summary from DNA biosensors to gene chips. *Nucleic Acids Research*, *28*(16), pp.3011-3016.

Wang, J., Palecek, E., Nielsen, P.E., Rivas, G., Cai, X., Shiraishi, H., Dontha, N., Luo, D. and Farias, P.A., 1996. Peptide nucleic acid probes for sequence-specific DNA biosensors. *Journal of the American Chemical Society*, *118*(33), pp.7667-7670.

Wang, J., Rivas, G., Cai, X., Palecek, E., Nielsen, P., Shiraishi, H., Dontha, N., Luo, D., Parrado, C., Chicharro, M. and Farias, P.A.M., 1997. DNA electrochemical biosensors for environmental monitoring. A review. *Analytica Chimica Acta*, *347*(1), pp.1-8.

Wang, Q.H., Jin, Z., Kim, K.K., Hilmer, A.J., Paulus, G.L., Shih, C.J., Ham, M.H., Sanchez-Yamagishi, J.D., Watanabe, K., Taniguchi, T. and Kong, J., 2012. Understanding and controlling the substrate effect on graphene electron-transfer chemistry via reactivity imprint lithography. *Nature Chemistry*, *4*(9), pp.724-732.

Wang, W., Wang, Y., Tu, L., Klein, T., Feng, Y. and Wang, J.P., 2013. Surface modification for Protein and DNA immobilization onto GMR biosensor. *IEEE Transactions on Magnetics*, *49*(1), pp.296-299.

Wang, X., Zhi, L. and Müllen, K., 2008. Transparent, conductive graphene electrodes for dye-sensitized solar cells. *Nano Letters*, *8*(1), pp.323-327.

Wang, Y., 2008. Theoretical Evidence for the Stronger Ability of Thymine to Disperse SWCNT than Cytosine and Adenine: self-stacking of DNA bases vs their cross-stacking with SWCNT. *The Journal of Physical Chemistry C*, *112*(37), pp.14297-14305.

Wang, Y., Li, Z., Wang, J., Li, J. and Lin, Y., 2011. Graphene and graphene oxide: biofunctionalization and applications in biotechnology. *Trends in Biotechnology*, *29*(5), pp.205-212.

Wang, Y.H., Deng, H.H., Liu, Y.H., Shi, X.Q., Liu, A.L., Peng, H.P., Hong, G.L. and Chen, W., 2016. Partially reduced graphene oxide as highly efficient DNA nanoprobe. *Biosensors and Bioelectronics*, *80*, pp.140-145.

Wang, Y.Y. and Burke, P.J., 2013. A large-area and contamination-free graphene transistor for liquid-gated sensing applications. *Applied Physics Letters*, *103*(5), p.052103.

Wang, Z., Zhang, J., Chen, P., Zhou, X., Yang, Y., Wu, S., Niu, L., Han, Y., Wang, L., Boey, F. and Zhang, Q., 2011. Label-free, electrochemical detection of methicillin-resistant

staphylococcus aureus DNA with reduced graphene oxide-modified electrodes. *Biosensors and Bioelectronics*, *26*(9), pp.3881-3886.

Weber, C.M., Eisele, D.M., Rabe, J.P., Liang, Y., Feng, X., Zhi, L., Müllen, K., Lyon, J.L., Williams, R., Bout, D.A.V. and Stevenson, K.J., 2010. Graphene-based optically transparent electrodes for spectroelectrochemistry in the UV–Vis region. *Small*, *6*(2), pp.184-189.

Wells, D.B., Belkin, M., Comer, J. and Aksimentiev, A., 2012. Assessing graphene nanopores for sequencing DNA. *Nano Letters*, *12*(8), pp.4117-4123.

Wetmur, J.G. and Fresco, J., 2008. DNA probes: applications of the principles of nucleic acid hybridization. *Critical Reviews in Biochemistry and Molecular Biology*.

Williams, G., Seger, B. and Kamat, P.V., 2008. TiO2-graphene nanocomposites. UV-assisted photocatalytic reduction of graphene oxide. *ACS Nano*, *2*(7), pp.1487-1491.

Wolcott, M.J., 1992. Advances in nucleic acid-based detection methods. *Clinical Microbiology Reviews*, *5*(4), pp.370-386.

Wolfe, A., Shimer Jr, G.H. and Meehan, T., 1987. Polycyclic aromatic hydrocarbons physically intercalate into duplex regions of denatured DNA. *Biochemistry*, *26*(20), pp.6392-6396.

Wong, I.Y. and Melosh, N.A., 2010. An electrostatic model for DNA surface hybridization. *Biophysical Journal*, *98*(12), pp.2954-2963.

Wong, R.S. and Passaro, E., 1990. DNA technology. *The American Journal of Surgery*, *159*(6), pp.610-614.

Wu, A.H., Sun, J.J., Zheng, R.J., Yang, H.H. and Chen, G.N., 2010. A reagentless DNA biosensor based on cathodic electrochemiluminescence at a C/C x O 1− x electrode. *Talanta*, *81*(3), pp.934-940.

Wu, C.C., Ko, F.H., Yang, Y.S., Hsia, D.L., Lee, B.S. and Su, T.S., 2009. Label-free biosensing of a gene mutation using a silicon nanowire field-effect transistor. *Biosensors and Bioelectronics*, *25*(4), pp.820-825.

Wu, L., Feng, L., Ren, J. and Qu, X., 2012. Electrochemical detection of dopamine using porphyrin-functionalized graphene. *Biosensors and Bioelectronics*, *34*(1), pp.57-62.

Wu, M., Kempaiah, R., Huang, P.J.J., Maheshwari, V. and Liu, J., 2011. Adsorption and desorption of DNA on graphene oxide studied by fluorescently labeled oligonucleotides. *Langmuir*, *27*(6), pp.2731-2738.

Wu, T.C., Rahman, M. and Norton, M.L., 2014. From nonfinite to finite 1D arrays of origami tiles. *Accounts of Chemical Research*, *47*(6), pp.1750-1758.

Xie, L., Ling, X., Fang, Y., Zhang, J. and Liu, Z., 2009. Graphene as a substrate to suppress fluorescence in resonance Raman spectroscopy. *Journal of the American Chemical Society*, *131*(29), pp.9890-9891.

Xiu-Ling, M.A.O., Jian, W.U. and Yi-Bin, Y.I.N.G., 2008. Application of electrochemical biosensors in fermentation. *Chinese Journal of Analytical Chemistry*, *36*(12), pp.1749-1755.

Xu, D., Evans, K.O. and Nordlund, T.M., 1994. Melting and premelting transitions of an oligomer measured by DNA base fluorescence and absorption. *Biochemistry*, *33*(32), pp.9592-9599.

Xu, M., Endres, R.G. and Arakawa, Y., 2007. The electronic properties of DNA bases. *Small*, *3*(9), pp.1539-1543.

Yan, J., Zhang, Y., Kim, P. and Pinczuk, A., 2007. Electric field effect tuning of electron-phonon coupling in graphene. *Physical Review Letters*, *98*(16), p.166802.

Yan, P., Lei, P., Xiao-Juan, C., Ting-Ting, Y., Wei-Jun, L. and Xin-Yu, L., 2011. Dispersion effect on the current voltage characteristic of AlGaN/GaN high electron mobility transistors. *Chinese Physics B*, *20*(9), p.097305.

Yang, X., Tang, S., Ding, G., Xie, X., Jiang, M. and Huang, F., 2011. Layer-by-layer thinning of graphene by plasma irradiation and post-annealing. *Nanotechnology*, *23*(2), p.025704.

Yapp, C., and Fairman, R., 2006. Factors affecting food safety compliance within small and medium-sized enterprises: implications for regulatory and enforcement strategies. *Food Control*, 17: 42–51.

Yim, C., McEvoy, N. and Duesberg, G.S., 2013. Characterization of graphene-silicon Schottky barrier diodes using impedance spectroscopy. *Applied Physics Letters*, *103*(19), p.193106.

Yin, Z., He, Q., Huang, X., Zhang, J., Wu, S., Chen, P., Lu, G., Zhang, Q., Yan, Q. and Zhang, H., 2012. Real-time DNA detection using Pt nanoparticle-decorated reduced graphene oxide field-effect transistors. *Nanoscale*, *4*(1), pp.293-297.

Yoo, K.H., Ha, D.H., Lee, J.O., Park, J.W., Kim, J., Kim, J.J., Lee, H.Y., Kawai, T. and Choi, H.Y., 2001. Electrical conduction through poly (dA)-poly (dT) and poly (dG)-poly (dC) DNA molecules. *Physical Review Letters*, *87*(19), p.198102.

Yoon, D., Moon, H., Son, Y.W., Choi, J.S., Park, B.H., Cha, Y.H., Kim, Y.D. and Cheong, H., 2009. Interference effect on Raman spectrum of graphene on SiO 2/Si. *Physical Review B*, *80*(12), p.125422.

Yoshinaga, H., Nakano, K., Soh, N., Ishimatsu, R. and Imato, T., 2012. A Pivot-Hinge-Style DNA Immobilization Method with Adaptable Surface Concentration Based on Oligodeoxynucleotide-Phosphorothioate Chemisorption on Gold Surfaces. *Analytical Sciences*, *28*(11), pp.1059-1064.

Yu Wang, Y. and Burke, P.J., 2013. A large-area and contamination-free graphene transistor for liquid-gated sensing applications. *Applied Physics Letters*, *103*(5), p.052103.

Yu, A., Roes, I., Davies, A. and Chen, Z., 2010. Ultrathin, transparent, and flexible graphene films for supercapacitor application. *Applied Physics Letters*, *96*(25), p.253105.

Zach, L., Doyle, M.E., Bier, V. and Czuprynski, C., 2012. Systems and governance in food import safety: A US perspective. *Food Control*, *27*(1), pp.153-162.

Zan, R., Ramasse, Q.M., Bangert, U. and Novoselov, K.S., 2012. Graphene reknits its holes. *Nano Letters*, *12*(8), pp.3936-3940.

Zeng, S., Chen, L., Wang, Y. and Chen, J., 2015. Exploration on the mechanism of DNA adsorption on graphene and graphene oxide via molecular simulations. *Journal of Physics D: Applied Physics*, *48*(27), p.275402.

Zhang, B., Song, J., Yang, G. and Han, B., 2014. Large-scale production of high-quality graphene using glucose and ferric chloride. *Chemical Science*, *5*(12), pp.4656-4660.

Zhang, J., Lang, H.P., Yoshikawa, G. and Gerber, C., 2012. Optimization of DNA hybridization efficiency by pH-driven nanomechanical bending. *Langmuir*, *28*(15), pp.6494-6501.

Zhang, L., Wang, Z., Lu, Z., Shen, H., Huang, J., Zhao, Q., Liu, M., He, N. and Zhang, Z., 2013. PEGylated reduced graphene oxide as a superior ssRNA delivery system. *Journal of Materials Chemistry B*, *1*(6), pp.749-755.

Zhang, Q., Qiao, Y., Hao, F., Zhang, L., Wu, S., Li, Y., Li, J. and Song, X.M., 2010. Fabrication of a Biocompatible and Conductive Platform Based on a Single-Stranded DNA/Graphene Nanocomposite for Direct Electrochemistry and Electrocatalysis. *Chemistry–A European Journal*, *16*(27), pp.8133-8139.

Zhang, X. and Hu, H., 2014. DNA molecules site-specific immobilization and their applications. *Open Chemistry*, *12*(10), pp.977-993.

Zhao, J., Feng, M., Yang, J. and Petek, H., 2009. The superatom states of fullerenes and their hybridization into the nearly free electron peaks of fullerites. *ACS Nano*, *3*(4), pp.853-864.

Zhou, M., Zhai, Y. and Dong, S., 2009. Electrochemical sensing and biosensing platform based on chemically reduced graphene oxide. *Analytical Chemistry*, *81*(14), pp.5603-5613.

Zhou, R., 2015. *Modeling of Nanotoxicity*. Springer. pp. 60-73.

Zhu, X., Han, K. and Li, G., 2006. Magnetic nanoparticles applied in electrochemical detection of controllable DNA hybridization. *Analytical Chemistry*, *78*(7), pp.2447-2449.

Zuker, M., 2003. Mfold web server for nucleic acid folding and hybridization prediction. *Nucleic Acids Research*, *31*(13), pp.3406-3415.

Appendix A: Design of a label-free ssDNA probe

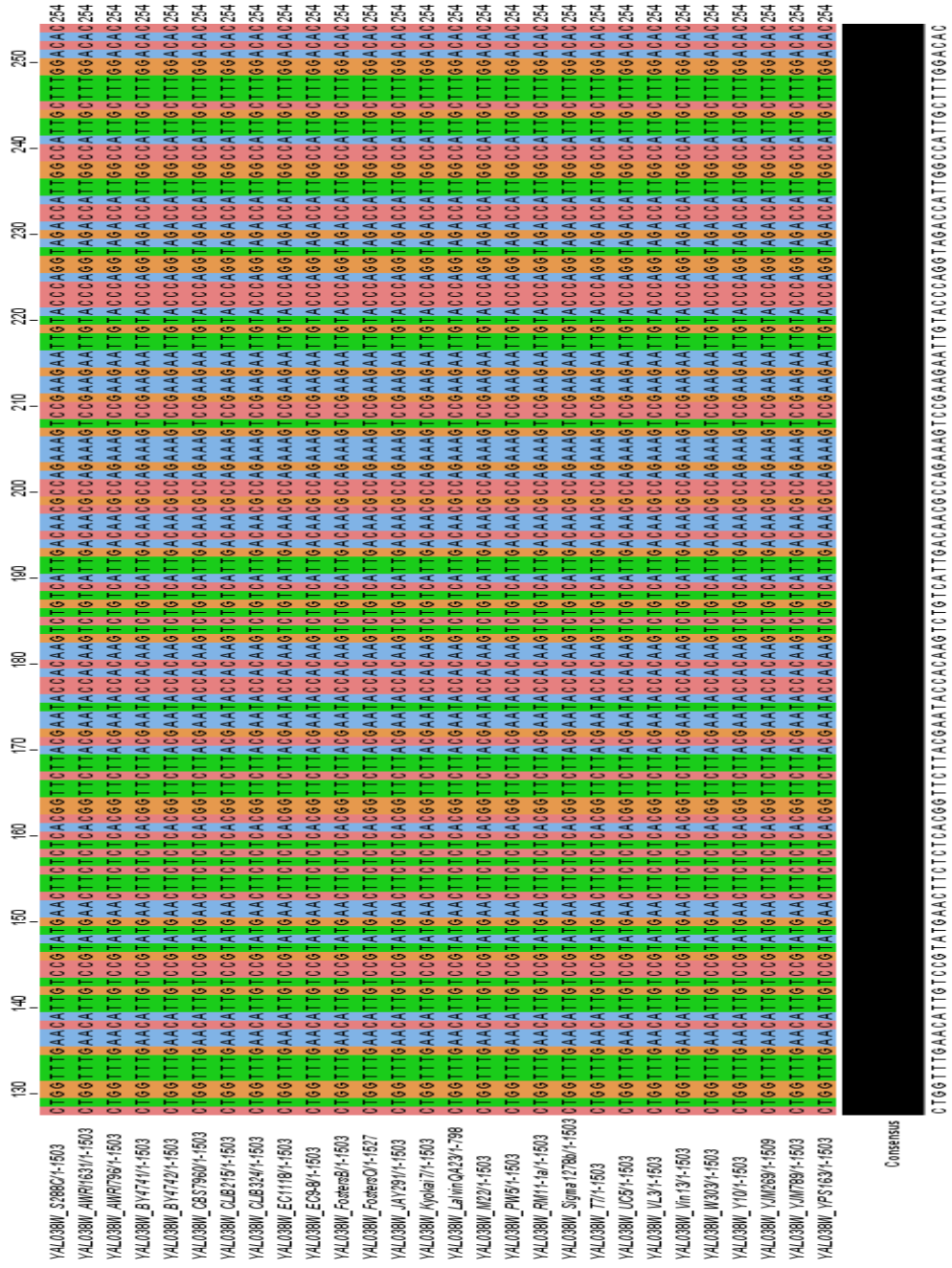

Figure A0.1 Jalview Kalign (version 2.03) alignment of CDC19 gene sequences in ClustalW format identifying the conserved sequence region across 28 S.cerevisiae strains found in SGD

Appendix B: List presentations at conferences, seminars and workshops

1. **G.N. Hlongwane**, D. Wamwangi, S.E. Iyuke. 2012. Tracking and tracing of a brewery product using a DNA/graphene sensor. South African Institute of Chemical Engineers (SAICHE) Conference. September 16-19, Drakensberg, South Africa (Poster).

2. **G.N. Hlongwane**, D. Wamwangi, S.E. Iyuke. 2013. Label-free DNA/graphene based electrochemical DNA hybridisation sensor. DST/NRF Centre of Excellence in Strong materials Annual Meeting. May 23, University of the Witwatersrand, South Africa (Poster).

3. **G.N. Hlongwane**, D. Wamwangi, S.E. Iyuke. 2013. 6th Science Conclave (A Congregation of Nobel. December 08-14, IIIT Allahabad, India (Invited Young Researcher).

4. **G.N. Hlongwane**, D. Wamwangi, S.E. Iyuke. 2014. Label-free refractometric detection of DNA hybridization on Graphene. DST/NRF Centre of Excellence in Strong materials Annual Meeting. April 16, University of the Witwatersrand, South Africa (Poster).

5. **G.N. Hlongwane**, D. Wamwangi, S.E. Iyuke. 2015. DNA hybridisation on Graphene leads to variable DNA duplex motifs. DST/NRF Centre of Excellence in Strong materials Annual Meeting. April 23, University of the Witwatersrand, South Africa (Poster).

6. **G.N. Hlongwane**, D. Wamwangi, S.E. Iyuke. 2015. Fabrication of label-free DNA/graphene based DNA hybridisation sensor. African Materials Science and Engineering Network (AMSEN) Workshop. May 27-29, Boksburg, South Africa (Oral).

7. **G.N Hlongwane**, D. Wamwangi, S. Iyuke. 2015. Workshop: Regional Initiative in Science and Education (RISE). Planet Earth Institute #scienceAfrica UnConference. July 21, Ravensbourne, United Kingdom (Panellist).

8. **G.N Hlongwane**, D. Wamwangi, S. Iyuke. 2015. Conformational Changes of DNA on Graphene. 8th Conference of the African Materials Research Society (AMRS). December 7-10, Accra, Ghana (Oral).

9. **G.N Hlongwane**, D. Wamwangi, S. Iyuke. 2016. Fabrication of label-free DNA/graphene based DNA hybridisation sensor. 7th Wits Cross Faculty Postgraduate Symposium. March 01-02, University of the Witwatersrand, South Africa (Oral).

10. **G.N Hlongwane**, D. Wamwangi, S. Iyuke. 2016. Regional Initiative in Science and Education (RISE) Meeting. April 19-22, Nairobi, Kenya (Closed session).

11. **G.N Hlongwane**, D. Wamwangi, S. Iyuke. 2016. Raman Fingerprints of DNA Hybridisation on Graphene. DST/NRF Centre of Excellence in Strong materials Annual Meeting. May 26, University of the Witwatersrand, South Africa (Poster).

Appendix C: List of articles in peer-reviewed journals

1. **G.N. Hlongwane**, D. Dodoo-Arhin, D. Wamwangi, M.O. Daramola, S.E. Iyuke. Geometric interpretation of current-voltage measurements: A new approach toward a consistent output signal in graphene based DNA biosensors. *Biosensors and Bioelectronics* (submitted).

2. **G.N. Hlongwane**, D. Dodoo-Arhin, D. Wamwangi, M.O. Daramola, S.E. Iyuke. A novel UV-Vis spectroscopy method for label-free detection of DNA adsorption and desorption on graphene. *Talanta* (submitted).

3. **G.N. Hlongwane**, D. Dodoo-Arhin, D. Wamwangi, M.O. Daramola, S.E. Iyuke. Raman fingerprint of DNA hybridisation on graphene. (Manuscript in preparation).

4. **G.N. Hlongwane**, D. Dodoo-Arhin, D. Wamwangi, M.O. Daramola, S.E. Iyuke. DNA hybridisation Sensors for Product authentication and tracing: state of the art and challenges (Manuscript in preparation).